Engineered Biofilms for Environmental Applications

Engineered Biofilms for Environmental Applications

A dissertation presented

by

Pei Kun Richie Tay

to

The School of Engineering and Applied Sciences

in partial fulfillment of the requirements

for the degree of

Doctor of Philosophy

in the subject of

Engineering Sciences

Harvard University

Cambridge, Massachusetts

October 2017

Dissertation Advisor: Prof. Neel S. Joshi Pei Kun Richie Tay

Engineered Biofilms for Environmental Applications

Abstract

As anthropogenic waste continues to pollute the environment with toxic metals, radionuclides and organic compounds, there is a need for new strategies of waste containment and waste management that are cost-effective and sustainable. This thesis explores the engineering of biofilms—populations of microorganisms in an extracellular matrix—as novel biotechnological tools for the removal of pollutants and the recovery of valuable resources from waste streams, using *E. coli* biofilms as a model system to highlight design principles. The guiding hypothesis is that we can program materials and living systems to be targeted biosorbents by genetic modification of both the cellular and the extracellular components of biofilms.

We first demonstrate the environmentally-triggered production of a mercury biosorbent in *E. coli* using a synthetic gene circuit that couples mercury sensing to the production of curli fibers—extracellular protein amyloids that have a natural affinity for mercury. The circuit is sensitive to mercury in the presence of other metals, and tunes curli production according to environmental mercury concentrations. This response persists over multiple cell generations. The work suggests that biofilms could potentially operate as autonomous sensor-actuator systems for *in situ* bioremediation. We then describe the development of filters based on curli fibers that have been genetically programmed to display customizable tags. The filters were successfully applied towards the selective recovery of rare earth metals from complex metal mixtures. This work paves

the way for designing extracellular amyloids in a range of biofilms for rapid, scalable and selective resource recovery from anthropogenic waste. Taken together, the results presented in this thesis show how a confluence of synthetic biology and materials science can potentially transform biofilms into specialized biosorbents for environmental applications.

Contents

Acknowledgements

A few people to thank for pulling me through this tumultuous and disillusioning, but ultimately humbling and rewarding, journey.

Neel, for challenging me to take on something new and unknown; for believing in me despite the endless shenanigans; for being a generous mentor and genuine person.

Peter, for endless insights and artistic inspiration; for offering a life raft in stormy seas.

Pete, for down-to-earth discussions and gentle but insistent nudging; and Dave, for invaluable practical advise.

Multiple lab members: Zsofia for help early on; Bom for his good humor; Martin for providing humor, Anna for being the subject of humor (sorry!), Noémie for playing along. We had some fun times.

Most importantly, my dear family, who gave me the freedom to pursue what I wanted, even if it meant an extended expatriation; who then stoically suffered my absence through several family and health crises; whose kind words of support were unfailing rays of hope, even if beamed through a mobile phone or computer screen. We are all stronger now.

1

Introduction

Urbanization and human industry—especially mining, agriculture and manufacturing—generate a constant stream of waste, often laden with chemical contaminants. Some of these are well-recognized toxins (e.g. heavy metals, pesticides),[1] but many others, ranging from pharmaceuticals and personal care products, to new agrochemicals, plasticizers, surfactants and dyes, are emerging pollutants, whose environmental persistence and impact on ecological and human health are still being unraveled.[2-4] There are also species (e.g. precious metals, plastics and biopolymers) with reuse potential, and their recovery from waste streams could be vital for future resource sustainability.[5-7] This dissertation focuses on the remediation of toxic metals and the recovery of valuable ones using rationally engineered biofilms—microbial communities held together by an extracellular matrix. We first discuss the issues of current methods for metal removal, and how engineered biofilms could overcome some of those challenges.

1.1 Abiotic approaches to metal remediation

Common physicochemical approaches to treating and removing metal pollutants include chemical precipitation, solvent extraction, redox stabilization, electrodialysis, reverse osmosis, ion exchange, and adsorption using granular activated carbon (GAC) or other porous matrices.[8, 9] In chemical precipitation, metal species are isolated in a solid form for disposal through the use of coagulants like alum, lime, iron salts and organic polymers. The analogous liquid-phase isolation is carried out through solvent extraction using water-immiscible solvents that can selectively dissolve certain metal complexes. Redox stabilization seeks to convert toxic metal species into less mobile and more benign forms (e.g. CrO_4^{2-} to Cr^{3+}, Hg^{2+} to Hg) using chemical oxidants or

reductants. Electrodialysis and reverse osmosis both rely on semi-permeable membranes to retain metal ions as waste liquid is directed past the membranes through an applied electric potential (the former) or a pressure gradient (the latter). In ion-exchange, charged resins take the place of membranes as selective filters for ionic species. Finally, meso- and microporous materials like GAC, mineral clays and zeolites adsorb metals through a combination of electrostatic and hydrogen-bonding interactions.

While many of these processes have been used for decades, they suffer from one or more weaknesses.[8, 9] First, they can be ineffective at low metal concentrations, typically less than 100 ppm (100 mg/L) for chemical precipitation and electrochemical methods.[9, 10] Second, a large amount of toxic sludge or other waste products can be produced that require further treatment and careful disposal, thus adding to operational costs and overall environmental burden; this is especially true of precipitation and solvent extraction. Third, the processes can incur significant capital and running costs associated with expensive materials (e.g. ion-exchange resins, selective membranes, mesoporous matrices) or high-energy operations (e.g. reverse osmosis, electrodialysis). Fourth, the filters can be poisoned by organics and not easily regenerated for reuse. Finally, most of these methods are non-specific in the species they remove, and it can be difficult to introduce selectivity for the recovery of high-value metals.

1.2 Biofilms for metal remediation

Biological methods offer eco-friendly and often more efficient and cost-effective alternatives to conventional physicochemical remediation of waste metals. Microorganisms, in particular, can degrade organic pollutants and sorb, transport, complex and transform metals, metalloids and radionuclides autonomously and efficiently without the generation of toxic by-

products.[11-15] They are easily propagated in large bioreactors or fermenters, or obtained inexpensively as fermentation waste from the pharmaceutical or food industries. In the form of activated sludge, they have been integral to wastewater treatment systems for decades, helping to remove and degrade excess nutrients and organic pollutants.[16, 17] They could also be applied for *in situ* decontamination of polluted sites—in a process called bioaugmentation—without significant disruption to the surrounding environment or generation of large sludge pools.[18-22] Bacteria have evolved mechanisms for interacting with metals for various reasons: most species require Fe^{3+} and other trace metals to thrive, chemoautotrophs like *Acidithiobacillus sp.* oxidize metallic ores for energy, and species growing in contaminated environments need to sense and detoxify harmful metals for survival. Living cells have the capacity to metabolize metals, accumulate them intracellularly, or produce surfactants or metal oxides that bind up metals.[23, 24] However, their need for a constant nutrient supply and susceptibility to poisoning when faced with high concentrations of toxic metals has limited their use for bioremediation. It is also difficult to recover metals that have accumulated within cells. Instead, metal removal is more often carried out with dead biomass, through passive adsorption to a range of hydrophilic and charged groups present on bacterial cell walls.[25-28] A variety of Gram-negative and -positive species have been investigated for their ability to bind heavy metals, radionuclides and precious metals.[25]

Biofilms are sessile communities of microorganisms surrounded by a secreted matrix of extracellular polymeric substances (EPS). They are the preferred mode of existence for many bacteria because they maintain a hydrated, nutrient-rich environment while providing enhanced resistance or tolerance to external stresses and antimicrobial agents.[29] Although notorious for their involvement in medical device contamination, biofouling of process water and microbially-influenced corrosion,[30-32] biofilms have also been exploited in recent decades in biotechnology—

as biocatalysts in chemical and biofuel production; in microbial fuel cells; in bioleaching for metal extraction; and in the treatment of wastewater and solid waste.[33-35] For the sorption of metals, biofilms are advantageous compared to suspended cultures because the vast EPS network greatly increases the surface area available for metal binding; the growth and attachment of biofilms to substrates also make them easier to handle than cell suspensions. Biosorption in existing biofilm reactors mostly rely on non-specific interactions between target metal species and the cell surface or EPS components. Because the nature of these interactions is often unknown, there are limited options for optimizing metal binding capabilities or developing more advanced technologies to recover specific metals. Genetic engineering of biofilm components—cells and EPS—offers a means to direct specific metal interactions to improve biosorption efficiency, and also potentially to tailor biofilm production to specific metal species.

1.3 *E. coli curli fibers and the BIND platform*

Previous research has demonstrated that bacteria can be engineered to display metal binding groups on their surface for enhanced metal sorption,[36, 37] however, not much effort has been made to modify the EPS, which constitutes most of the biomass of a biofilm.[38] The composition of the extracellular matrix varies across bacterial species, though it generally consists of polysaccharides, extracellular DNA, and proteins.[38] Polysaccharides like alginate, cellulose and colanic acid are most abundant, but they are difficult to engineer due to their complex biosynthetic pathways and the need to chemically alter the sugar monomers. Extracellular DNA is released upon cell lysis, thus its production is necessarily self-limited. In contrast, proteins can be facilely manipulated using standard genetic engineering techniques, and most protein polymers in biofilm

EPS are assembled extracellularly from secreted monomers, thus protein engineering offers a good starting point for building specialized nanomaterials for biosorption.

Our lab and others have developed a platform for displaying peptide motifs and small protein domains on protein nanofibers called curli fibers in *E. coli* biofilms; we call this Biofilm Integrated Nanofiber Display (BIND).[39-44] The curli monomeric unit is a protein called CsgA; it is secreted via a dedicated export apparatus that also guides its extracellular self-assembly into amyloid nanofibers.[45] The secretion machinery can accommodate the addition of domains at the C-terminus of CsgA—moieties as large as 260-residue nanobodies have been successfully exported with minimal impact on fiber assembly.[46] Functionalized curli fibers have been used to capture and template the growth of metal nanoparticles to build conductive materials.[39, 40] We hypothesize that bacterial biofilms can be engineered as specialized biosorbents for waste metals by manipulating the production and properties of functional amyloid fibers in the biofilms.

1.4 Thesis outline

The overall goal of this thesis is to explore principles of designing biofilms as materials and living systems for targeted biosorption. We used *E. coli* and curli fibers native to *E. coli* biofilms as a genetically tractable starting point for the implementation of our designs, while the biosorption of metals provided a practical framework for examining the limitations of our approaches and how they compare to current strategies. It was not our intent to engineer optimized products or processes for commercial exploitation, so a rigorous examination of yields, efficiencies and design parameters that would be crucial in final application was beyond the scope of this thesis.

We first looked at engineering the cellular component of biofilms for "on-demand" *in situ* bioremediation. Chapter 2 demonstrates the design and implementation of a gene circuit to couple

the detection of toxic mercury to the production of a mercury-binding curli protein network in *E. coli* biofilms. The sensitivity and robustness of the response was tested under exposure to various mercury concentrations and mixed-metal environments. We showed that curli production and mercury sorption led to a consolidation of the biomass so that the mercury was not readily released.

We then explored engineering curli fibers for fabrication into biosorption filters with customizable targets. Chapter 3 discusses the modification of curli biogenesis to create extensive fibrous meshes, and also the isolation and immobilization of these meshes using a rapid and scalable filtration process we developed. The use of curli-based filters functionalized with lanthanide-binding tags to recover lanthanides is described in Chapter 4. We examined the adsorption selectivity in complex metal mixtures—including the ability to resolve groups of lanthanides—and also the feasibility of recovering the metals using acidic washes. The ability to operate the filters in batch and continuous flow modes was demonstrated.

Finally, Chapter 5 provides a summary of the results, the implications and limitations of the current research, and directions that could be taken by future researchers.

1.5 References

[1] Agency, U. S. E. P. (2014) Appendix A to Part 423 - 126 Priority Pollutants, In *Title 40*.

[2] Daughton, C. G., and Ternes, T. A. (1999) Pharmaceuticals and personal care products in the environment: agents of subtle change?, *Environmental Health Perspectives 107*, 907-938.

[3] Deblonde, T., Cossu-Leguille, C., and Hartemann, P. (2011) Emerging pollutants in wastewater: A review of the literature, *International Journal of Hygiene and Environmental Health 214*, 442-448.

[4] Gavrilescu, M., Demnerová, K., Aamand, J., Agathos, S., and Fava, F. (2015) Emerging pollutants in the environment: present and future challenges in biomonitoring, ecological risks and bioremediation, *New Biotechnology 32*, 147-156.

[5] Puyol, D., Batstone, D. J., Hülsen, T., Astals, S., Peces, M., and Krömer, J. O. (2016) Resource Recovery from Wastewater by Biological Technologies: Opportunities, Challenges, and Prospects, *Frontiers in Microbiology 7*, 2106.

[6] van der Hoek, J. P., de Fooij, H., and Struker, A. (2016) Wastewater as a resource: Strategies to recover resources from Amsterdam's wastewater, *Resources, Conservation and Recycling 113*, 53-64.

[7] van Loosdrecht, M. C., and Brdjanovic, D. (2014) Water treatment. Anticipating the next century of wastewater treatment, *Science (New York, N.Y.) 344*, 1452-1453.

[8] Gadd, G. M. (2009) Biosorption: critical review of scientific rationale, environmental importance and significance for pollution treatment, *Journal of Chemical Technology & Biotechnology 84*, 13-28.

[9] Lo, Y.-C., Cheng, C.-L., Han, Y.-L., Chen, B.-Y., and Chang, J.-S. (2014) Recovery of high-value metals from geothermal sites by biosorption and bioaccumulation, *Bioresource Technology 160*, 182-190.

[10] Crini, G. (2006) Non-conventional low-cost adsorbents for dye removal: A review, *Bioresource Technology 97*, 1061-1085.

[11] Alencar, F. L. S., Navoni, J. A., and Do Amaral, V. S. (2017) The use of bacterial bioremediation of metals in aquatic environments in the twenty-first century: a systematic review, *Environmental Science and Pollution Research 24*, 16545-16559.

[12] Dolinova, I., Strojsova, M., Cernik, M., Nemecek, J., Machackova, J., and Sevcu, A. (2017) Microbial degradation of chloroethenes: a review, *Environmental Science and Pollution Research 24*, 13262-13283.

[13] Edwards, C., and Lawton, L. A. (2009) Bioremediation of cyanotoxins, *Advances in applied microbiology 67*, 109-129.

[14] Ncibi, M. C., Mahjoub, B., Mahjoub, O., and Sillanpaa, M. (2017) Remediation of Emerging Pollutants in Contaminated Wastewater and Aquatic Environments: Biomass-Based Technologies, *Clean-Soil Air Water 45*.

[15] Pacwa-Płociniczak, M., Płaza, G. A., Piotrowska-Seget, Z., and Cameotra, S. S. (2011) Environmental Applications of Biosurfactants: Recent Advances, *International Journal of Molecular Sciences 12*, 633-654.

[16] Lewandowski, Z., and Boltz, J. P. (2011) Biofilms in Water and Wastewater Treatment, In *Treatise on Water Science*, pp 529-570, Elsevier, Oxford.

[17] Walden, C., and Zhang, W. (2016) Biofilms Versus Activated Sludge: Considerations in Metal and Metal Oxide Nanoparticle Removal from Wastewater, *Environmental Science & Technology 50*, 8417-8431.

[18] Herrero, M., and Stuckey, D. C. (2015) Bioaugmentation and its application in wastewater treatment: A review, *Chemosphere 140*, 119-128.

[19] Mrozik, A., and Piotrowska-Seget, Z. (2010) Bioaugmentation as a strategy for cleaning up of soils contaminated with aromatic compounds, *Microbiological Research 165*, 363-375.

[20] Nzila, A., Razzak, S. A., and Zhu, J. (2016) Bioaugmentation: An Emerging Strategy of Industrial Wastewater Treatment for Reuse and Discharge, *International Journal of Environmental Research and Public Health 13*, 846.

[21] Jiang, Y., Brassington, K. J., Prpich, G., Paton, G. I., Semple, K. T., Pollard, S. J. T., and Coulon, F. (2016) Insights into the biodegradation of weathered hydrocarbons in contaminated soils by bioaugmentation and nutrient stimulation, *Chemosphere 161*, 300-307.

[22] Vásquez-Murrieta, M. S., Hernández-Hernández, O. J., Cruz-Maya, J. A., Cancino-Díaz, J. C., and Jan-Roblero, J. (2016) Approaches for Removal of PAHs in Soils: Bioaugmentation, Biostimulation and Bioattenuation, Soil Contamination - Current Consequences and Further Solutions, (Larramendy, M., Ed.), InTech.

[23] Hennebel, T., De Gusseme, B., Boon, N., and Verstraete, W. (2009) Biogenic metals in advanced water treatment, *Trends in biotechnology 27*, 90-98.

[24] Pacwa-Plociniczak, M., Plaza, G. A., Piotrowska-Seget, Z., and Cameotra, S. S. (2011) Environmental applications of biosurfactants: recent advances, *International journal of molecular sciences 12*, 633-654.

[25] Vijayaraghavan, K., and Yun, Y.-S. (2008) Bacterial biosorbents and biosorption, *Biotechnology Advances 26*, 266-291.

[26] Volesky, B. (2007) Biosorption and me, *Water research 41*, 4017-4029.

[27] Aksu, Z. (2005) Application of biosorption for the removal of organic pollutants: a review, *Process Biochemistry 40*, 997-1026.

[28] Vieira, R. H., and Volesky, B. (2000) Biosorption: a solution to pollution?, *International microbiology : the official journal of the Spanish Society for Microbiology 3*, 17-24.

[29] Flemming, H.-C., Wingender, J., Szewzyk, U., Steinberg, P., Rice, S. A., and Kjelleberg, S. (2016) Biofilms: an emergent form of bacterial life, *Nat Rev Micro 14*, 563-575.

[30] Little, B. J., and Lee, J. S. (2014) Microbiologically influenced corrosion: an update, *International Materials Reviews 59*, 384-393.

[31] Wingender, J., and Flemming, H.-C. (2011) Biofilms in drinking water and their role as reservoir for pathogens, *International Journal of Hygiene and Environmental Health 214*, 417-423.

[32] (2009) *The Role of Biofilms in Device-Related Infections*, Springer-Verlag Berlin Heidelberg.

[33] Halan, B., Buehler, K., and Schmid, A. (2012) Biofilms as living catalysts in continuous chemical syntheses, *Trends in biotechnology 30*, 453-465.

[34] Kaiser, P., Reich, S., Leykam, D., Willert-Porada, M., Greiner, A., and Freitag, R. (2017) Electrogenic Single-Species Biocomposites as Anodes for Microbial Fuel Cells, *Macromol. Biosci. 17*, 10.

[35] Vera, M., Schippers, A., and Sand, W. (2013) Progress in bioleaching: fundamentals and mechanisms of bacterial metal sulfide oxidation--part A, *Applied microbiology and biotechnology 97*, 7529-7541.

[36] Gupta, S., and Singh, D. (2017) Role of Genetically Modified Microorganisms in Heavy Metal Bioremediation, In *Advances in Environmental Biotechnology* (Kumar, R., Sharma, A. K., and Ahluwalia, S. S., Eds.), pp 197-214, Springer Singapore, Singapore.

[37] Perpetuo, E. A., Souza, C. B., and Nascimento, C. A. O. (2011) Engineering Bacteria for Bioremediation, Progress in Molecular and Environmental Bioengineering - From Analysis and Modeling to Technology Applications, (Carpi, P. A., Ed.), InTech.

[38] Flemming, H. C., and Wingender, J. (2010) The biofilm matrix, *Nature reviews. Microbiology 8*, 623-633.

[39] Chen, A. Y., Deng, Z., Billings, A. N., Seker, U. O. S., Lu, M. Y., Citorik, R. J., Zakeri, B., and Lu, T. K. (2014) Synthesis and patterning of tunable multiscale materials with engineered cells, *Nature materials 13*, 515-523.

[40] Nguyen, P. Q., Botyanszki, Z., Tay, P. K. R., and Joshi, N. S. (2014) Programmable biofilm-based materials from engineered curli nanofibres, *5*, 4945.

[41] Zhong, C., Gurry, T., Cheng, A. A., Downey, J., Deng, Z., Stultz, C. M., and Lu, T. K. (2014) Strong underwater adhesives made by self-assembling multi-protein nanofibres, *Nat Nano 9*, 858-866.

[42] Botyanszki, Z., Tay, P. K. R., Nguyen, P. Q., Nussbaumer, M. G., and Joshi, N. S. (2015) Engineered catalytic biofilms: Site-specific enzyme immobilization onto E. coli curli nanofibers, *Biotechnology and Bioengineering 112*, 2016-2024.

[43] Nussbaumer, M. G., Nguyen, P. Q., Tay, P. K. R., Naydich, A., Hysi, E., Botyanszki, Z., and Joshi, N. S. (2017) Bootstrapped biocatalysis: biofilm-derived materials as reversibly functionalizable multi-enzyme surfaces, *ChemCatChem*, n/a-n/a.

[44] Seker, U. O. S., Chen, A. Y., Citorik, R. J., and Lu, T. K. (2017) Synthetic Biogenesis of Bacterial Amyloid Nanomaterials with Tunable Inorganic–Organic Interfaces and Electrical Conductivity, *ACS Synthetic Biology 6*, 266-275.

[45] Van Gerven, N., Klein, R. D., Hultgren, S. J., and Remaut, H. (2015) Bacterial Amyloid Formation: Structural Insights into Curli Biogensis, *Trends in Microbiology 23*, 693-706.

[46] Van Gerven, N., Goyal, P., Vandenbussche, G., De Kerpel, M., Jonckheere, W., De Greve, H., and Remaut, H. (2014) Secretion and functional display of fusion proteins through the curli biogenesis pathway, *Molecular microbiology 91*, 1022-1035.

2

A synthetic gene circuit for mercury bioremediation using environmentally-triggered biofilm production

Parts of the work described in this chapter have been reproduced with permission from Tay *et al, ACS Synth Biol*, 2017, 6 (10), pp 1841–1850.

2.1 Abstract

Synthetic biology approaches to bioremediation are a key sustainable strategy to leverage the self-replicating and programmable aspects of biology for environmental stewardship. The increasing spread of anthropogenic mercury pollution into our habitats and food chains is a pressing concern. Here, we explore the use of programmed bacterial biofilms to aid in the sequestration of mercury. We demonstrate that by integrating a mercury-responsive promoter and an operon encoding a mercury-absorbing self-assembling extracellular protein nanofiber, we can engineer bacteria that can detect and sequester toxic mercury ions from the environment. This work paves the way for the development of on-demand biofilm living materials that can operate autonomously as heavy-metal absorbents.

2.2 Introduction

Industrial processes such as mining, materials processing and coal combustion result in the unnatural dissemination and accumulation of mercury compounds in land, freshwater, and marine habitats.[1] Mercury is a particularly insidious pollutant, as its accumulation in ecological niches

increases up through the food chain, a process known as biomagnification.[2] Humans are typically exposed to toxic mercury compounds through the ingestion of contaminated food sources such as fish or shellfish, leading to damage to tissues of the brain, kidney, and lung.[3] *In utero* exposure results in severe developmental abnormalities, resulting in EPA-FDA advisories against eating fish during pregnancy.[4] Recent studies have found that mercury contamination in the environment is much more prevalent than previously thought,[5] hence the need for innovative approaches to remediating contaminated sites. Of particular interest are scalable, low-cost, and sustainable biological approaches for the detection and sequestration of mercury ions (Hg^{2+}).

Bioengineered mercury sensor circuits employ naturally occurring mercury-responsive transcriptional regulators, such as the MerR regulator.[6] MerR regulates the expression of the *mer* operon—a widespread and ancient bacterial operon family found in plasmids and transposons—which encodes enzymes for mercury detoxification.[7] Upon binding to Hg^{2+}, the MerR repressor undergoes a conformational change resulting in de-repression of the *mer* operon. By replacing the *mer* operon genes with a reporter such as luciferase or GFP, [8, 9] mercury-inducible biosensors have been developed that allow for bacterial reporting of environmental mercury. Besides mercury reporters, a number of attempts have been made to use bacteria to bind and sequester mercury. For example, intracellular accumulation of mercury has been engineered into bacteria by the overexpression of heavy metal-binding metallothioneins, with the goal of remediating mercury-contaminated water.[10] However, it was found that the addition of a Hg^{2+} transport system, encoded by the *merT* and *merP* genes, were essential for mercury sequestration. An alternative strategy uses cell-surface displayed mercury-binding proteins, such as a metallothioneins,[11] phytochelatins,[12] or the MerR metal binding domain,[13] to create engineered cellular biosorbents. These examples of engineered bacterial circuits for sensing and mercury absorption demonstrate

the potential of green biological strategies for the remediation of mercury remediation. However, the sequestration strategies described above employed externally added chemical inducers (e.g., IPTG) rather than having the cell react dynamically to environmental mercury. Furthermore, these strategies used the cell biomass itself as the mercury sink, which required continuous energetic investment in biomass synthesis, and would end up poisoning the cell.

One promising alternative is to exploit the extracellular material (ECM) of bacterial biofilms to act as biosorbent. The high surface area of the ECM could potentially provide much larger adsorption capacities than cell surface-based strategies and prevent mercury-induced toxicity to the cell, allowing sustained production of the mercury-binding material. A number of studies have investigated naturally-occurring biofilms for heavy metal absorption,[14, 15] but to our knowledge, there has not been a rationally designed dynamic gene circuit for the production of a mercury-absorbing bacterial ECM. A robust and autonomously operating biofilm that is able to sequester mercury could act as a sink for *in situ* remediation of anthropogenic mercury at heavily contaminated sites.

Our strategy builds upon efforts by others that use renewable biomaterials, often purified and assembled into a filter matrix *in vitro*, as materials for heavy metal adsorption. These materials include animal and plant-derived biomaterials such as keratin or cellulose fibers as binding agents for the sequestration of various heavy metal contaminants.[16, 17] Of particular interest is the recent exploration of synthetic composites containing self-assembling amyloid fibers for the removal of heavy metal pollutants.[18] Amyloids have been known to interact specifically with heavy metals,[19-21] and these complexes can be redox active.[18, 22, 23] Such properties have led to a number of amyloid-based emerging technologies.[24-26] Although using purified amyloids to create purification membranes has the advantage of precise control over the final composition of the material, it still

requires purification and engineered assembly steps which may add to cost and complexity of the system. Here, we explore the potential of integrating amyloid materials with synthetic biological principles to create engineered living systems capable of functional sequestration *in situ* only when the pollutant is detected.[27, 28]

Escherichia coli and *Salmonella spp.* biofilms contain functional amyloids called curli, which are self-assembling extracellular protein nanofibers.[29] We and others have recently re-engineered curli fibers for the functional display of peptides and proteins to create dynamic engineered living materials.[30-33] Curli and similar functional amyloids have evolved as a key biofilm component enabling substrate adhesion,[34] structural reinforcement of the biofilm,[35] and host cell invasion.[36] A recent study by Hidalgo and colleagues suggested that curli might also serve a protective function, specifically by shielding bacteria in biofilms from extracellular mercury through adsorption of the heavy metal.[37]

Based on these findings, we designed and engineered a synthetic circuit that is able to detect mercury in the environment (via MerR) and direct the synthesis of curli nanofibers to sequester mercury ions in an extracellular matrix. The circuit utilizes the divergently regulated MerR promoter (P_{merR}) derived from a *Shigella flexneri* plasmid, engineered such that MerR is constitutively expressed and represses transcription of either a reporter (YFP) or the curli operon. When present, mercury ions bind to MerR to trigger an allosteric change and allow transcription and expression of the desired output (Figure 2.1).

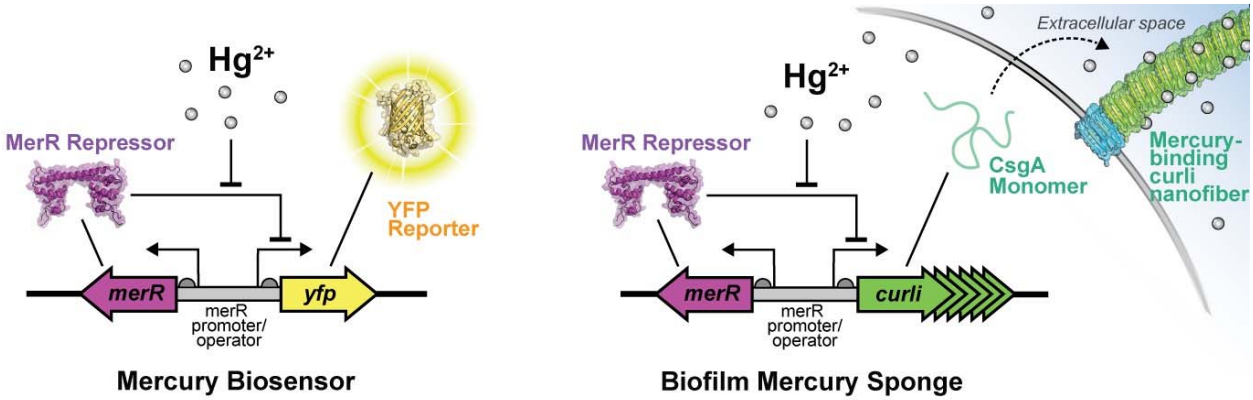

Figure 2.1. Schematic of the MerR-regulated Hg^{2+}-binding curli biofilm circuit. The reporter gene in the MerR-based mercury biosensing circuit was replaced with a curli operon encoding the synthesis and export of self-assembling functional amyloids that are able to bind mercury ions.

2.3 Materials and methods

Cloning

The P_{merR}:YFP mercury reporter plasmid was constructed by Gibson assembly of synthesized DNA fragments (Thermo Fisher Scientific). The *merR* gene and promoter region was taken from the *mer* operon of Shigella flexneri 2b plasmid R100. The *csgBAC* and *csgDEF* divergent curli operons derived from *E. coli* LSR10 were subcloned into a pET30a vector to obtain a single synthetic *csgBACEFG* operon as previously described.[38] To create the P_{merR}:curli operon, the *csgBACEFG* operon was subcloned in place of *yfp* gene. The negative control plasmid was obtained by completely excising the T7-LacO promoter region from pET30a using Gibson cloning. All plasmids were transformed into PQN4 cells, an engineered *E. coli* MC4100 strain in which the curli operon was removed by lambda Red recombineering and the T7 RNA polymerase gene integrated into the genome using a DE3 lysogenization kit (Merck Millipore). All cells were plated on LB agar or grown in bacterial medium supplemented with 50 μg/mL kanamycin.

Cell culture and metal exposure

Metals were diluted from 1000 ppm stocks in 2% HNO_3 (High Purity Standards) to the desired final concentrations. Overnight cultures were expanded to OD_{600} ~0.7 at 37°C in LB. All subsequent experiments involving mercury exposure were performed in supplemented minimal media (GCMM) comprising: 6.78 g/L Na_2HPO_4, 3 g/L KH_2PO_4, 0.5 g/L NaCl, 1 g/L NH_4Cl, 2 mM $MgSO_4$, 0.1 mM $CaCl_2$, 0.4% w/v glucose, and 1% (w/v) casamino acids. Congo Red plates were prepared with GCMM and agarose (Lonza) supplemented with 25 μg/mL Congo Red, 10 μg/mL Coomassie Brilliant Blue and the appropriate concentration of Hg^{2+}. Agarose was used to

reduce non-specific binding of mercury to normal bacteriological agar. For protein expression on plates, expanded cultures were pelleted and resuspended in GCMM, and 5 µl spotted on Congo Red plates, which were incubated at 30°C overnight. For protein expression in suspension, metal was added to GCMM-resuspended cultures to the appropriate final concentration and cultured for at least 18 hrs in 1 mL deep-well plates (30°C, 900 rpm). Three replicate cultures were used for each condition tested. Statistical analysis was performed using the Student's t-test with a 95% confidence interval. For experiments involving cycling of cells between different mercury concentrations, four single clonal colonies were expanded in LB to an OD_{600} ~0.7. The cultures were pelleted and resuspended in GCMM with or without 1 ppm Hg^{2+}, and allowed to grow for at least 18 hr. Samples were collected for TEM imaging, OD_{600} measurement and quantification of curli expression using the Congo Red assay as described below. The cultures were then normalized to OD_{600} =1, diluted 250x into fresh LB, and the cycling repeated four times.

Quantitation of protein expression

100 µL of metal-exposed cultures were passed through a 96-well filter plate (MultiScreen Isopore, Millipore). Wells were washed once with PBS and shaken with 100 µL of 15 µg/mL Congo Red solution for 5 min. The suspension was filtered and the absorbance at 490 nm of the unbound Congo Red in the filtrate was read on a BioTek H1 plate reader, and used to determine the amount of Congo Red bound to the cultures. Wells were subsequently shaken with 100 µL deionized water, and YFP fluorescence was determined on the plate reader (Ex: 485 nm / Em: 550 nm).

Transmission electron microscopy

Cell culture samples (5 μL) were applied to plasma-cleaned formvar/carbon film nickel TEM grids for 1 minute, then washed with 5 μL of ultrapure water for 1 minute, and subsequently negative-stained with fresh 2% uranyl formate for 15 seconds. The samples were allowed to dry for 10 minutes, and then imaged on a JEM-1400 Transmission Electron Microscope at 80 kV accelerating voltage.

Scanning electron microscopy

Nuclepore filter membrane discs containing immobilized metal-exposed cultures were fixed overnight in 2% glutaraldehyde / 2% *para*-formaldehyde at 4°C. The discs were immersed in a series of dehydrating ethanol solutions (25%, 50%, 75%, 100% v/v ethanol), then dried on a Tousimis Autosamdri-931 CO_2 critical point dryer. SEM images were obtained on a Zeiss Ultra Plus FE-SEM.

Quantitation of metal binding

350-450 μL of metal-exposed cultures were pelleted, frozen and lyophilized and the dry weights measured. Pellets were taken up in 250 μL concentrated HNO_3 (69% v/v, trace-metal grade, Fisher), then briefly heated to 95°C and sonicated for complete resuspension. The mixture was left to digest at 25°C for 1 hr with shaking. Acid-digested samples were diluted in 2% HNO_3 and their metal content analyzed on an Agilent 7700x ICP-MS. Bismuth was used as an internal standard. Statistical analysis was performed using the Student's t-test with a 95% confidence interval.

Cell flocculation studies

Liquid cultures of PQN4 transformants with the negative control plasmid, P_{merR}-YFP, or P_{merR}-curli were grown for 24 hours in LB with and without 800 ppb Hg^{2+}. The resulting cultures, after thorough resuspension, were allowed to settle at ambient conditions and were photographed every 2 hours. The flocculation was also quantitatively measured in triplicate by monitoring the absorbance at 600 nm of 1 ml cultures in cuvettes in an Agilent Cary 300 UV-Vis spectrophotometer over the course of 720 minutes. Representative microscopy images of the cultures showing cell suspensions or flocs were imaged on an EVOS FL Cell Imaging System.

2.4 Results

To demonstrate that our circuit responds to mercury, the pET30a-P_{merR}-curli plasmid was transformed into a previously engineered *E. coli* strain, PQN4, in which the entire curli operon has been deleted.[38] The parental *E. coli* strain is the MC4100 strain, which does not produce any other extracellular materials (e.g. polysaccharides, fimbrae, flagella) that may complicate analysis. The MC4100 strain has been used extensively in mechanistic and genetic studies of the curli operon.[39-41] In the wild-type MC4100 background, as in most other wild *E. coli* strains, induction of the genomically-encoded curli operon occurs only under conditions of low osmolarity and/or starvation.[42, 43] By placing this operon instead under the control of a mercury-inducible promoter, we have decoupled curli production from these narrow conditions and have now coupled them instead to the presence of environmental mercury, creating an engineered living material that fabricates a heavy-metal sequestering nanomaterial in response to the detection of that specific pollutant.

The pET30a-P_{merR}-YFP and a pET30a control vector were used as controls. Colonies of overnight cultures were spotted onto minimal media agar containing the amyloid-specific dye Congo Red, with or without ionic mercury (Hg^{2+}), and left to grow at 30°C overnight. Minimal media was chosen to reduce the effect of media components on metal binding. As shown in Fig. 2.2, curli production was tightly regulated by P_{merR} and high expression required the presence of Hg^{2+}. The P_{merR}-YFP biosensor transformants exhibited mercury-induced fluorescence, indicating proper functioning of the MerR-regulated promoter (Fig. 2.3). There was a graded response, with more curli produced at higher Hg^{2+} concentrations.

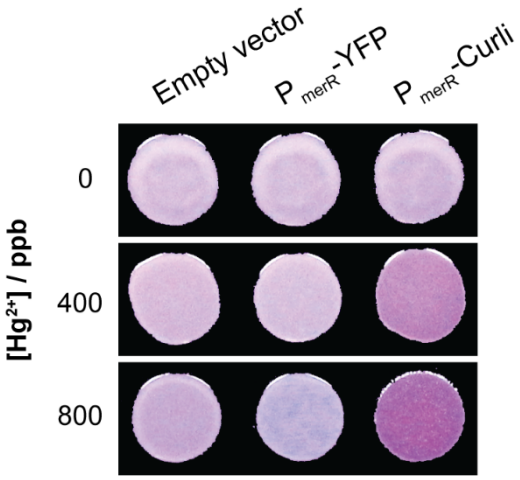

Figure 2.2. Curli nanofiber production is regulated by environmental mercury (Hg^{2+}) concentration. The MerR circuit activates the output genes in the presence of Hg^{2+}, as seen with P_{merR}-curli cells spotted on plates containing the amyloid-specific dye Congo Red.

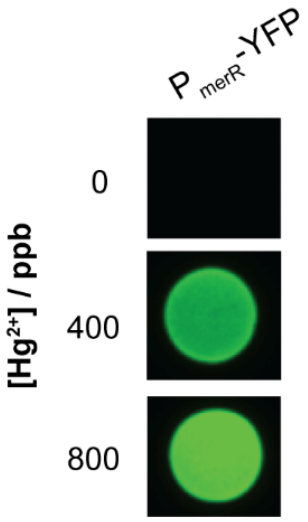

Figure 2.3. YFP expression from the P_{merR} promoter is regulated by environmental mercury concentration. Fluorescent images of plates were taken on a ProteinSimple FluorChem M imager.

This concentration-dependent expression was further demonstrated by culturing cells in suspension overnight with exposure to a range of Hg^{2+} concentrations. The curli content of the cultures was measured using a Congo Red quantification assay and normalized to the OD_{600} of the cultures. We confirmed that the presence of mercury did not affect Congo Red binding to curli (Fig. 2.4). In our MerR-regulated curli circuit, induction in liquid media occurred at 600 ppb and above. Induction of curli plateaued at 1000 ppb and was sustained at the maximum concentration tested, 1400 ppb (Fig. 2.5), but significant amounts beyond background was not detected in the absence of Hg^{2+} as measured by our CR-binding assay. To examine potential toxic effects of high mercury concentrations on the viability of the cell, we measured the density of the cultures after 24 hours growth for each of the concentrations. At mercury concentrations above 1000 ppb, cell densities only decreased for the P_{merR}-curli expressing cells. In contrast, transformants harboring the P_{merR}-YFP or negative control plasmid showed no reduced cell density up to 1400 ppb (Fig. 2.6a). Previous reports have established a Hg^{2+} MIC of 2 ppm for *E. coli*.[44] The results demonstrate that at these higher mercury concentrations, any negative impact on growth for the P_{merR}-curli cells was likely due to the metabolic burden of induced protein overproduction rather than mercury toxicity effects on the cell. We also observed similar negative impacts on cell health when the curli operon under control of the strong $P_{T7/lacO}$ promoter was overexpressed upon IPTG induction (Fig. 2.6b). These findings lend support to the utility of our sensing feedback-regulated circuit, in which a metabolically costly nanofiber matrix is fabricated by the cell for sequestering mercury only when mercury is detected in the environment.

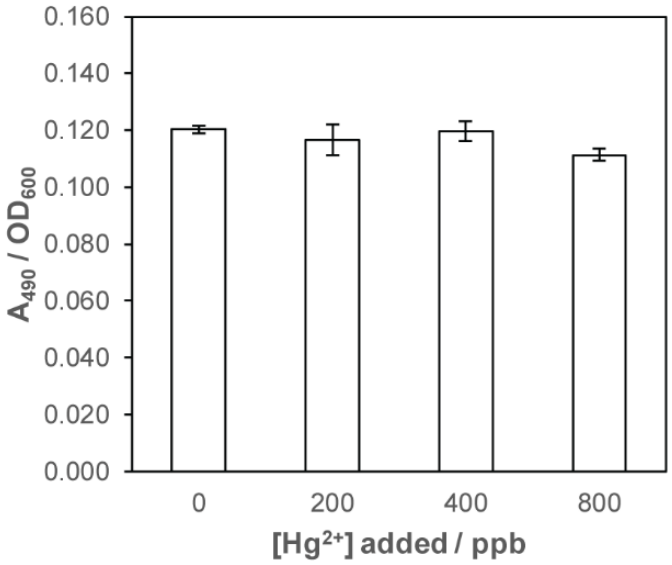

Figure 2.4. Congo red assay on IPTG-induced curli shows no effect of mercury on CR binding. PQN4 cells were transformed with a pET30a-$P_{T7/lacO}$-curli plasmid with the *csgBACEFG* operon under the control of a T7/lacO promoter. Overnight cultures were expanded in GCMM (with glucose replaced by an equivalent concentration of glycerol) to an OD_{600} of ~0.8, and curli expression was induced with 0.3 mM IPTG overnight at 30°C. Hg^{2+} of different concentrations were subsequently added to the cultures and incubated at 30°C for 1 hr. Three replicates were used for each concentration tested. Curli content was quantified using Congo Red as described in Methods section.

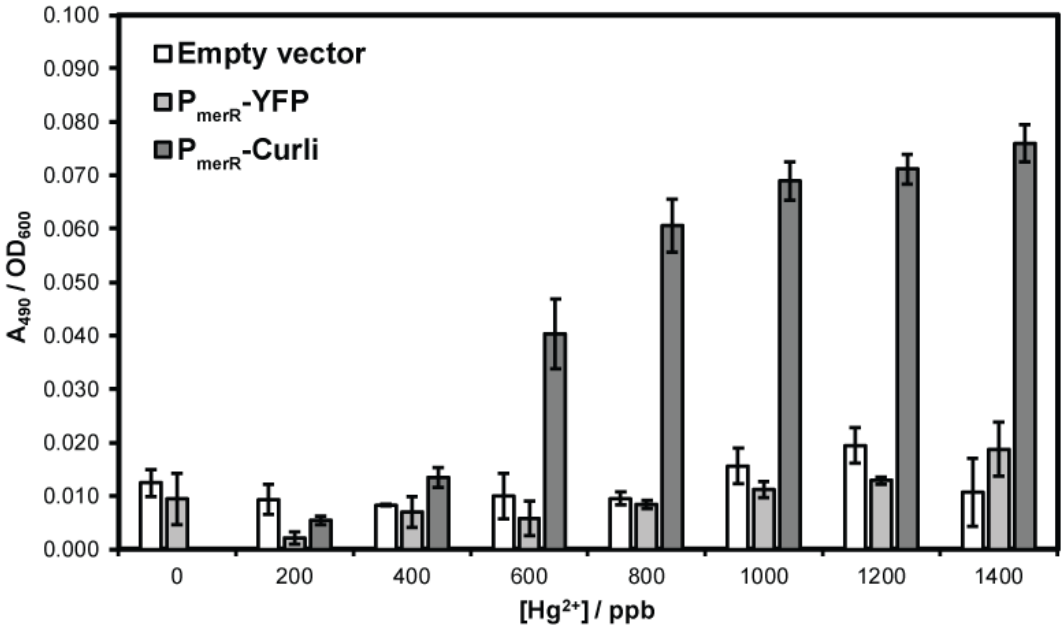

Figure 2.5. Cells grown in suspension were exposed to a range of Hg^{2+} concentrations overnight. Quantitation of curli production showed concentration-dependent expression.

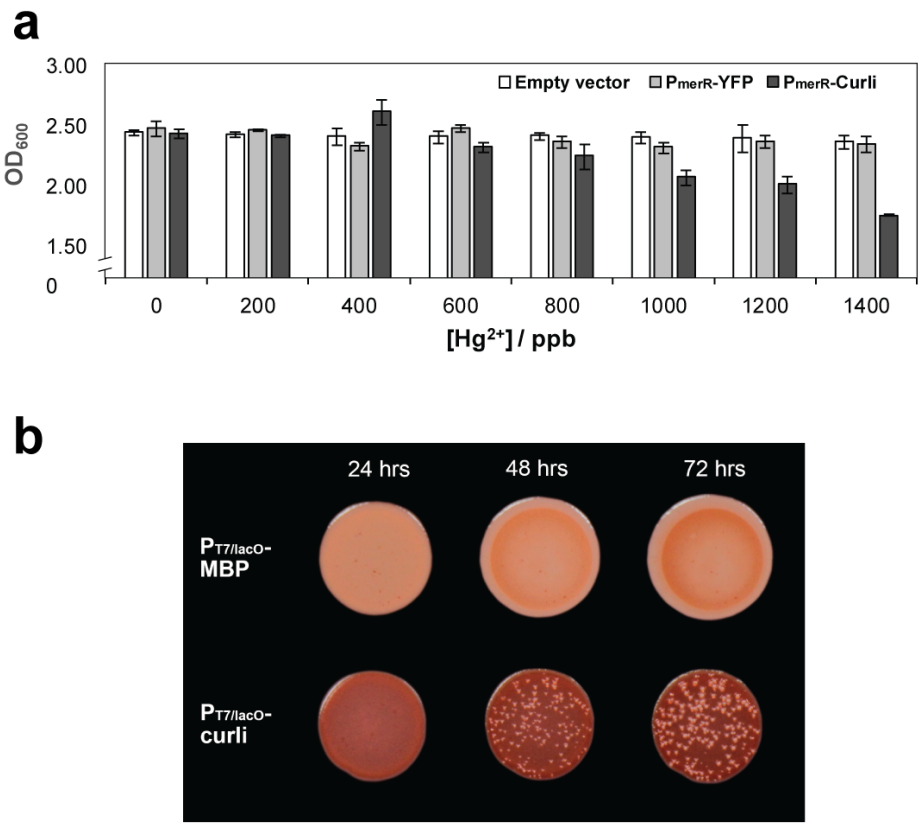

Figure 2.6. Curli operon induction using the P_{merR} promoter results in impaired cellular growth at higher mercury concentrations (a). PQN4 cells were transformed with pET30a-$P_{T7/lacO}$-regulated plasmids expressing either maltose-binding protein or the curli operon. Cultures were normalized to OD_{600} = 0.5 and spotted onto LB-congo red induction plates supplemented with 50 μg/mL kanamycin and 0.150 mM IPTG. The punctate spots which emerged for the $P_{T7/lacO}$-curli macrocolonies at 48 hours do not stain with Congo Red, and are thought to be escape colonies (b).

As a proxy for solid media such as contaminated soil, mercury-laden agar was used to perform induction experiments on macrocolonies (Fig. 2.7). On solid media, the curli induction response as detected by a quantitative congo red assay appears to be more sensitive to mercury concentrations, occurring at 200 pbb and above. This lower induction threshold in comparison to

liquid media is likely due to altered gene expression between the different modes of growth that may influence P_{mer} mercury induction and/or the increased likelihood for curli polymerization on solid media due to retarded diffusion. These results demonstrate that such a circuit for generating a mercury-absorbing extracellular matrix can be applied to different forms of contaminated media. We visually confirmed the presence of dense nanofibers by scanning electron microscopy (Fig. 2.8). Our circuit was active at mercury concentrations defined for mercury-contaminated sites,[45] thus making it potentially useful for environmental Hg^{2+} remediation. Further, the dynamic response of the circuit, as shown for single clonal populations propagated through multiple generations, persisted through repeated changes in environmental mercury concentration (Fig. 2.9).

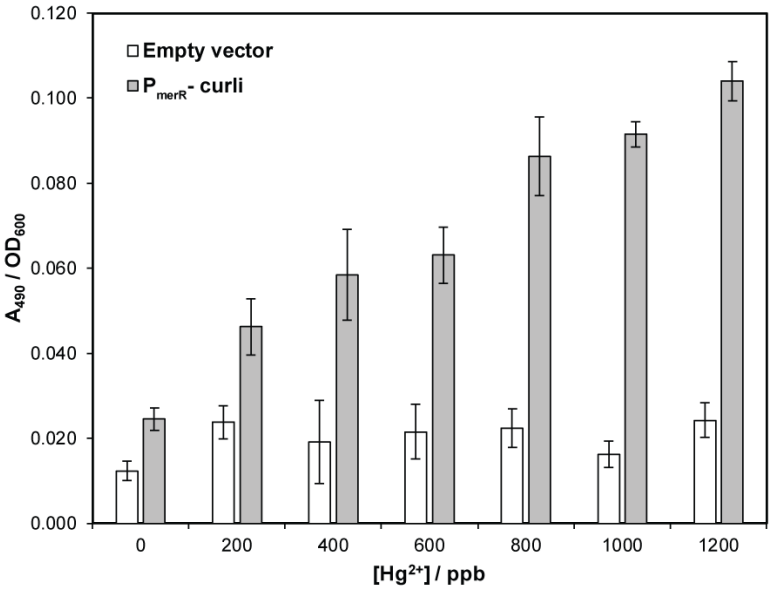

Figure 2.7. MerR-regulated curli operon performance on solid agar media. Macrocolonies spotted onto GCMM-agar plates supplemented with the indicated concentrations of mercury were grown on the agar for 48 hours, carefully scraped from the agar and resuspended into the same volume. Data shown is Congo Red absorbed normalized for cell density in the resuspension (n = 3).

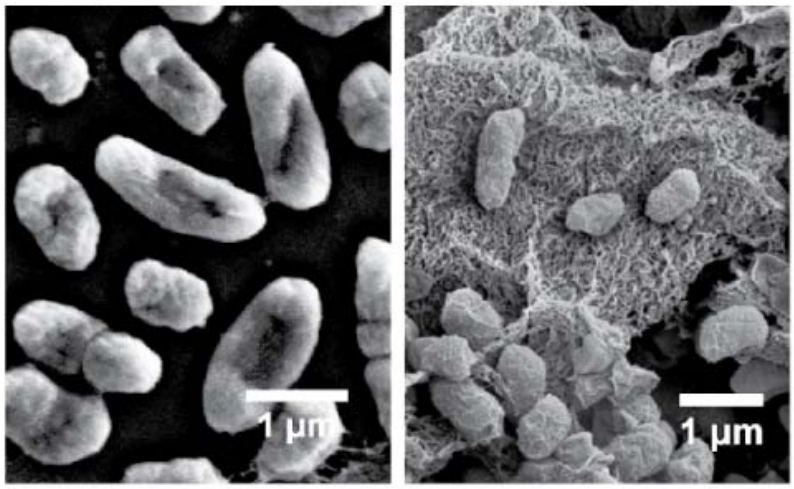

Figure 2.8. Scanning electron micrographs of cells containing empty plasmid (left) and P_{merR}-curli plasmid (right), exposed to Hg^{2+}. Only the latter showed abundant production of extracellular curli nanofibers.

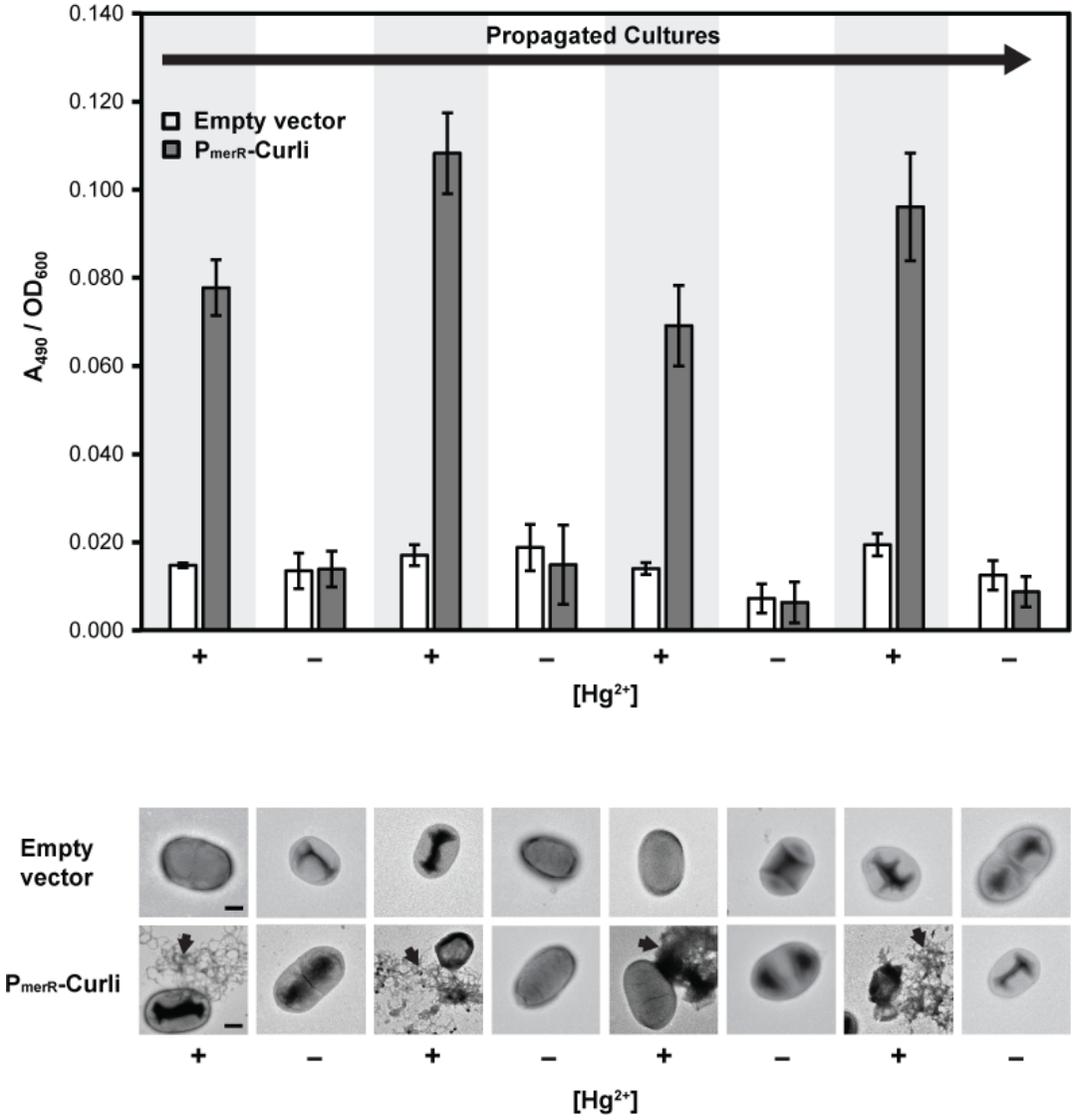

Figure 2.9. (Top) Curli production in individually propagated cultures exposed to alternating conditions of 1000 ppb of mercury and no mercury, demonstrating dynamic control of nanofiber production only in the presence of environmental mercury. For each transformation type, individual clones were propagated in quadruplicate. (Bottom) Representative transmission electron micrographs of cells from the top panel, showing the presence of curli (arrows) only for the P_{merR}-curli cells exposed to mercury. Scale bars: 500 nm.

We next investigated the extent of mercury sequestration by curli-producing cultures. Cultures exposed overnight to Hg^{2+} were pelleted, dried and analyzed for their mercury content by inductively coupled plasma mass spectrometry (ICP-MS). Curli-expressing bacteria bound 4.5x more mercury on a dry weight basis than cells containing the empty vector when exposed to 1200 ppb Hg^{2+} (Fig. 2.10). Cells expressing the P_{merR}-YFP circuit showed the same low level of mercury binding as cells with the empty vector (Fig. 2.10), demonstrating that activation of the circuit alone was not responsible for enhanced mercury sequestration, and the latter was a consequence of curli production. Furthermore, IPTG-induced curli fibers generated by a $P_{T7/lacO}$ promoter instead of P_{merR} also bound to mercury at equivalent levels (Fig. 2.11a, b), indicating that mercury adsorption is due only to the curli fibers and that these nanofibers are functionally identical regardless of the promoter system. TEM analysis also indicates the same ultrastructure for curli fibers produced regardless of the regulating promoter (Fig. 2.11c).

The dependence of mercury binding on curli synthesis was more apparent when we looked at P_{merR}-curli cells exposed to different concentrations of mercury. The quantity of mercury bound in the biomass correlated significantly to the curli content of the cultures (Fig. 2.10 inset), thus bacteria exposed to higher levels of mercury also sequestered more mercury via the production of more extracellular curli fibers, creating a self-governing mercury-binding system. Curliated cultures were able to retain mercury for over ten days, even after several washes (Fig. 2.12). The mechanism of mercury binding to curli is unclear; there are no cysteine residues in CsgA, though the presence of multiple glutamic and aspartic acid residues along the backbone of assembled fibers suggests an electrostatic interaction. CsgA could also have an inherent ability to reduce Hg^{2+}, as has been demonstrated for the amyloidogenic Aβ peptide and its reduction of Cu^{2+}.[46]

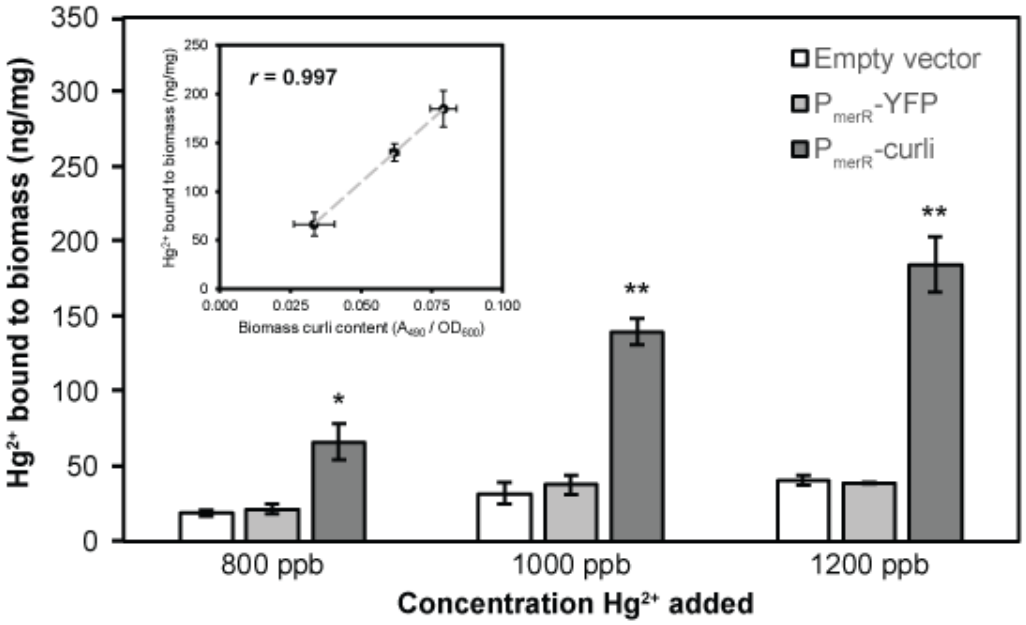

Figure 2.10. Cultures expressing curli showed higher Hg^{2+} sequestration after overnight exposure compared to non-curliated cultures, as measured by ICP-MS quantitation of bound mercury. The amount of Hg^{2+} bound correlated positively with the curli content of the culture (inset, r = calculated Pearson correlation coefficient). * represents $p < 0.05$; ** represents $p < 0.01$.

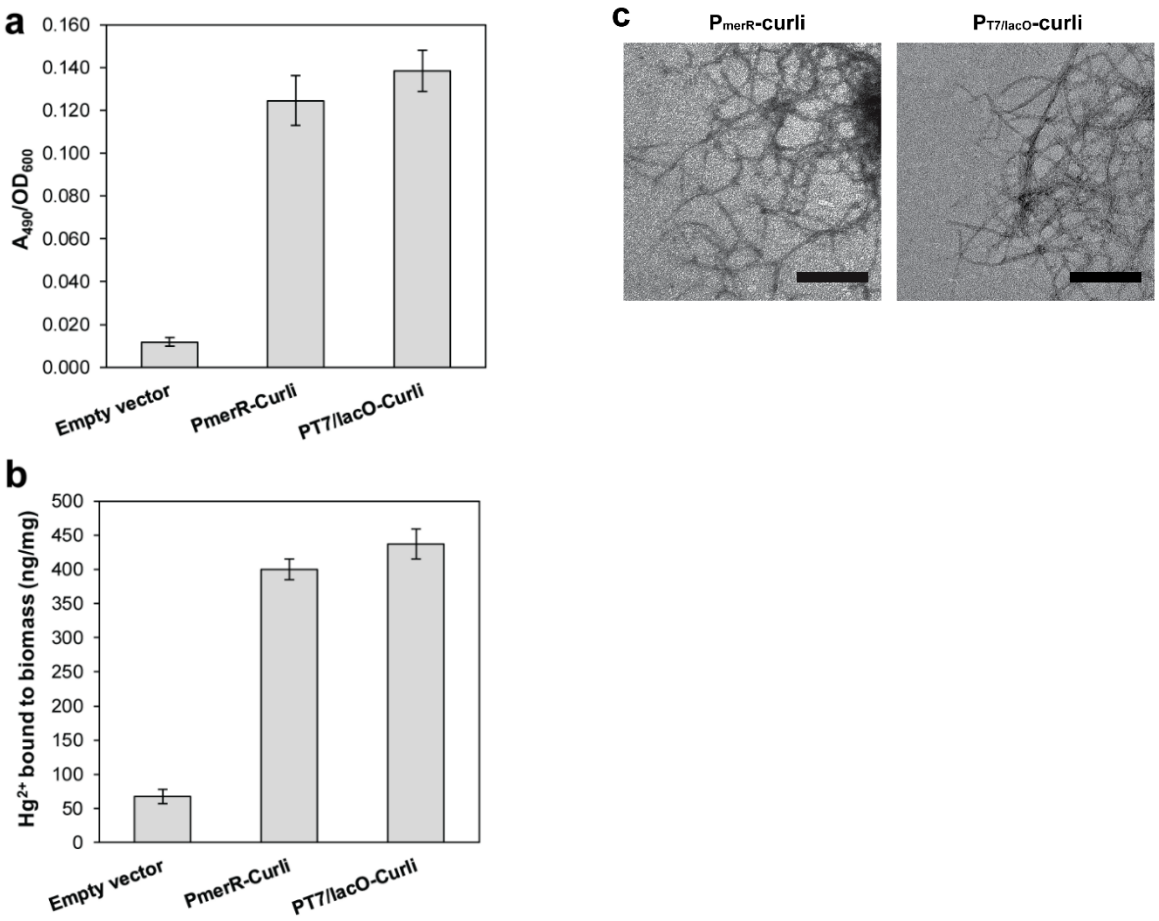

Figure 2.11. Nanofibers generated from the curli operon produced by different promoters are functionally and structurally similar. Cells containing empty vector, P_{merR}-Curli or $P_{T7/lacO}$-Curli were expanded in LB to $OD_{600} = 0.7$, pelleted and resuspended in GCMM containing 1 ppm Hg^{2+} (with glucose replaced by an equivalent concentration of glycerol), and allowed to express overnight. Determination of OD_{600}, curli production and mercury content of cell pellets were performed as described in the Methods section. Regardless of the regulating operon, normalized amounts of curli (a) bound to similar levels of mercury (b). TEM analysis also indicated similar nanofiber ultrastructure (c); scale bars: 250 nm.

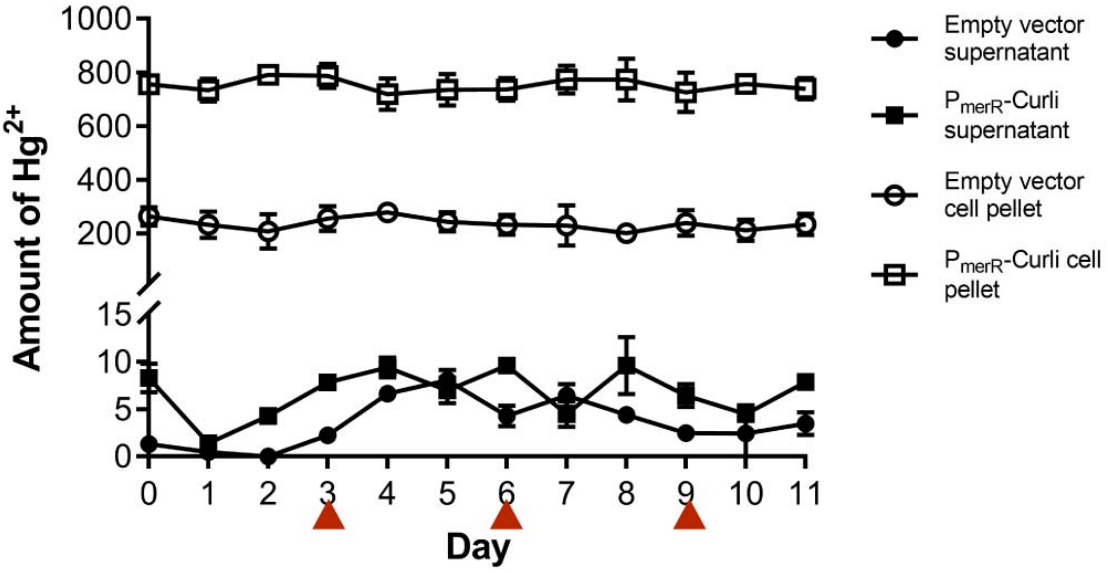

Figure 2.12. Curliated cultures retained bound mercury over multiple washes. Cells containing the empty vector and P_{MerR}-Curli were cultured overnight in GCMM containing 1 ppm Hg^{2+}. The cultures were pelleted & resuspended in MOPS buffer (20 mM MOPS, 100 mM NaCl, 0.05% NaN_3, pH 7) and allowed to settle at room temperature. 500 µl samples from these cultures were taken and pelleted daily, and the mercury content of the supernatant and dried cell pellets were determined using ICP-MS as described previously. On specified days (red arrow), the entire culture was pelleted and resuspended in fresh MOPS buffer and allowed to settle again. The amount of mercury is reported in ng for the supernatant and ng Hg^{2+}/mg biomass for cell pellets.

Because mercury-contaminated sites could also contain other metal pollutants,[47] we exposed P_{merR}-curli cells to different metal cocktails to determine their impact on circuit activation and mercury binding to curli. MerR is known to be cross-selective for several other metals (Au^{3+}, Zn^{2+}, Ag^{+}, Cd^{2+}), though higher concentrations of those metals (2-3 orders of magnitude relative to mercury) are required for transcriptional activation.[48] We tested four divalent metals (Cd^{2+}, Pb^{2+}, Cu^{2+}, Zn^{2+}), none of which induced curli production when used individually or as a mixture at concentrations equivalent to 1000 ppb Hg^{2+} (Fig. 2.13). Interestingly however, Cd^{2+} and Cu^{2+} gave a further increase in curli production when used in equimolar combination with Hg^{2+}, even though Cu^{2+} is not known to interact with MerR.[48, 49] This hitherto undescribed hetero-bimetallic activation of MerR expands the range of environments in which our circuit could be useful (for instance, in mercury-contaminated sites near copper mines) and its mechanism warrants further investigation. Importantly, the amount of mercury bound by curli-expressing cultures as measured by ICP-MS was not compromised in mixed-metal environments and was actually substantially higher in all cases, although it no longer scaled with curli content, possibly due to interference from the other metals (Fig. 2.14). One possibility is that the metals could be forming multi-metallic complexes on the curli fibers, which would facilitate Hg^{2+} deposition and explain improved mercury binding from metal cocktails.

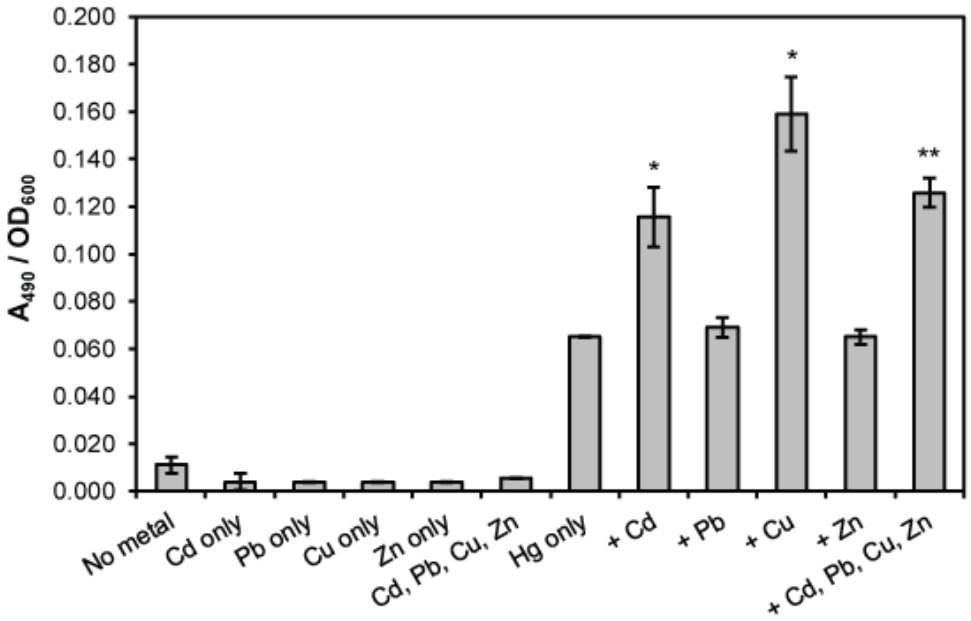

Figure 2.13. The MerR circuit is selective for Hg^{2+}, although some divalent metals (Cd^{2+}, Cu^{2+}) could act synergistically with Hg^{2+} to further enhance curli production. All metals were added at 5 μM. * represents $p < 0.05$; ** represents $p < 0.01$.

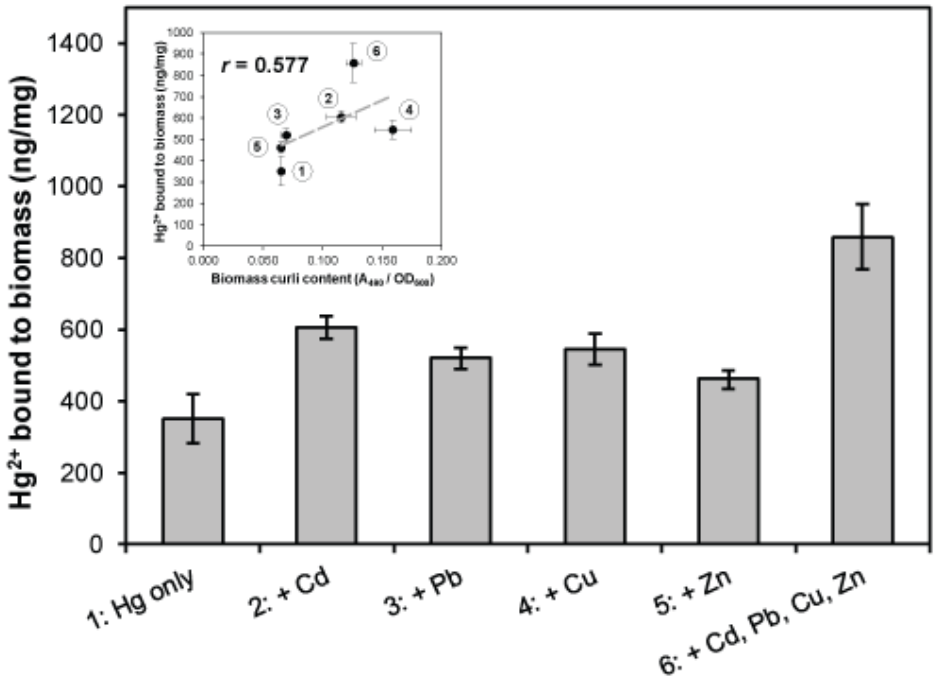

Figure 2.14. Hg^{2+} sequestration by curli fibers was not compromised in the presence of a metal mixture as determined by ICP-MS. Inset shows the Pearson coefficient between the amount of Hg^{2+} bound and the curli content.

Flocculation of cellular biomass driven by mercury-induced biofilms would particularly aid in the sequestration of mercury by generating a precipitated mass that would consolidate and extract the heavy metal when the contaminant media is liquid, such as leachate or mine tailings. Rapid flocculation was observed for P_{merR}-curli transformants cultured in the presence of Hg^{2+}, whereas this was not observed for P_{merR}-YFP or empty vector transformants (Fig. 2.15a, b). Microscopy examination of the cultures showed the presence of large cellular aggregates only when cells containing the P_{merR}-curli circuit were exposed to Hg^{2+} (Fig. 2.15c). Further studies are warranted to establish any potential influence of mercury cations on curli aggregation, as heavy metals have been found to participate in the aggregation of other amyloids.[50]

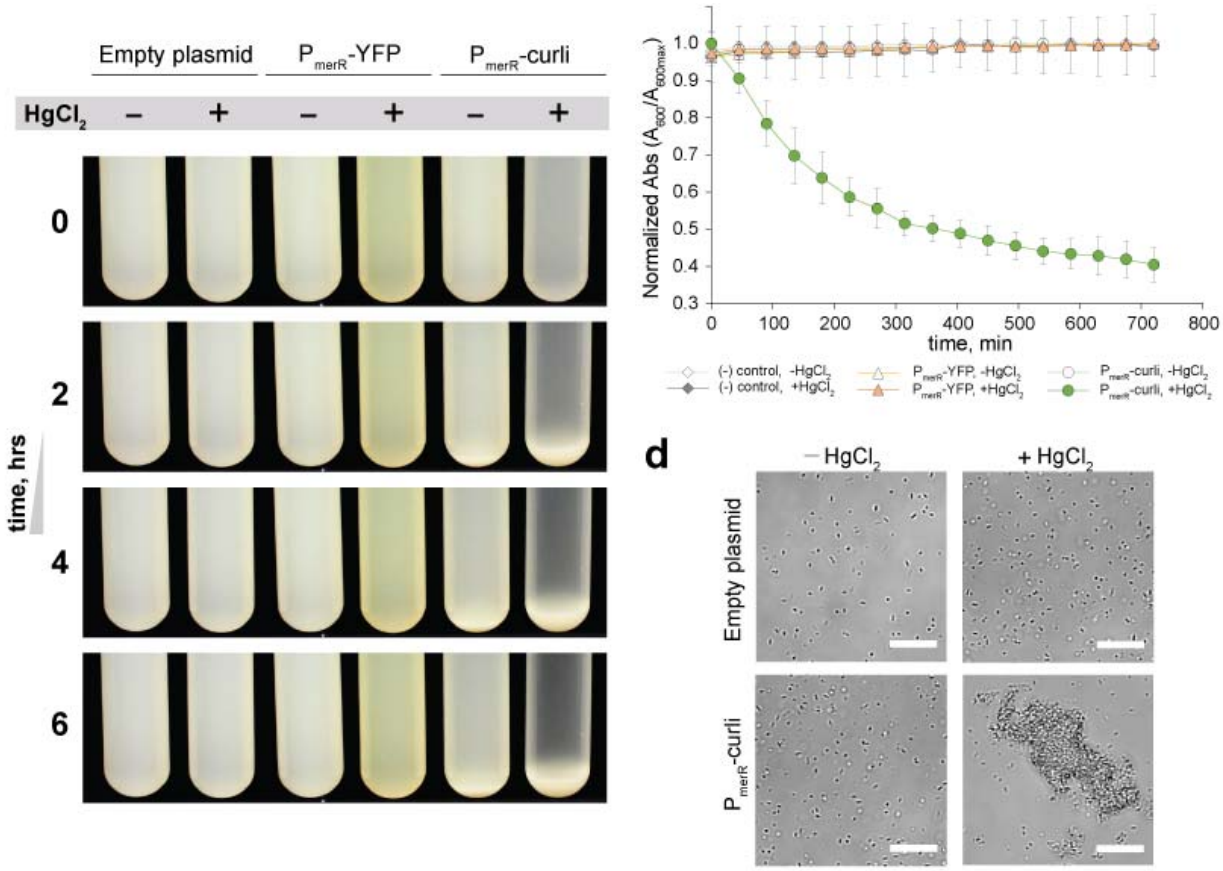

Figure 2.15. Mercury-induced biofilm flocculation removes mercury-bound biomass from suspension. (a) Images of transformants with no mercury or exposed to 800 ppb of mercury that have been allowed to flocculate and settle over 6 hours. (b) Quantitative sedimentation of the cultures by absorbance measurements. Shown as $n = 3$, S.D. (c) Representative microscopy images of cell cultures showing floc formation for P_{merR}-curli transformants either exposed to no mercury or 800 ppb of mercury. Scale bars: 15 μm.

2.5 Discussion

Current heavy metal bioremediation strategies face several limitations: where natural biofilms are used, large quantities of biomass are often necessary to compensate for unpredictable and non-specific metal sorption, and even with bacteria genetically engineered to improve their metal binding capacity, the need for costly chemical inducers to sustain the expression of metal binding groups has limited large-scale deployment of these organisms. These engineered systems could theoretically be designed for constitutive or bistable (toggle) expression, but this would result in metabolically wasteful protein production when no heavy metal is present, and compromise the viability of the bacteria in field applications. Such metabolic burden manifests as impaired cellular growth which we observe when the curli operon is overexpressed. These barriers to scalability and robustness have led to synthetic biology efforts to engineer self-regulating dynamic circuits capable of efficient feed-back controlled gene expression.[51-53] For metabolically costly products such as a large-scale extracellular protein matrix, one of the most efficient regulatory strategies is a feedback-controlled graded response. A number of studies have shown that implementation of in-cell dynamic feedback systems increases the robustness and predictability of engineered synthetic biology circuits and leads to productivity increases.[54, 55]

By combining a metal sensing promoter and a metal binding effector protein nanofiber in a single genetic circuit, we have created bacteria that dynamically generate mercury-binding curli amyloid fibers in the presence of environmental mercury. The circuit described herein is responsive to mercury in a sensitive range (above 400 ppb) that is below that of the trigger threshold for contaminated sites (which ranges from 1–10 ppm mercury, depending on country) and the mercury MIC (2 ppm) of *E. coli*,[44] yet above the experimentally established tolerable limit (0.13 ppm) for soil health in terms of plants and micro-organisms.[56] This adds a level of precise

autonomous selectivity to bioremediation efforts, where metal removal efficiently occurs *in situ* only in response to a detected contaminant. Our circuit was also selective for mercury even in mixed metal environments which commonly occurs for contaminated sites of previous mining or metal processing facilities,[57, 58] and the curli fibers produced induced flocculation of the cells, further facilitating mercury sequestration and biomass retrieval. The bound mercury was not easily washed off the biomass. Curli nanofibers are highly stable, being resistant to proteases,[59] harsh chemicals,[30] and detergents and high temperatures.[60] This makes them ideal for sequestering mercury in a matrix that will not easily break down. Furthermore, the curli fibers formed dense nanofibrous networks with an extremely high surface area that would be ideal as an engineered sponge for adsorbing mercury. Additional engineering of the CsgA protein to incorporate metal binding groups could further improve the efficiency of metal removal, although attempts to engineer a small set of mercury-binding motifs into our BIND curli display system resulted in poor secretion and mercury binding inferior to wild-type curli.

Here we have presented a synthetic biology circuit in which a mercury-absorbing extracellular self-assembling nanomaterial is fabricated under the control of a mercury-sensing regulatory system. Our initial characterization of this circuit was performed in *E. coli*, as the genetics[61] and biophysics[62] of the curli functional amyloid system in *E. coli* is the most well characterized to date. However, one potential drawback is the relatively low mercury toxicity threshold of *E. coli*, at 2 ppm. Given that the curli functional amyloid is phylogenetically widespread,[63] exploration of other bacterial chassis that may confer specific phenotypic advantages could greatly expand the operational range, induction sensitivity, and robustness of this circuit for practical deployment. In particular, the circuit could potentially be introduced into a microbe that is uniquely adapted for widespread colonization of the target environment, for

instance, the soil bacteria *Bacillus* spp. or *Shewanella* spp., or one that is highly tolerant to mercury[14], allowing for improved organismal fitness in contaminated environments. One key area for future optimization of our circuit would be improving the induction response of the merR promoter to further increase the sensitivity or alter the response dynamics of induction. This could be undertaken by introducing a transporter for mercuric ions to increase the intracellular mercury levels[10] or engineering of the MerR regulatory protein.[64, 65] Further engineering to induce toxin precipitation or mineralization within the biofilm[66, 67] would facilitate toxin removal upon disposal of the biofilm or sequester the mercury to prevent it from mobilizing through the biosphere. Given further engineering efforts such as that described above, a mercury-sensing and absorbing engineered living material could be practically implemented in a variety of ways.

One implementation is known as ex situ bioremediation (ESB), which employs fixed- or moving-bed bioreactors and have been implemented in the field for heavy metal decontamination of various media.[68, 69] However, ESB requires excavation of the contaminated media for feedstock as well as downstream separation of the contaminants from the soil or water, which often increases costs. In contrast, in situ bioremediation (ISB) efforts have been investigated as cost-effective green solutions for environmental remediation, and numerous pilot studies have been performed in which bacteria have been injected (in a process known as 'bioaugmentation') into contaminated soil[70-72] or even deep into the bedrock.[73, 74] While most ISB efforts attempt to utilize wild bacterial isolates that can be surprisingly competitive with the indigenous microbial population[75], there is immense potential for the development of remediation-focused synthetic organisms that can be readily programmable for specific growth conditions or contaminants.[76] Such genetically-modified bacteria specifically engineered for enhanced bioremediation have already undergone field testing at contaminated sites.[77, 78]

We can envision sentinel bacteria populations capable of responding to a variety of environmental toxins by the *in situ* production of biofilm sponges to sequester toxins at their source, thus preventing significant leaching into surrounding soil or water bodies. Such solidification/stabilization (S/S) strategies focus on binding or sequestering the toxins at their source in a stabilized mass, trapping the toxins in an insoluble format and reducing mobilization throughout the ecosphere, preventing leaching into highly mobile media (e.g., groundwater) that would facilitate poisoning of food chains. S/S approaches are the most frequently used strategy to treat soil, sludge, and liquid that is contaminated with mercury.[69] A synthetic biology approach for the implementation of a genetically engineered living material for bioremediation that is able to sequester mercury in a highly stable amyloid matrix at contaminated sites for different forms of media could be considered to be a hybrid approach of ISB and S/S strategies. As contaminated sites are often highly heterogeneous with spatially localized hot spots, the engineered biofilms would selectively populate the regions around the hot spots that are below their toxicity threshold, biosynthesizing mercury-adsorbing curli nanofibers *in situ*. Local sequestration of mercury would allow the cells to expand their zone of colonization, producing more curli and binding more mercury in the process. Given the diversity of metal-responsive promoters,[79] the range of biofilm-specific functional amyloid proteins available for genetic manipulation,[80] and recent advances towards displaying functional heterologous peptide and proteins domains on these amyloid scaffolds,[28] this strategy of environmentally-triggered production of engineered biosorptive extracellular matrices could potentially be adapted for the remediation of various toxic metals and environmental pollutants.

2.6 References

[1] Driscoll, C. T., Mason, R. P., Chan, H. M., Jacob, D. J., and Pirrone, N. (2013) Mercury as a Global Pollutant: Sources, Pathways, and Effects, *Environmental Science & Technology 47*, 4967-4983.

[2] Suedel, B. C., Boraczek, J. A., Peddicord, R. K., Clifford, P. A., and Dillon, T. M. (1994) Trophic Transfer and Biomagnification Potential of Contaminants in Aquatic Ecosystems, In *Reviews of Environmental Contamination and Toxicology* (Ware, G. W., Ed.), pp 21-89, Springer New York, New York, NY.

[3] Guzzi, G., and La Porta, C. A. (2008) Molecular mechanisms triggered by mercury, *Toxicology 244*, 1-12.

[4] Florek, J., Giret, S., Juere, E., Lariviere, D., and Kleitz, F. (2016) Functionalization of mesoporous materials for lanthanide and actinide extraction, *Dalton Transactions 45*, 14832-14854.

[5] Eagles-Smith, C. A., Wiener, J. G., Eckley, C. S., Willacker, J. J., Evers, D. C., Marvin-DiPasquale, M. C., Obrist, D., Fleck, J., Aiken, G. R., Lepak, J. M., Jackson, A. K., Webster, J., Stewart, R., Davis, J., Alpers, C. N., and Ackerman, J. (2016) Mercury in western North America: A synthesis of environmental contamination, fluxes, bioaccumulation, and risk to fish and wildlife, *Science of the Total Environment 568*, 1213-1226.

[6] O'Halloran, T., and Walsh, C. (1987) Metalloregulatory DNA-binding protein encoded by the merR gene: isolation and characterization, *Science (New York, N.Y.) 235*, 211-214.

[7] Summers, A. O. (1992) Untwist and shout: a heavy metal-responsive transcriptional regulator, *Journal of Bacteriology 174*, 3097-3101.

[8] Virta, M., Lampinen, J., and Karp, M. (1995) A Luminescence-Based Mercury Biosensor, *Analytical Chemistry 67*, 667-669.

[9] Hakkila, K., Maksimow, M., Karp, M., and Virta, M. (2002) Reporter genes lucFF, luxCDABE, gfp, and dsred have different characteristics in whole-cell bacterial sensors, *Analytical biochemistry 301*, 235-242.

[10] Chen, S., and Wilson, D. B. (1997) Construction and characterization of Escherichia coli genetically engineered for bioremediation of Hg(2+)-contaminated environments, *Appl Environ Microbiol 63*, 2442-2445.

[11] Lin, K. H., Chien, M. F., Hsieh, J. L., and Huang, C. C. (2010) Mercury resistance and accumulation in Escherichia coli with cell surface expression of fish metallothionein, *Appl Microbiol Biotechnol 87*, 561-569.

[12] Bae, W., Wu, C. H., Kostal, J., Mulchandani, A., and Chen, W. (2003) Enhanced Mercury Biosorption by Bacterial Cells with Surface-Displayed MerR, *Applied and Environmental Microbiology 69*, 3176-3180.

[13] Qin, J., Song, L., Brim, H., Daly, M. J., and Summers, A. O. (2006) Hg(II) sequestration and protection by the MerR metal-binding domain (MBD), *Microbiol 152*, 709-719.

[14] Francois, F., Lombard, C., Guigner, J. M., Soreau, P., Brian-Jaisson, F., Martino, G., Vandervennet, M., Garcia, D., Molinier, A. L., Pignol, D., Peduzzi, J., Zirah, S., and Rebuffat, S. (2012) Isolation and characterization of environmental bacteria capable of extracellular biosorption of mercury, *Appl Environ Microbiol 78*, 1097-1106.

[15] Meliani, A., Bensoltane, A. (2016) Biofilm-Mediated Heavy Metals Bioremediation in PGPR Pseudomonas, *J. Bioremediation Biodegrad. 7*.

[16] Malik, D. S., Jain, C. K., and Yadav, A. K. (2016) Removal of heavy metals from emerging cellulosic low-cost adsorbents: a review, *Appl Water Sci*.

[17] Ishikawa, S., and Suyama, K. (1998) Recovery and refining of au by gold-cyanide ion biosorption using animal fibrous proteins, *Appl Biochem Biotechnol 70*, 719-728.

[18] Bolisetty, S., and Mezzenga, R. (2016) Amyloid–carbon hybrid membranes for universal water purification, *Nature nanotechnology 11*, 365-371.

[19] Hane, F., Tran, G., Attwood, S. J., and Leonenko, Z. (2013) Cu2+ Affects Amyloid-β (1–42) Aggregation by Increasing Peptide-Peptide Binding Forces, *PLOS ONE 8*, e59005.

[20] Rufo, C. M., Moroz, Y. S., Moroz, O. V., Stöhr, J., Smith, T. A., Hu, X., DeGrado, W. F., and Korendovych, I. V. (2014) Short peptides self-assemble to produce catalytic amyloids, *Nat Chem 6*, 303-309.

[21] Sarell, C. J., Syme, C. D., Rigby, S. E., and Viles, J. H. (2009) Copper(II) binding to amyloid-beta fibrils of Alzheimer's disease reveals a picomolar affinity: stoichiometry and coordination geometry are independent of Abeta oligomeric form, *Biochemistry 48*, 4388-4402.

[22] Eskici, G., and Axelsen, P. H. (2012) Copper and Oxidative Stress in the Pathogenesis of Alzheimer's Disease, *Biochemistry 51*, 6289-6311.

[23] Sternisha, A., and Makhlynets, O. (2017) Catalytic Amyloid Fibrils That Bind Copper to Activate Oxygen, *Methods in molecular biology (Clifton, N.J.) 1596*, 59-68.

[24] Knowles, T. P., and Mezzenga, R. (2016) Amyloid Fibrils as Building Blocks for Natural and Artificial Functional Materials, *Advanced materials (Deerfield Beach, Fla.) 28*, 6546-6561.

[25] Seker, U. O. S., Chen, A. Y., Citorik, R. J., and Lu, T. K. (2017) Synthetic Biogenesis of Bacterial Amyloid Nanomaterials with Tunable Inorganic–Organic Interfaces and Electrical Conductivity, *ACS Synth Biol 6*, 266-275.

[26] Shen, Y., Posavec, L., Bolisetty, S., Hilty, F. M., Nyström, G., Kohlbrecher, J., Hilbe, M., Rossi, A., Baumgartner, J., Zimmermann, M. B., and Mezzenga, R. (2017) Amyloid fibril systems reduce, stabilize and deliver bioavailable nanosized iron, *Nature nanotechnology 12*, 642-647.

[27] Chen, A. Y., Zhong, C., and Lu, T. K. (2015) Engineering Living Functional Materials, *ACS Synth Biol 4*, 8-11.

[28] Nguyen, P. Q. (2017) Synthetic biology engineering of biofilms as nanomaterials factories, *Biochemical Society transactions 45*, 585-597.

[29] Chapman, M. R., Robinson, L. S., Pinkner, J. S., Roth, R., Heuser, J., Hammar, M., Normark, S., and Hultgren, S. J. (2002) Role of Escherichia coli curli operons in directing amyloid fiber formation, *Science (New York, N.Y.) 295*, 851-855.

[30] Botyanszki, Z., Tay, P. K. R., Nguyen, P. Q., Nussbaumer, M. G., and Joshi, N. S. (2015) Engineered catalytic biofilms: Site-specific enzyme immobilization onto E. coli curli nanofibers, *Biotechnology and Bioengineering 112*, 2016-2024.

[31] Chen, A. Y., Deng, Z., Billings, A. N., Seker, U. O., Lu, M. Y., Citorik, R. J., Zakeri, B., and Lu, T. K. (2014) Synthesis and patterning of tunable multiscale materials with engineered cells, *Nature materials 13*, 515-523.

[32] Nguyen, P. Q., Botyanszki, Z., Tay, P. K., and Joshi, N. S. (2014) Programmable biofilm-based materials from engineered curli nanofibres, *Nature communications 5*, 4945.

[33] Zhong, C., Gurry, T., Cheng, A. A., Downey, J., Deng, Z., Stultz, C. M., and Lu, T. K. (2014) Strong underwater adhesives made by self-assembling multi-protein nanofibres, *Nature nanotechnology 9*, 858-866.

[34] Pawar, D. M., Rossman, M. L., and Chen, J. (2005) Role of curli fimbriae in mediating the cells of enterohaemorrhagic Escherichia coli to attach to abiotic surfaces, *Journal of applied microbiology 99*, 418-425.

[35] Kikuchi, T., Mizunoe, Y., Takade, A., Naito, S., and Yoshida, S. (2005) Curli fibers are required for development of biofilm architecture in Escherichia coli K-12 and enhance bacterial adherence to human uroepithelial cells, *Microbiology and immunology 49*, 875-884.

[36] Uhlich, G. A., Gunther, N. W., Bayles, D. O., and Mosier, D. A. (2009) The CsgA and Lpp Proteins of an Escherichia coli O157:H7 Strain Affect HEp-2 Cell Invasion, Motility, and Biofilm Formation, *Infection and Immunity 77*, 1543-1552.

[37] Hidalgo, G., Chen, X., Hay, A. G., and Lion, L. W. (2010) Curli Produced by Escherichia coli PHL628 Provide Protection from Hg(II), *Applied and Environmental Microbiology 76*, 6939-6941.

[38] Dorval Courchesne, N.-M., Duraj-Thatte, A., Tay, P. K. R., Nguyen, P. Q., and Joshi, N. S. (2016) Scalable Production of Genetically Engineered Nanofibrous Macroscopic Materials via Filtration, *ACS Biomaterials Science & Engineering*.

[39] Andersson, E. K., Bengtsson, C., Evans, M. L., Chorell, E., Sellstedt, M., Lindgren, A. E., Hufnagel, D. A., Bhattacharya, M., Tessier, P. M., Wittung-Stafshede, P., Almqvist, F., and Chapman, M. R. (2013) Modulation of curli assembly and pellicle biofilm formation by chemical and protein chaperones, *Chemistry & biology 20*, 1245-1254.

[40] Barnhart, M. M., and Chapman, M. R. (2006) Curli biogenesis and function, *Annual review of microbiology 60*, 131-147.

[41] Wang, X., Hammer, N. D., and Chapman, M. R. (2008) The molecular basis of functional bacterial amyloid polymerization and nucleation, *The Journal of biological chemistry 283*, 21530-21539.

[42] Arnqvist, A., Olsen, A., Pfeifer, J., Russell, D. G., and Normark, S. (1992) The Crl protein activates cryptic genes for curli formation and fibronectin binding in Escherichia coli HB101, *Molecular microbiology 6*, 2443-2452.

[43] Jubelin, G., Vianney, A., Beloin, C., Ghigo, J. M., Lazzaroni, J. C., Lejeune, P., and Dorel, C. (2005) CpxR/OmpR interplay regulates curli gene expression in response to osmolarity in Escherichia coli, *J Bacteriol 187*, 2038-2049.

[44] Nies, D. H. (1999) Microbial heavy-metal resistance, *Appl Microbiol Biotechnol 51*, 730-750.

[45] Bell, L. (2016) Guidance on the Identification, Management and Remediation of Mercury-Contaminated Sites, ((IPEN), I. P. E. N., Ed.).

[46] Huang, X. D., Atwood, C. S., Hartshorn, M. A., Multhaup, G., Goldstein, L. E., Scarpa, R. C., Cuajungco, M. P., Gray, D. N., Lim, J., Moir, R. D., Tanzi, R. E., and Bush, A. I. (1999) The A beta peptide of Alzheimer's disease directly produces hydrogen peroxide through metal ion reduction, *Biochemistry 38*, 7609-7616.

[47] Hseu, Z. Y., Huang, Y. T., and Hsi, H. C. (2014) Effects of remediation train sequence on decontamination of heavy metal-contaminated soil containing mercury, *Journal of the Air & Waste Management Association (1995) 64*, 1013-1020.

[48] Ralston, D. M., and Ohalloran, T. V. (1990) Ultrasensitivity and heavy-metal selectivity of the allosterically modulated merR transcription complex, *Proceedings of the National Academy of Sciences of the United States of America 87*, 3846-3850.

[49] Chu, L., Mukhopadhyay, D., Yu, H. G., Kim, K. S., and Misra, T. K. (1992) Regulation of the Staphylococcus aureus plasmid-pi258 mercury resistance operon, *Journal of Bacteriology 174*, 7044-7047.

[50] House, E., Collingwood, J., Khan, A., Korchazkina, O., Berthon, G., and Exley, C. (2004) Aluminium, iron, zinc and copper influence the in vitro formation of amyloid fibrils of Abeta42 in a manner which may have consequences for metal chelation therapy in Alzheimer's disease, *Journal of Alzheimer's disease : JAD 6*, 291-301.

[51] Liu, D., Xiao, Y., Evans, B. S., and Zhang, F. (2015) Negative Feedback Regulation of Fatty Acid Production Based on a Malonyl-CoA Sensor–Actuator, *ACS Synth Biol*

4, 132-140.

[52] Oyarzún, D. A., Lugagne, J.-B., and Stan, G.-B. V. (2015) Noise Propagation in Synthetic Gene Circuits for Metabolic Control, *ACS Synth Biol 4*, 116-125.

[53] Stapleton, J. A., Endo, K., Fujita, Y., Hayashi, K., Takinoue, M., Saito, H., and Inoue, T. (2012) Feedback Control of Protein Expression in Mammalian Cells by Tunable Synthetic Translational Inhibition, *ACS Synth Biol 1*, 83-88.

[54] Bansal, K., Yang, K., Nistala, G. J., Gennis, R. B., and Bhalerao, K. D. (2010) A positive feedback-based gene circuit to increase the production of a membrane protein, *Journal of biological engineering 4*, 6.

[55] Harrison, M. E., and Dunlop, M. J. (2012) Synthetic feedback loop model for increasing microbial biofuel production using a biosensor, *Front Microbiol 3*, 360.

[56] Tipping, E., Lofts, S., Hooper, H., Frey, B., Spurgeon, D., and Svendsen, C. (2010) Critical Limits for Hg(II) in soils, derived from chronic toxicity data, *Environmental pollution (Barking, Essex : 1987) 158*, 2465-2471.

[57] Bueno, P. C., Bellido, E., Rubí, J. A. M., and Ballesta, R. J. (2009) Concentration and spatial variability of mercury and other heavy metals in surface soil samples of periurban waste mine tailing along a transect in the Almadén mining district (Spain), *Environmental Geology 56*, 815-824.

[58] Fashola, M. O., Ngole-Jeme, V. M., and Babalola, O. O. (2016) Heavy Metal Pollution from Gold Mines: Environmental Effects and Bacterial Strategies for Resistance, *International journal of environmental research and public health 13*.

[59] Collinson, S. K., Parker, J. M. R., Hodges, R. S., and Kay, W. W. (1999) Structural predictions of AgfA, the insoluble fimbrial subunit of Salmonella thin aggregative fimbriae1, *J Mol Biol 290*, 741-756.

[60] Hammar, M., Bian, Z., and Normark, S. (1996) Nucleator-dependent intercellular assembly of adhesive curli organelles in Escherichia coli, *Proc Natl Acad Sci USA 93*, 6562-6566.

[61] Evans, M. L., and Chapman, M. R. (2014) Curli biogenesis: order out of disorder, *Biochimica et biophysica acta 1843*, 1551-1558.

[62] Sleutel, M., Van den Broeck, I., Van Gerven, N., Feuillie, C., Jonckheere, W., Valotteau, C., Dufrene, Y. F., and Remaut, H. (2017) Nucleation and growth of a bacterial functional amyloid at single-fiber resolution, *Nat Chem Biol advance online publication*.

[63] Dueholm, M. S., Albertsen, M., Otzen, D., and Nielsen, P. H. (2012) Curli functional amyloid systems are phylogenetically widespread and display large diversity in operon and protein structure, *PLoS One 7*, e51274.

[64] Hakkila, K. M., Nikander, P. A., Junttila, S. M., Lamminmaki, U. J., and Virta, M. P. (2011) Cd-specific mutants of mercury-sensing regulatory protein MerR, generated by directed evolution, *Appl Environ Microbiol 77*, 6215-6224.

[65] Li, L., Liang, J., Hong, W., Zhao, Y., Sun, S., Yang, X., Xu, A., Hang, H., Wu, L., and Chen, S. (2015) Evolved bacterial biosensor for arsenite detection in environmental water, *Environ Sci Technol 49*, 6149-6155.

[66] Anbu, P., Kang, C.-H., Shin, Y.-J., and So, J.-S. (2016) Formations of calcium carbonate minerals by bacteria and its multiple applications, *SpringerPlus 5*, 250.

[67] Harris, D., Ummadi, J. G., Thurber, A. R., Allau, Y., Verba, C., Colwell, F., Torres, M. E., and Koley, D. (2016) Real-time monitoring of calcification process by Sporosarcina pasteurii biofilm, *Analyst 141*, 2887-2895.

[68] Hazen, T. C., and Tabak, H. H. (2005) Developments in Bioremediation of Soils and Sediments Polluted with Metals and Radionuclides: 2. Field Research on Bioremediation of Metals and Radionuclides, *Rev Environ Sci Bio/Technol 4*, 157-183.

[69] (2007) Treatment Technologies for Mercury in Soil, Waste, and Water, (Agency, U. S. E. P., Ed.).

[70] Abouseoud, M., Yataghene, A., Amrane, A., and Maachi, R. (2008) Biosurfactant production by free and alginate entrapped cells of Pseudomonas fluorescens, *J Indust Microbiol Biotechnol 35*, 1303-1308.

[71] Menendez-Vega, D., Gallego, J. L. R., Pelaez, A. I., Fernandez de Cordoba, G., Moreno, J., Muñoz, D., and Sanchez, J. (2007) Engineered in situ bioremediation of soil and groundwater polluted with weathered hydrocarbons, *Eur J Soil Biol 43*, 310-321.

[72] Mrozik, A., and Piotrowska-Seget, Z. (2010) Bioaugmentation as a strategy for cleaning up of soils contaminated with aromatic compounds, *Microbiological research 165*, 363-375.

[73] Riis, C. E., Christensen, A. G., Mortensen, A. P., and Jannerup, H. (2010) Bioremediation of TCE in a fractured limestone aquifer using a novel horizontal passive biobarrier, *Remed J 20*, 27-43.

[74] Ross, N., and Bickerton, G. (2002) Application of Biobarriers for Groundwater Containment at Fractured Bedrock Sites, *Remed J 12*, 5-21.

[75] (2010) FRTR Cost and Performance Case Studies, (Roundtable, F. R. T., Ed.).

[76] Singh, J. S., Abhilash, P. C., Singh, H. B., Singh, R. P., and Singh, D. P. (2011) Genetically engineered bacteria: an emerging tool for environmental remediation and future research perspectives, *Gene 480*, 1-9.

[77] Sayler, G. S., and Ripp, S. (2000) Field applications of genetically engineered microorganisms for bioremediation processes, *Current opinion in biotechnology 11*, 286-289.

[78] Valls, M., and de Lorenzo, V. (2002) Exploiting the genetic and biochemical capacities of bacteria for the remediation of heavy metal pollution, *FEMS microbiology reviews 26*, 327-338.

[79] Fernandez-López, R., Ruiz, R., de la Cruz, F., and Moncalián, G. (2015) Transcription factor-based biosensors enlightened by the analyte, *Frontiers in Microbiology 6*, 648.

[80] Nielsen, P. H., Dueholm, M. S., Thomsen, T. R., Nielsen, J. L., and Otzen, D. (2011) Functional Bacterial Amyloids in Biofilms, In *Biofilm Highlights* (Flemming, H.-C., Wingender, J., and Szewzyk, U., Eds.), pp 41-62, Springer Berlin Heidelberg, Berlin, Heidelberg.

3

Acellular biofilm-derived materials for biosorption

3.1 Introduction

Biosorption is the passive sequestration of organic or inorganic species to a biomass, which can be derived from microorganisms, plants or animals. As a biotechnology for environmental applications, biosorption has been touted as a cost-effective way of remediating a wide range of pollutants and recovering valuable compounds from waste streams. Yet despite a dramatic increase in publications in this research area and significant progress in our understanding of this complex phenomenon (Fig. 3.1), commercial and industrial exploitation of biosorption technologies is still very limited, hindered in part by the lack of specificity and lower robustness of biomass-based systems compared with competing technologies like ion-exchange resins.[1]

Most biosorption research has focused on microbial biosorbents, since microbes like bacteria and fungi can often be obtained at low cost, are generally easy to cultivate, have a very high surface area : volume ratio, and their cell walls and extracellular polymers feature a rich array of chemical groups (e.g. carboxylates, phosphates, hydroxyls, carbonyls, thiols) and a range of binding interactions that cannot be achieved with most other biopolymers without chemical modification.[2] Practical implementation of microbial biosorbents presents several challenges. Live cells require a constant source of nutrition and are susceptible to poisoning when exposed to high pollutant concentrations. Also, suspended biomass is not durable for repeated long-term application and is difficult to separate from treated effluent. To increase the robustness of microbial sorbents, they are used in dried immobilized preparations, obtained either by culturing cells on supports and drying them, or encapsulating dried cell matter in porous materials.[3] However, there

is still a risk of cellular material sloughing off supports and contaminating effluent streams or clogging flow lines. A bigger concern for microbial biosorption is the lack of binding specificity, thus many cell types have to be screened to identify optimal sorbents for particular sorbates, and sorbent performance is highly susceptible to fluctuations in environmental conditions. Although much progress has been made to genetically engineer bacteria and fungi to display binding groups on the cell surface to increase binding specificity and affinity,[4] it might not be economically viable to develop these organisms solely as biosorbents unless they are also used in other fermentation processes.

We have developed an alternative approach to introduce greater specificity to bacterial biosorbents, by genetically engineering extracellular protein nanofibers in *E. coli* biofilms to display peptide motifs or protein domains.[5, 6] The curli amyloid fibers associate extracellularly to form extensive networks, offering a high density of binding sites not unlike the surface of cells, but with potentially larger specific sorption surface areas, and greater resistance to harsh sorption conditions. The isolation of these fibrous networks away from the cells would be advantageous for several reasons: (a) the bacteria are not tied up in the biosorbent and could be reused for further amyloid production, or repurposed for other fermentation applications or less-selective biosorption processes; (b) there is potentially less shedding of sorbent material over time from immobilized acellular fibers compared to whole biofilms, thus extending the lifetime of the biosorbent and reducing contamination of effluent streams; (c) swelling of cell bodies will not occlude binding sites on the fibers or affect the dynamics of adsorption to the fibers; (d) the selectivity conferred by the engineered fibers is not undermined by non-specific adsorption to cells; and (e) valuable metal or organic species will not be entrapped in cell bodies and are more readily recovered.

In the curli biogenesis pathway, secreted CsgA monomers self-assemble into nanofibers by seeding onto a membrane-anchored nucleation protein, CsgB.[7] CsgB is tethered to the cell surface by its fifth repeating unit (R5),[8, 9] aided by another outer membrane-associated accessory protein, CsgF, which also helps to chaperone the nucleating function of the CsgB subunit.[10] In strains without CsgF or with a truncated mutant CsgB ($CsgB^{\Delta R5}$), CsgB is secreted into the surrounding medium and curli assembly is much diminished.[8, 10] *In vitro*, purified CsgA was able to self-assemble in the absence of CsgB, but a 1-2 hr lag phase occurred before significant fiber growth.[11, 12] Several gatekeeper residues are believed to temper CsgA assembly to ensure that fibrillation and localization are under the control of CsgB and CsgF.[13] A CsgA mutant lacking all the gatekeeper residues (CsgA*) showed rapid polymerization with a limited lag phase even without CsgB, however, the fibers were formed away from the cell surface, and overexpression of CsgA* induced significant cell toxicity.[13]

The native curli operon in wild-type *E. coli* is induced to produce curli only under conditions of low osmolarity and/or starvation.[14, 15] To decouple curli production from these stringent conditions, we previously assembled the major *csg* genes into a synthetic *csgBACEFG* operon, which could be placed under the control of common promoters to provide the entire machinery for curli biosynthesis.[16, 17] Large curli networks were formed following expression from the operon, but they were tethered to the cells and difficult to separate (Fig. 3.4a). Previous attempts to purify the extracellular fibers involved shearing with low-intensity sonication and pelleting with ultracentrifugation,[5, 18] though these methods are impractical for larger-scale separations. This chapter examines several strategies to engineer curli networks that are more easily separated from cells, including: (a) expression of CsgA* under low induction to reduce toxicity to cells; (b) expression of truncated CsgB ($CsgB^{\Delta R5}$) or (c) deletion of CsgB and/or CsgF

to allow nucleation and fiber assembly away from the cell surface. The chapter will also describe the development of a filtration protocol for rapid separation of curli from cells.

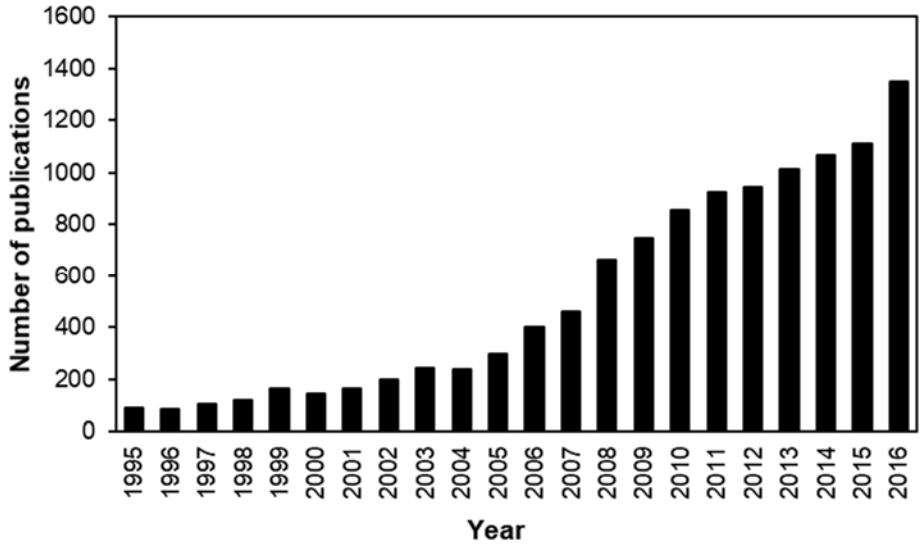

Figure 3.1. The number of papers appearing with "biosorption" in the topic as listed in the ISI Web of Science database for "All Years" (1995–2016) (out of a total of 11,465 articles). Database searched 7 Aug 2017).

3.2 Materials and methods

Cloning

The synthetic *csgBACEFG* operon (Chapter 2) was subcloned into a pET21d vector for use in all subsequent cloning experiments. Variants BΔR5, CsgA* and ΔB were generated by subcloning synthesized DNA fragments (Integrated DNA Technologies) containing, respectively, $csgB^{\Delta R5}A$, *csgA** and *csgA* (wild-type) in place of the *csgBA* genes, using standard Gibson assembly protocols. Similarly, variant ΔBF was generated from variant ΔB by subcloning a synthesized DNA fragment containing *csgE* (wild-type) in place of the *csgEF* genes. 6×His variants of corresponding constructs were produced by subcloning of a DNA fragment containing the 6×His gene via Gibson assembly. To create the negative control plasmid, the gene for maltose-binding protein (MBP) was subcloned from a pET28a-SpyTagMBP plasmid (Addgene 35050) into pET21d in place of the *csg* genes, as there was some cell toxicity from overexpression of the empty plasmid. The *E. coli* PQN4 strain was used for curli expression (see Chapter 2).

Curli expression

For expression in suspension, overnight cultures were expanded in LB supplemented with 10 μg/ml carbenicillin and 1% w/v glucose to an OD_{600} of 0.7. The cultures were pelleted and resuspended in LB/carbenicillin containing IPTG, and protein expression allowed to occur overnight at 30°C with shaking. Cultures were diluted 10× for OD_{600} measurement. To quantify curli production, 500 μl cultures were pelleted and resuspended in 15 μg/ml Congo Red for 5 min. The suspension was re-pelleted and the absorbance of the supernatant was read at 490 nm and used to determine the amount of Congo Red bound. Three sets of cultures were used for each expression study. For expression on plates, LB agar plates were first prepared supplemented with 25 μg/mL

Congo Red, 10 μg/mL Coomassie Brilliant Blue and 0.1 mM IPTG. Expanded cultures were pelleted and resuspended in LB, and 10 μl spotted on the Congo Red plates, which were then incubated at 30°C overnight. Statistical analysis was performed using the Student's t-test with a 95% confidence interval.

Separation of CsgA-6×His fiber networks from cells

A 200 ml culture of ΔBF-6×His cells was induced with 0.1 mM IPTG overnight at 30°C to allow production of CsgA-6×His fiber networks. The culture was then mixed with 5 ml buffer-washed NiNTA beads (Qiagen) and left to settle at 4°C overnight. The supernatant was carefully decanted and the beads transferred to a polypropylene chromatography column. The beads were then washed with 4×5 ml wash buffer (50 mM phosphate buffer, 0.5 M NaCl, pH 7), followed by 4×5 ml wash buffer containing 40 mM imidazole to remove non-specifically bound proteins. The two washes were separately pooled. Elution was carried out with 4×5 ml wash buffer containing 0.5 M imidazole. The eluate was spin-concentrated in a 3 kDa Amicon filter and dialyzed with 50 mM phosphate buffer. The concentrated sample was suspended in hexafluoroisopropanol (HFIP) and left to shake overnight to disassemble the fibers. After blowing off the HFIP under a stream of air, the dried sample was resuspended in water and immediately run on an SDS-PAGE gel along with the column washes.

Scanning electron microscopy

Samples were filtered onto nanoporous membrane discs (Whatman® Nuclepore™ Track-Etched Membranes), and the membranes were fixed overnight in 2% glutaraldehyde / 2% *para*-formaldehyde at 4°C. The discs were immersed in a series of dehydrating ethanol solutions (25%,

50%, 75%, 100% v/v ethanol), then dried on a Tousimis Autosamdri-931 CO_2 critical point dryer. SEM images were obtained on a Zeiss Ultra Plus FE-SEM.

Nanogold labeling and transmission electron microscopy

NiNTA-nanogold labelling of 6×His tags displayed on CsgA was performed as previously described.[19] 200-mesh formvar/carbon-coated nickel TEM grids (Electron Microscopy Sciences) were placed coated side-down on 20 µl droplets of samples on parafilm for 2 min. The grid was rinsed with ultrapure water, then with selective binding buffer (1×PBS, 0.487 M NaCl, 80 mM imidazole, 0.2% v/v Tween 20), and placed face-down in a 50 µl droplet of selective binding buffer containing 10 nM 5 nm NiNTA-AuNP particles (Nanoprobes). The TEM grid and droplet on parafilm was covered with a petri dish to minimize evaporation and allowed to incubate for 30 min. The grid was then washed 5× with selective binding buffer, 3× with ultrapure water, and negative-stained with fresh 2% uranyl formate for 15 sec. The samples were allowed to dry for 10 minutes, then imaged on a JEM-1400 Transmission Electron Microscope at 80 kV accelerating voltage.

Filtration-immobilization of curli fiber networks

To overnight cultures containing curli fiber mats, guanidinium chloride (GdmCl) was added to a final concentration of 0.8 M, and the mixture was kept at 4°C for 1–2 hr. Gdm-containing cultures were then vacuum-filtered onto polycarbonate filter membranes (47 mm diameter, 10 µm pore size, EMD Millipore) until the membranes were saturated. The filtered biomass was incubated successively with 5 mL of 8 M GdmCl for 5 min, 5 mL of an aqueous solution of nuclease (Benzonase, Sigma-Aldrich, 1.5 U/ml with 2 µM $MgCl_2$) for 10 min, and 5 mL of 5% w/v sodium

dodecyl sulfate (SDS) in water for 5 min, and rinsed with 3×5 mL deionized water after each treatment step.

YFP labeling of filter-immobilized of curli displaying functional tags

Venus yellow fluorescent protein constructs (Venus-SpyTag, Venus-SpyCatcher) were cloned into and expressed from a pDEST14 backbone (Addgene #35044), followed by purification using a Ni-NTA affinity column.[20] The Venus fusion protein solutions were diluted to 10 μM in 50 mM phosphate buffer (pH 7.2), and incubated with filter membranes (90 min, 4°C) containing immobilized CsgA-SpyTag or CsgA-SpyCatcher nanofibers. The membranes were then rinsed with 5×5 mL of deionized water. To exclude non-specific binding on filter membranes, the following controls were also incubated with Venus-SpyCatcher or Venus-SpyTag: (1) immobilized CsgA-6×His, (2) cells expressing only MBP and subjected to the same filtration treatment, and (3) bare filter membranes.

3.3 Results and discussion

Variants of a synthetic *csgBACEFG* operon were constructed to investigate the production of cell-detached curli networks. Consistent with previous findings, there was significant toxicity associated with the overexpression of CsgA*,[13] even at low inducer concentrations (20 μM IPTG) and with concurrent overexpression of other curli proteins (Fig. 3.2). Conversely, no cytotoxicity was observed for variants with truncated CsgB (BΔR5), or deleted CsgB (ΔB) and CsgF (ΔBF) (Fig. 3.2). Comparison of curli production using a Congo Red pull-down assay showed that all of the latter three variants produced a comparable amount of curli to wild-type, with BΔR5 consistently giving slightly higher production than wild-type (Fig. 3.3). Since $CsgB^{\Delta R5}$ retained the ability to self-assemble *in vitro* (albeit at a slower rate than native CsgB),[9] the increased Congo Red signal might reflect the formation of $CsgB^{\Delta R5}$ fibers, which are undesirable as they reduce the density of displayed groups on curli networks and might also occlude those groups. Scanning electron microscopy showed that, unlike wild-type curli fibers, which were attached to and enveloped the bacteria, curli fibers from the variants aggregated extensively to form large extracellular mats tens of microns in size that were not associated with the cells (Fig. 3.4). Detachment of curli fibers from cells was confirmed with colonies grown on agar (Fig. 3.5).[8] When cells were scraped off the colonies, distinct pink discs tracing the shape of the colonies were observed for BΔR5 and ΔBF variants, indicating significant fiber assembly within the agar away from the cell colony; this staining pattern was not observed for wild-type colonies. Since CsgB and CsgF were not necessary for the formation of extensive curli networks, we selected the ΔBF variant as the most streamlined construct for cell-untethered curli production.

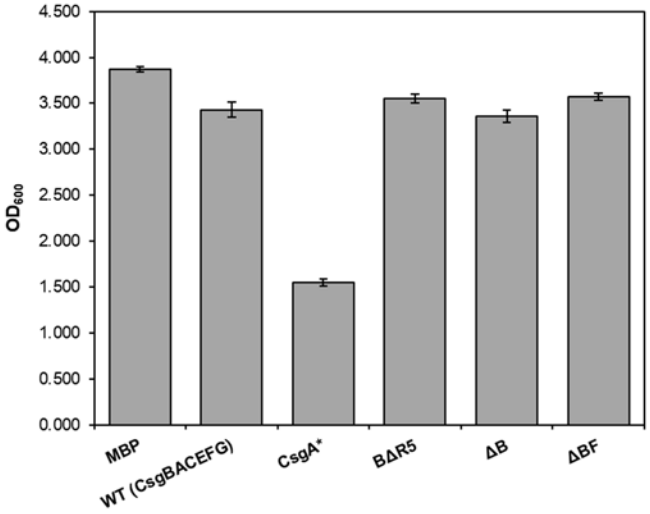

Figure 3.2. Cell density after overnight curli production from the different variants. Cultures at OD_{600}~0.7 were induced with 20 µM IPTG and allowed to express for at least 16 hr at 30°C with shaking. Growth of the CsgB variants (BΔR5, ΔB and ΔBF) were comparable to that of the wild-type operon. Overexpression of CsgA* led to cytotoxicity even at a low inducer concentration.

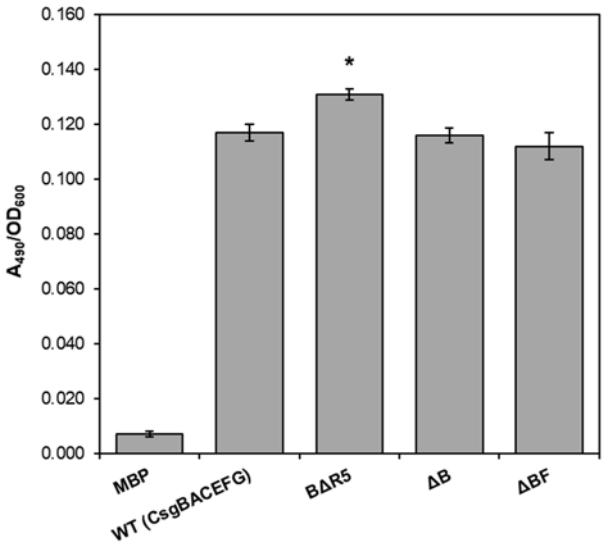

Figure 3.3. Comparative curli production from the variants as determined by the Congo Red pull-down assay. Cells were induced with 75 µM IPTG and allowed to express for at least 16 hr at 30°C with shaking. All variants produced comparable amount of curli fibers to the wild-type operon. * represents $p < 0.05$.

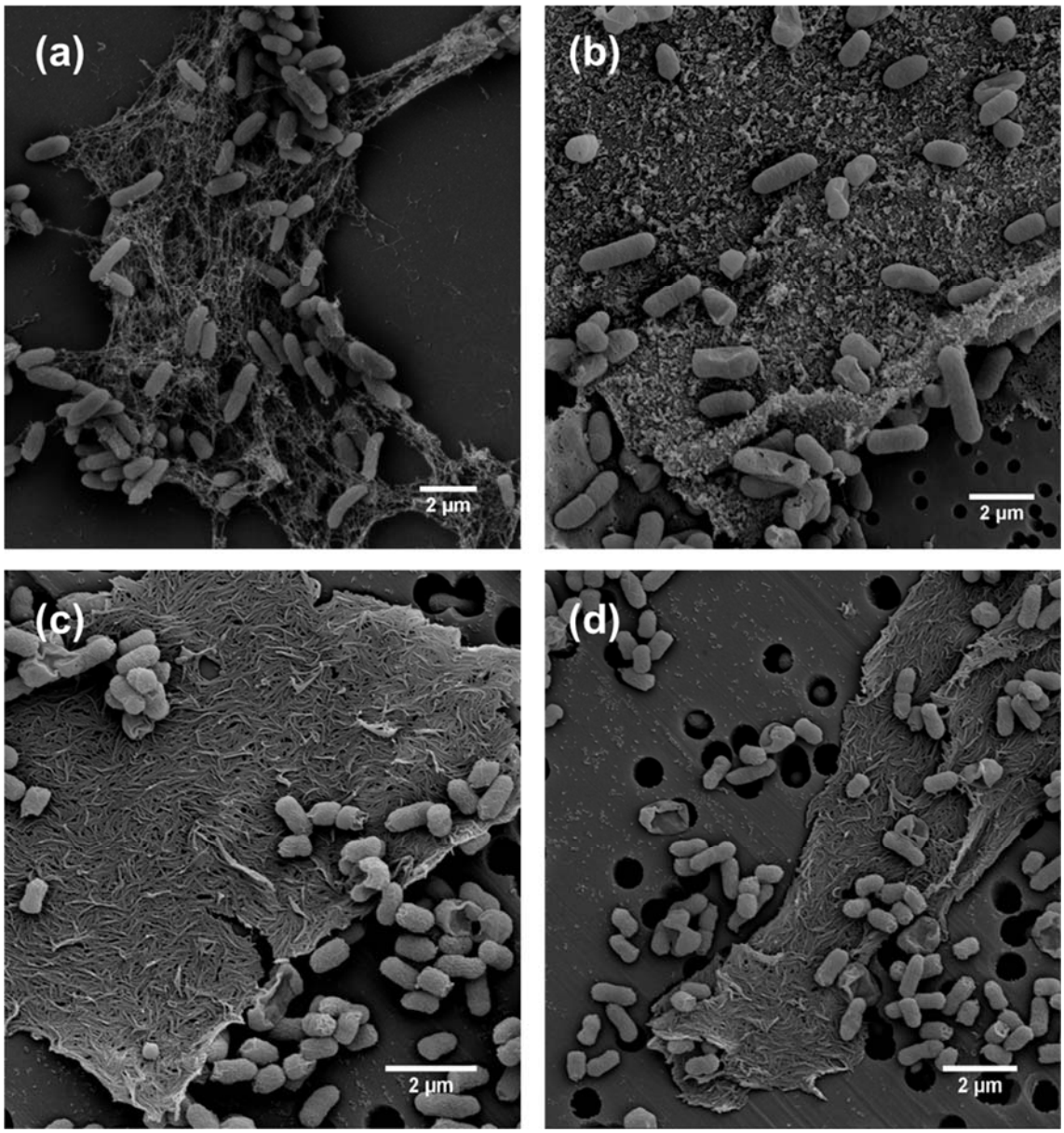

Fig 3.4. Scanning electron micrographs of curli networks expressed using: (a) the full synthetic *csgBACEFG* operon; (b) a $CsgB^{\Delta R5}$ variant of the operon (BΔR5); (c) a *csgACEFG* variant (ΔB); and (d) a *csgACEG* variant (ΔBF). Unlike wild-type expression, where curli fibers were tethered to the cells, expression from the three variants gave rise to extensive fiber meshes that were largely separate from the cells.

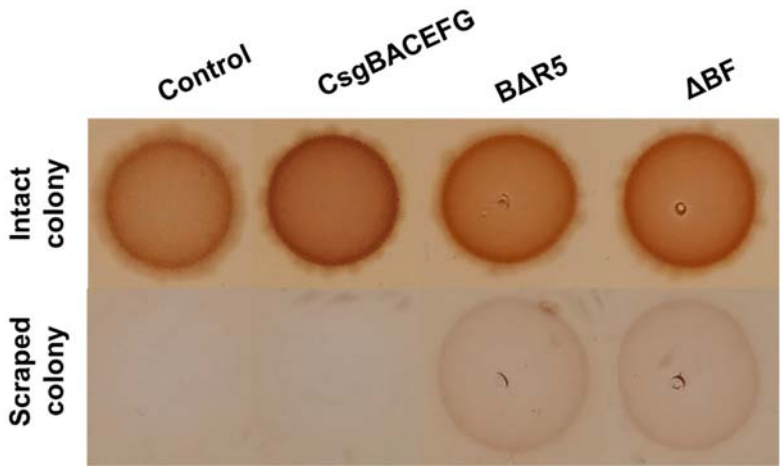

Figure 3.5. Curli production from wild-type and variants grown on agar. 10 µl of cultures (OD_{600}~0.7) were spotted on LB agar containing Congo Red and 0.1 mM IPTG, and plates were incubated at 30°C overnight. Intact colonies are shown on the top panel, and the bottom panel depicts the same colonies after the cells have been scraped off, showing that significant curli assembly occurred within the agar at a distance from the cells for the BΔR5 and ΔBF variants.

To separate the curli fiber meshes from the bacteria, we initially explored the use of affinity tags. NiNTA beads were used to separate curli fibers displaying 6×His tags from overnight cultures. Elution of the fibers using imidazole showed that a significant quantity of fibers was bound to the beads in the ΔBF variant, whereas no fibers were recovered from wild-type cultures (Fig. 3.6). This also demonstrated that the curli meshes retained BIND capabilities despite the fibers being in an aggregated state. Nanogold labeling of eluted fiber meshes confirmed that the bulk of the mesh surface was available for specific binding (Fig. 3.7). Nonetheless, coating of the beads was not uniform and was easily disrupted under flow or mechanical agitation (Fig. 3.8), a consequence of the large size of the curli meshes. The cost of the functionalized beads also prohibits scaling up the process—an issue with affinity-based separations in general. Moreover, the introduction of an

affinity tag potentially limits the display of other selective domains and could interfere with downstream sorption processes; removal of the tags would drive up costs even further. The use of porous substrates to entrap the curli networks is an attractive alternative, but suffers its own set of disadvantages. The substrates need to be loaded in specialized biofilm reactors,[21] then separated out once loading is complete for subsequent decellularization. The latter requires more stringent conditions to remove cells trapped in the pores. Further, there could be mass transfer limitations for sorption to porous materials. Overall, the separation of curli networks from cells should not involve a significant investment in cost and effort.

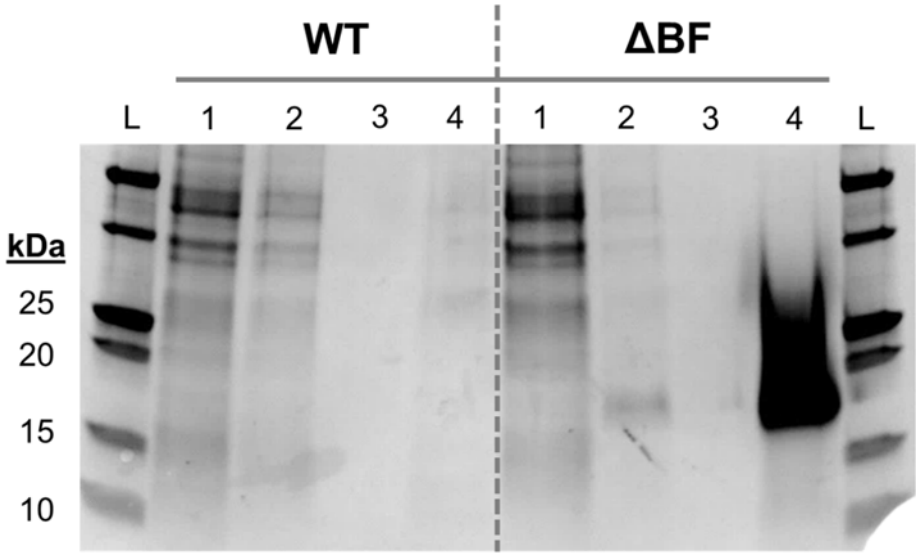

Figure 3.6. SDS-PAGE following affinity separation of His-tagged curli fiber mats using NiNTA beads. Numbers to the left denote protein molecular weights in the ladder. The lanes are as follow: 1. overnight cell culture; 2. flow-through buffer washes; 3. flow-through from buffer washes containing 40 mM imidazole; 4. eluted protein, after HFIP treatment.

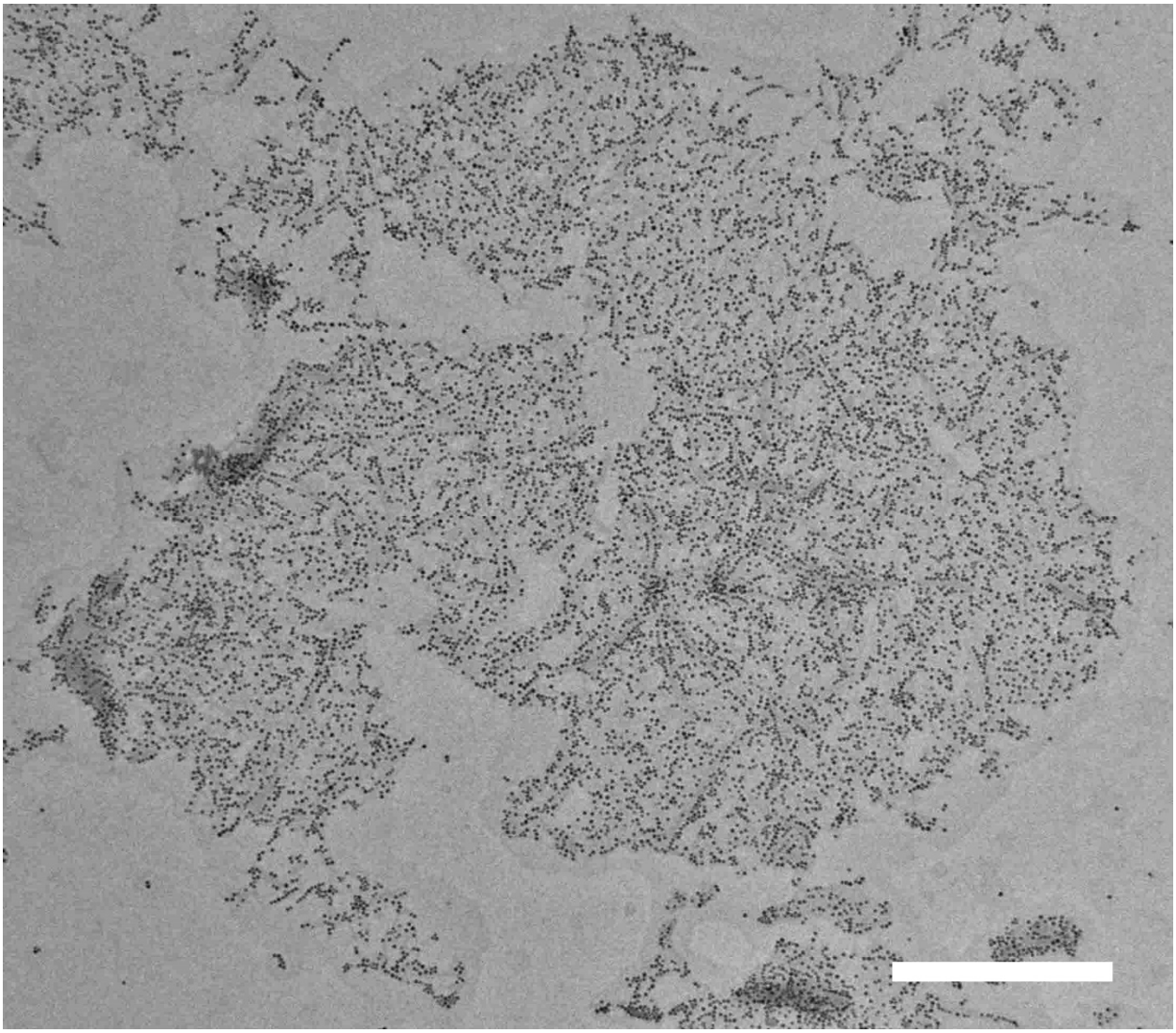

Figure 3.7. Transmission electron micrograph of NiNTA-nanogold-labeled CsgA-6×His curli networks that have been purified from cell culture, showing that the networks retained the ability to display functional groups on the vast majority of their surfaces. Scale bar: 500 nm.

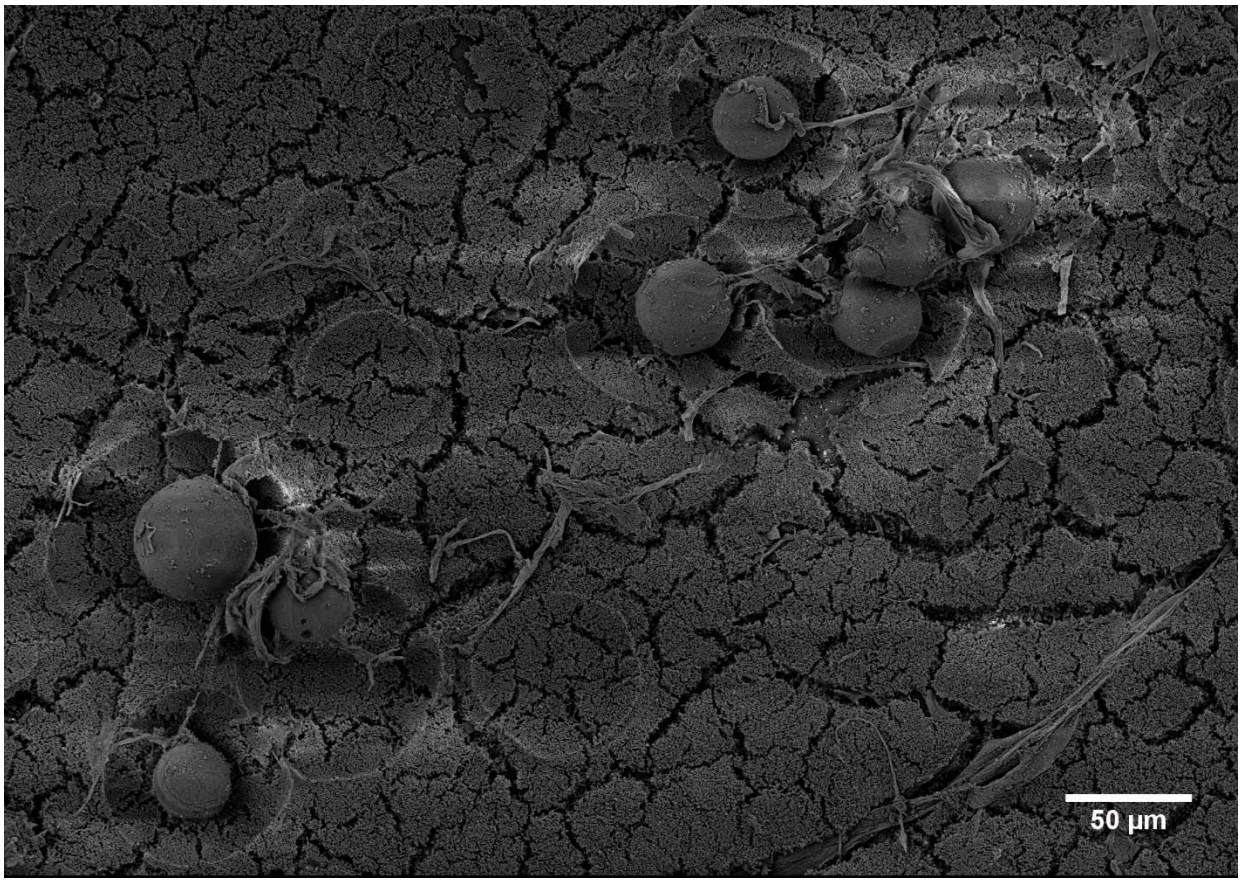

Figure 3.8. Scanning electron micrograph of NiNTA beads incubated with CsgA-6×His curli networks, showing non-uniform coating of the beads.

With that in mind, we developed a filtration-based protocol for isolating curli fibers, relying on the stability of the assembled meshes to denaturing conditions (Fig. 3.9).[16] Curli was first filter-immobilized under vacuum onto a microporous membrane, enabling the rapid removal of the bulk of the cells in a culture, while maintaining their viability for continued curli production. The membrane was then sequentially treated with denaturant (guanidinium hydrochloride) and nuclease to lyse remaining cells and remove contaminating proteins and nucleic acids. The immobilized fiber meshes offered good coverage of the filter surface, and were able to display functional groups for the customized binding of other molecules (Fig. 3.10). Treatment of the

filters with a detergent (sodium dodecylphosphate) allowed the fibers to be scraped off and the membranes to be reused for new cycles of immobilization. This process is rapid, independent of affinity tags, and scalable for the processing of large volumes of culture. The versatility of filtration was also recently exploited by Bolisetty *et al.* to fabricate composite materials based on β-lactoglobulin amyloids.[22] However, their use of purified proteins could be cost-prohibitive to scale up, and there is limited ability to functionalize the protein for more selective binding.

The polycarbonate membranes used in our pilot study could be replaced with more resilient polymers (e.g. Teflon) to withstand harsher downstream sorption processes, or with biodegradable materials like cellulose to reduce cost and environmental impact. Commercial biosorbents need to display good binding capacity, binding selectivity, regenerability, mass transfer kinetics, and be low in cost to manufacture. Filters based on immobilized functionalized curli or amyloid networks offer many of these features. The dense nanofibrous meshes provide a high specific surface area for sorption, while the compact filters could be shaped into a variety of forms to maximize space in a biosorption set-up without compromising mass transfer. Binding selectivity is conferred by the high-density display of customizable tags. The curli matrix is readily regenerated through fermentation, and the natural resilience of amyloids increases the lifetime of amyloid-based biosorbents, reducing operational costs. The next chapter explores the application of these filters for the selective biosorption of rare earth metals.

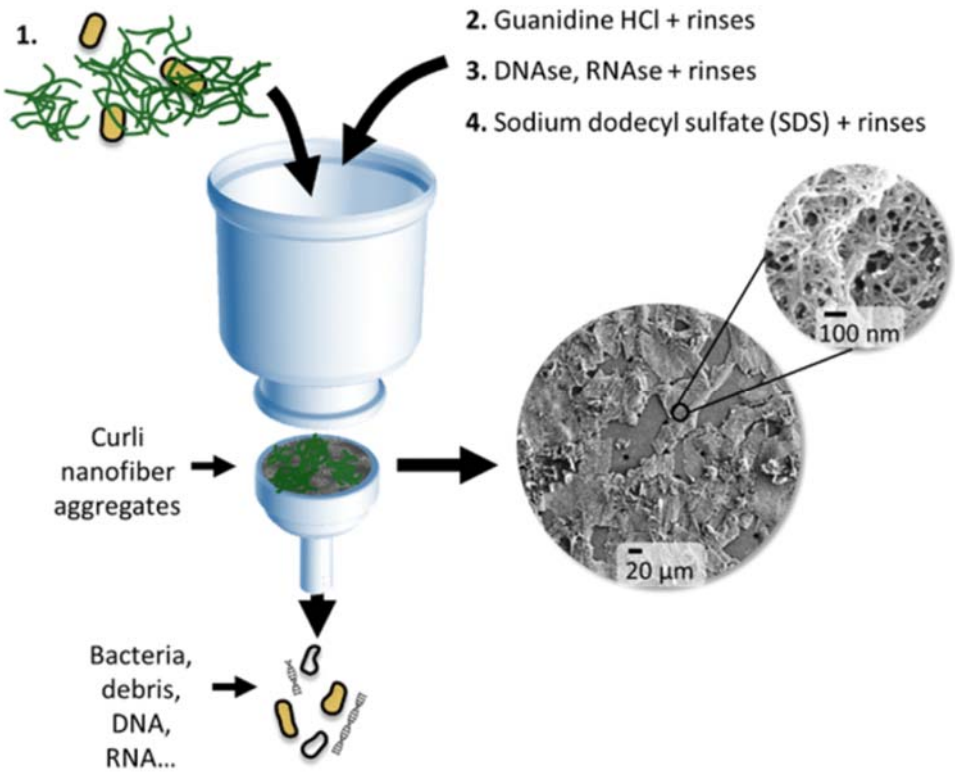

Figure 3.9. Schematic summarizing the filter-immobilization of large curli nanofiber aggregates. SEM images of the curli aggregates on a 10 µm polycarbonate membrane are shown. Reproduced with permission from Dorval Courchesne *et al*, *ACS Biomaterials and Engineering*, 3(5): 733-741.

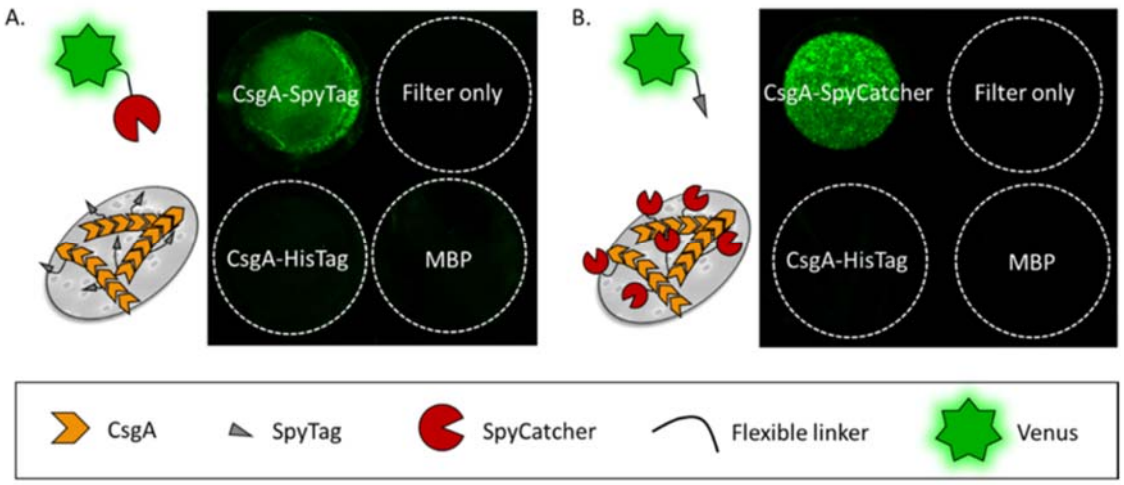

Figure 3.10. Curli meshes displaying small tags or larger protein domains remain functional after immobilization. SpyTag- (A) and SpyCatcher-displaying curli fibers (B) bind their cognate Venus-SpyCatcher and Venus-SpyTag proteins respectively. Filters prepared from MBP- and CsgA-6×His-expressing cultures did not show similar targeted binding specificity. Reproduced with permission from Dorval Courchesne *et al*, *ACS Biomaterials and Engineering*, 3(5): 733-741.

3.5 References

[1] Gadd, G. M. (2009) Biosorption: critical review of scientific rationale, environmental importance and significance for pollution treatment, *Journal of Chemical Technology & Biotechnology 84*, 13-28.

[2] Volesky, B. (2007) Biosorption and me, *Water Research 41*, 4017-4029.

[3] Park, D., Yun, Y.-S., and Park, J. M. (2010) The past, present, and future trends of biosorption, *Biotechnology and Bioprocess Engineering 15*, 86-102.

[4] Li, P.-S., and Tao, H.-C. (2015) Cell surface engineering of microorganisms towards adsorption of heavy metals, *Critical Reviews in Microbiology 41*, 140-149.

[5] Nguyen, P. Q., Botyanszki, Z., Tay, P. K. R., and Joshi, N. S. (2014) Programmable biofilm-based materials from engineered curli nanofibres, *5*, 4945.

[6] Nguyen, P. Q. (2017) Synthetic biology engineering of biofilms as nanomaterials factories, *Biochemical Society transactions 45*, 585-597.

[7] Van Gerven, N., Klein, R. D., Hultgren, S. J., and Remaut, H. (2015) Bacterial Amyloid Formation: Structural Insights into Curli Biogensis, *Trends in Microbiology 23*, 693-706.

[8] Hammer, N. D., Schmidt, J. C., and Chapman, M. R. (2007) The curli nucleator protein, CsgB, contains an amyloidogenic domain that directs CsgA polymerization, *Proceedings of the National Academy of Sciences of the United States of America 104*, 12494-12499.

[9] Hammer, N. D., McGuffie, B. A., Zhou, Y., Badtke, M. P., Reinke, A. A., Brannstrom, K., Gestwicki, J. E., Olofsson, A., Almqvist, F., and Chapman, M. R. (2012) The C-terminal repeating units of CsgB direct bacterial functional amyloid nucleation, *Journal of molecular biology 422*, 376-389.

[10] Nenninger, A. A., Robinson, L. S., and Hultgren, S. J. (2009) Localized and efficient curli nucleation requires the chaperone-like amyloid assembly protein CsgF, *Proceedings of the National Academy of Sciences of the United States of America 106*, 900-905.

[11] Wang, X., Smith, D. R., Jones, J. W., and Chapman, M. R. (2007) In vitro polymerization of a functional Escherichia coli amyloid protein, *The Journal of biological chemistry 282*, 3713-3719.

[12] Dueholm, M. S., Nielsen, S. B., Hein, K. L., Nissen, P., Chapman, M., Christiansen, G., Nielsen, P. H., and Otzen, D. E. (2011) Fibrillation of the Major Curli Subunit CsgA under a Wide Range of Conditions Implies a Robust Design of Aggregation, *Biochemistry 50*, 8281-8290.

[13] Wang, X., Zhou, Y., Ren, J. J., Hammer, N. D., and Chapman, M. R. (2010) Gatekeeper residues in the major curlin subunit modulate bacterial amyloid fiber biogenesis, *Proc Natl Acad Sci U S A 107*, 163-168.

[14] Arnqvist, A., Olsen, A., Pfeifer, J., Russell, D. G., and Normark, S. (1992) The Crl protein activates cryptic genes for curli formation and fibronectin binding in Escherichia coli HB101, *Molecular microbiology 6*, 2443-2452.

[15] Jubelin, G., Vianney, A., Beloin, C., Ghigo, J. M., Lazzaroni, J. C., Lejeune, P., and Dorel, C. (2005) CpxR/OmpR interplay regulates curli gene expression in response to osmolarity in Escherichia coli, *J Bacteriol 187*, 2038-2049.

[16] Dorval Courchesne, N.-M., Duraj-Thatte, A., Tay, P. K. R., Nguyen, P. Q., and Joshi, N. S. (2017) Scalable Production of Genetically Engineered Nanofibrous Macroscopic Materials via Filtration, *ACS Biomaterials Science & Engineering 3*, 733-741.

[17] Tay, P. K. R., Nguyen, P. Q., and Joshi, N. S. (2017) A Synthetic Circuit for Mercury Bioremediation Using Self-Assembling Functional Amyloids, *ACS Synthetic Biology*.

[18] Romling, U., Bokranz, W., Rabsch, W., Zogaj, X., Nimtz, M., and Tschape, H. (2003) Occurrence and regulation of the multicellular morphotype in Salmonella serovars important in human disease, *International journal of medical microbiology : IJMM 293*, 273-285.

[19] Chen, A. Y., Deng, Z., Billings, A. N., Seker, U. O. S., Lu, M. Y., Citorik, R. J., Zakeri, B., and Lu, T. K. (2014) Synthesis and patterning of tunable multiscale materials with engineered cells, *Nature materials 13*, 515-523.

[20] Nagai, T., Ibata, K., Park, E. S., Kubota, M., Mikoshiba, K., and Miyawaki, A. (2002) A variant of yellow fluorescent protein with fast and efficient maturation for cell-biological applications, *Nature biotechnology 20*, 87-90.

[21] Halan, B., Buehler, K., and Schmid, A. Biofilms as living catalysts in continuous chemical syntheses, *Trends in biotechnology 30*, 453-465.

[22] Bolisetty, S., and Mezzenga, R. (2016) Amyloid–carbon hybrid membranes for universal water purification, *Nat Nano 11*, 365-371.

4

Selective recovery of rare earth metals using engineered biofilm-derived filters

4.1 Abstract

The rare earth elements (REEs) are widely used in modern consumer electronics and clean technologies, but unpredictable supply and environmentally unsustainable extraction practices have spurred efforts into green methods of recovering the metals from waste streams. Here we present filters tailored for REE recovery, derived from curli amyloid fibers in *E. coli* biofilms that have been genetically modified to display lanthanide binding tags (LBTs). The curli-LBT filters showed lanthanide specificity in the presence of other metals, with a preference for binding several high-value heavy REEs. Bound lanthanides were readily recovered using an acid wash, and the filters could be re-used for multiple cycles of sorption and desorption with minimal loss of efficiency. Our engineered biofilm-derived filters provide a rapid, selective and scalable method for REE separation that is more robust compared to conventional cell-based sorbents, and this platform could be adapted to recover other precious metals or commodities.

4.2 Introduction

The rare earth elements (REEs), which comprise the lanthanide metals as well as scandium and yttrium, exhibit unique properties that make them useful in modern-day magnets, batteries, phosphors and catalysts. Though not particularly rare in terms of crustal abundance, REEs are found at fairly low concentrations in ores, and are difficult and costly to extract and refine due to

their physicochemical similarities. Global demand for REEs has grown steadily over the past few decades, a continuing trend driven by their importance to the consumer electronics industry and the clean-energy sector.[1] In recent reports, both the European Union and the United States Department of Energy have identified REEs to be critical to emerging low-carbon energy technologies,[2, 3] yet there are concerns that future REE availability could be compromised by monopolistic supply conditions—China currently controls over 95% of REE supplies—and environmentally unsustainable extraction practices.[1, 4] The most widely used separation method is solvent extraction, which requires several steps of pre-treatment with strong acids or bases followed by multiple extraction cycles using organic solvents.[5, 6] The solvent waste, if not contained, can create extensive environmental damage leading to the contamination of natural water streams. These detrimental effects, along with the need to establish more reliable supplies of the metals, have led to efforts to recover REEs from waste streams, e.g. mine tailings or consumer product waste.[7-9]

The use of microorganisms for the sustainable removal of toxic metals from industrial waste has been extensively investigated and reviewed.[10] Knowledge of the way some of these metals interact with microorganisms has helped to define remediation strategies, including the design of genetically engineered bacteria and fungi capable of bioaccumulating heavy metals intracellularly, on the cell surface or within an extracellular matrix.[11-13] Much less is known about the interactions between REEs and microbes. Several lanthanides have recently been discovered to function as cofactors in the alcohol dehydrogenases of bacteria, but it is not clear how the bacteria mobilize or metabolize these metals.[14-16]

Nonetheless, multiple studies in recent years have established that lanthanides passively adsorb to the cell surface of some bacteria and fungi (reviewed by Andres *et al.*[17] and Moriwaki *et*

al.[18]), and that carboxyate- and phosphate-containing entities in the cell wall are the main binding sites for the metals.[19-22] The bound lanthanides could be recovered by treating the cells with competing chelators (e.g. citrate, EDTA) or by washing with an acid, though the latter adversely affected cell viability.[23, 24] The majority of these studies were performed in batch using living cells,[23, 25-27] which required the growth and maintenance of large volumes of cultures, with the ensuing complication of having to separate the cells from the effluent stream. This has partly been resolved by immobilizing the biomass on solid supports like activated alumina, polymer beads and filter membranes. Fixed bed bioreactors assembled from these supports have enabled continuous-flow biosorption and streamlined multiple sorption/desorption cycles.[23, 24, 28] However, the long-term integrity of the immobilized biomass was not studied, and escape of cells or cell debris could potentially occlude flow lines. There have been efforts to reduce the reliance on living cells by using dried cell matter, but this has led to lower binding capacities.[26, 29]

Besides the cell surface, extracellular polymers (EPs) secreted by cells in biofilms are also known to bind metals.[30-33] Alginate, an anionic polysaccharide produced by seaweed and some algae, has shown affinity for some lanthanides.[34-36] Wang *et al.* used gel beads comprising a mix of alginate and poly-γ-glutamic acid (an biopolymer produced by *Bacillus sp.*) to recover Nd^{3+} over several sorption/desorption cycles.[37] An issue with alginate-based biosorbents is that the Ca^{2+} commonly used for crosslinking to yield stable gels is prone to be displaced during the binding and desorption phases, thus necessitating frequent replenishment to maintain the structural integrity of the sorbent. It is also difficult to alter the chemical composition of polysaccharides to increase binding affinity or introduce greater REE binding selectivity—a disadvantage in general of relying on non-specific adsorption to cell walls or exopolymers.

Other EPs commonly associated with bacterial biofilms are amyloid fibrils self-assembled from secreted protein monomers. Unlike with sugars, these protein monomers are more tractable to genetic engineering, and our group and others have successfully appended peptide tags and protein domains to one such monomer—the *E. coli* CsgA protein—to create functionalized curli fiber-based biofilms capable of capturing enzymes and metal nanoparticles.[38-43] Further, we have shown that these fibers could be untethered from the cell surface by removing the anchoring protein CsgB, allowing the formation of extensive cell-free fiber meshes (tens of microns in size) that were easily immobilized onto membranes via a filtration process.[44] Here we demonstrate that immobilized curli fiber mats displaying a genetically-encoded lanthanide-binding tag could be used for the binding and release of rare earth metal ions over multiple cycles.

Lanthanide-binding tags (LBTs) are oligopeptides originally developed as protein tags to study protein structure and interactions *in vitro* and *in vivo*.[45-51] They were evolved to chelate Tb^{3+} over metal ions of similar size (e.g. Ca^{2+}) and valence (e.g. Fe^{3+}), and showed nanomolar binding affinity for many lanthanides.[52] Being small, they could be inserted in loops of proteins or at their termini using standard molecular biology techniques with minimal impact on structure and function.[46, 53] Park *et al.* recently appended 8×LBT to the S-layer protein of *Caulobacter crescentus* for cell surface display.[54] The engineered bacteria bound several lanthanides with varying affinities, and the lanthanides were recovered using a citrate treatment. Although the cells were selective for Tb^{3+} over other metals, binding required the presence of Ca^{2+} and relied on batch sorption using living cells, with its attendant disadvantages as described previously. By displaying LBTs on extracellular amyloid fibers that could be separated from cells, we were able to assemble cell-free materials that retained a large surface area for lanthanide sorption, without the potential for cell contamination in downstream processes. Work by Mezzenga's group first showed that

amyloids immobilized on filters could be used to sequester heavy metals;[55] here we show that through genetic engineering, these protein-based materials could be further improved for more selective metal recovery.

4.2 Materials and methods

Cloning

Plasmids carrying CsgA-LBT variants were created by sub-cloning synthesized DNA fragments (Integrated DNA Technologies, USA) into a pET21d-P_{T7}-*csgACEG* plasmid via Gibson Assembly (Chapter 3). To create the negative control plasmid, the gene for maltose-binding protein (MBP) was subcloned from a pET21a-MBP-His plasmid (Addgene 38006) into pET21d in place of the *csg* genes. All plasmids were transformed into PQN4 cells (*csg,* λDE3).

Curli production

For curli fiber production, overnight cultures were expanded in LB supplemented with 10 μg/ml carbenicillin to an OD_{600} of 0.7, then 0.1 mM IPTG was added and protein expression allowed to occur overnight at 30°C with shaking. Cultures were diluted 10× for OD_{600} measurement. To quantify curli production, 500 μl cultures were pelleted and resuspended in 15 μg/ml Congo Red for 5 min. The suspension was re-pelleted and the absorbance of the supernatant was read at 490 nm and used to determine the amount of Congo Red bound. Three sets of cultures were used for each expression study.

Curli immobilization

Filter-immobilization of curli fiber mats was performed as described previously,[44] with some modifications. Overnight cultures were vacuum-filtered through 5 μm polycarbonate membranes (Whatman® Nuclepore™, 47 mm diameter, Millipore, USA) to the point of saturation. The filters were treated with 8 M guanidinium chloride at room temperature for 15 min and washed 3× with deionized water. They were then exposed to 50 U/ml benzonase (with 2 μM $MgCl_2$) at 25°C for 1

hr, and filter-rinsed 3× with deionized water. The cleaned filters were air-dried at 50°C overnight and weighed to determine the mass of immobilized material.

SDS-PAGE

Filter-immobilized fibers were carefully scraped off membranes in a minimal volume of deionized water, resuspended in 500 µl hexafluoroisopropanol (HFIP), sonicated for 1 hr, and left to shake at room temperature for 5 hr. The HFIP was carefully evaporated under an airstream, and the dried material was resuspended in 6 M urea and sonicated to resuspend before being loaded for SDS-PAGE (200 V, 30 min).

REE sorption

8 mm discs were punched from the filters for batch binding experiments. The filter discs were rinsed with and subsequently soaked in 0.2 M HEPES buffer (pH 7) for 1 hr prior to binding. Individual and mixed REE solutions were diluted from 1000 µg/ml stocks (High Purity Standards, USA) into HEPES buffer to the desired concentrations. Filters were exposed to REE solutions in 48-well plates with gentle shaking. Metal content of the supernatant was assayed using ICP-MS (Agilent Technologies, 7700x) with samples diluted in 2% HNO_3, using indium as an internal standard. For end-point measurements, the metal solutions were removed after 30 min and the filters washed once with HEPES buffer; the wash was pooled with the metal solution for ICP-MS quantitation. Three filters were used for each sorption/desorption experiment. To test binding under various pH conditions, the pH of the HEPES buffer was adjusted accordingly and re-confirmed after metal dilution. Filter luminescence following Tb^{3+} sorption (200 µM) was imaged

on a FluorChem M Imager under UV illumination with a 525 nm emission filter. Statistical analysis was performed using the Student's t-test with a 95% confidence interval.

***Determination of binding affinity* K_D**

The binding affinity of individual lanthanides to curli-LBT4 filters was determined using a series of metal concentrations (50–250 μM). The amount of metal bound at each concentration was calculated and used to determine K_D in GraphPad Prism using global non-linear regression analysis of total and non-specific binding. Binding data from wild-type curli filters was used as the non-specific contribution. Three sets of data were fitted for each metal.

REE desorption

8 mm filter discs were first exposed to 100 μM Tb^{3+} (or mixed Ln^{3+}) for 30 min to allow adsorption. The amount adsorbed was determined as above. For desorption, filters were gently shaken with dilute HNO_3 at different pH at room temperature. The amount of Tb^{3+} recovered was determined from the supernatant using ICP-MS. The fraction or percentage of metal recovered was calculated relative to the amount of metal sorbed. For multiple sorption/desorption cycles, filters were rinsed 2× with deionized water and 2× with 0.2 M HEPES buffer (pH 7) following acid treatment, then soaked in the same buffer for 1 hr prior to metal exposure. Filters were air-dried at 50°C overnight and weighed both before the first cycle and at the end of the third cycle. Samples of the filter discs were also taken for SEM imaging.

REE sorption under flow

To study sorption under continuous flow, a 47 mm curli-LBT4 filter was enclosed in a filter holder (50 mm outer diameter, Membrane Solutions, USA). A 20 μM binary mixture of Ce^{3+} and Tb^{3+} (in 0.2 M HEPES, pH 7) was delivered to the filter holder in Teflon tubing using a peristaltic pump (MasterFlex, Cole-Parmer, USA) in single-pass at a flow rate of 0.2 ml/min. The entire apparatus (tubing and filter holder without filter) was first rinsed with 2% HNO_3, then the REE mixture to determine background metal sorption for normalization. At fixed time points, the outflow from the filter holder was sampled, and the metal concentration of each species, C, was quantified using ICP-MS. At the end of the run, the total outflow volume was measured and its metal composition quantified to calculate the total amount of each metal species adsorbed by the filters. Breakthrough was determined for $C/C_0 = 0.05$, where $C_0 = 20$ μM. Three separate runs were conducted using individual curli-LBT4 filters to ensure reproducibility of the observed binding trends.

Scanning electron microscopy

SEM images were obtained on a Zeiss Ultra Plus FE-SEM operated at 5 kV in SE2 mode. Air-dried filters were immobilized on aluminum stubs and sputter-coated with 5 nm gold for imaging.

4.3 Results

Expression and immobilization of curli fibers displaying LBT repeats

CsgA appended with LBTs of various lengths was expressed in PQN4, a previously engineered *E. coli* strain in which the entire curli operon was deleted (Table 4.1). This strain does not produce any other exopolymers besides curli that might complicate analysis of lanthanide binding. Expression of 2×- and 4×- concatemeric LBT repeats compared favorably to wild-type CsgA (wt-CsgA), as determined by a pull-down assay using the amyloid-binding Congo Red dye, but a longer 6×-LBT variant gave lower curli production and a lower cell density at the end of expression, an indicator that the variant was toxic when overexpressed (Fig. 4.1). Toxicity could be a consequence of the large size of the appended domain or the large number of negative charges introduced by acidic residues in LBT (five per repeat). Previous studies have shown that large domains exceeding 250 amino acids could be exported successfully through the curli biogenesis pathway, so long as the domain was largely unstructured or its folded structure did not exceed 2.5 nm in diameter.[56] Since the lanthanide-binding tag is unstructured in the absence of lanthanide ions,[52] it is unlikely that the size of larger concatamers was limiting expression. On the other hand, the additional charges on large LBT repeats could disrupt the electrostatic interaction between CsgA and CsgC, a periplasmic chaperone that prevents the intracellular aggregation of unsecreted CsgA.[57, 58] Rampant periplasmic aggregation of CsgA could have led to cell lysis and limited overall curli production. When the LBT sequence was modified to switch all the acidic residues to glycine (LBT*), better expression was observed for 6×-LBT*, thus the highly-charged nature of high-repeat LBT variants was likely to have compromised curli production (Fig. 4.1).

All three LBT variants formed large extracellular fiber meshes (Fig. 4.2) as observed previously with wt-CsgA expressed in the absence of CsgB and CsgF (Chapter 3). WT, LBT2 and LBT4 variants were subsequently filter-immobilized on polycarbonate membranes for REE binding studies (~1 mg biomass per 47 mm filter).

Table 4.1. Peptide sequences for the lanthanide-binding tags (LBTs) used in the study.

LBT variant	Amino acid sequence
LBT2	YIDTNNDGWIEGDELYIDTNNDGWIEGDELLA
LBT4	YIDTNNDGWIEGDELYIDTNNDGWIEGDELYIDTNNDGWIEGDELYIDTNNDGWIEGDELLA
LBT6	YIDTNNDGWIEGDELYIDTNNDGWIEGDELYIDTNNDGWIEGDELYIDTNNDGWIEGDELYIDTNNDGWIEGDELYIDTNNDGWIEGDELLA
LBT2*	YIGTNNGGWIGGGGLYIGTNNGGWIGGGGLLA
LBT4*	YIGTNNGGWIGGGGLYIGTNNGGWIGGGGLYIGTNNGGWIGGGGLYIGTNNGGWIGGGGLLA
LBT6*	YIGTNNGGWIGGGGLYIGTNNGGWIGGGGLYIGTNNGGWIGGGGLYIGTNNGGWIGGGGLYIGTNNGGWIGGGGLYIGTNNGGWIGGGGLLA

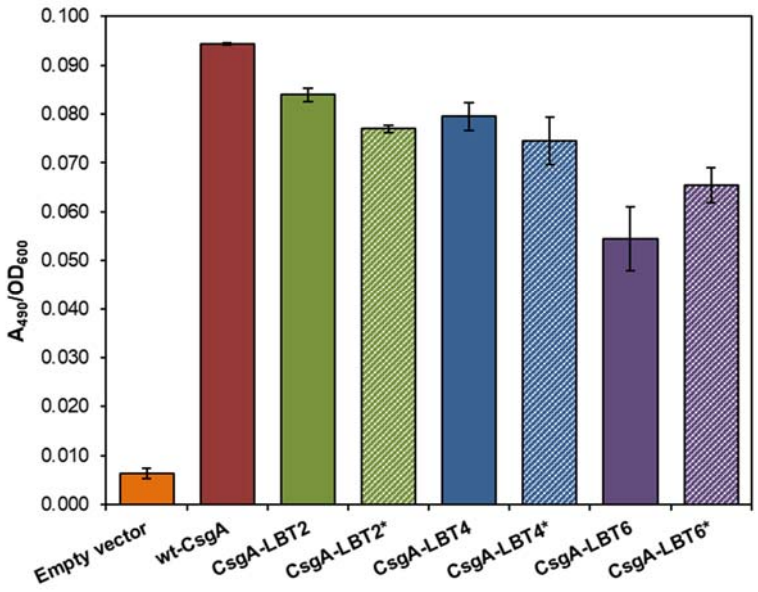

Figure 4.1. Expression of CsgA containing various concatamers of LBT, as determined by a Congo Red pull-down assay and normalized to cell density. The corresponding LBT* variants have their acidic residues switched to glycine. 2×- and 4×-LBT repeats expressed well relative to wt-CsgA, but a 6×-LBT variant showed significantly lower expression, which was partly alleviated by removing the charged residues.

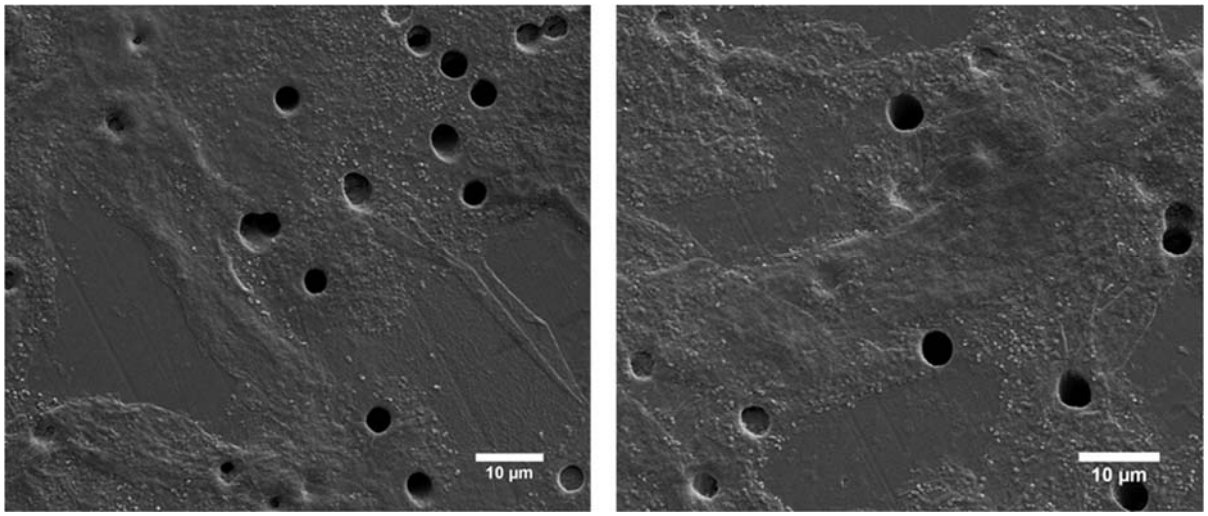

Figure 4.2. Scanning electron micrographs showing similar extensive fiber meshes formed by WT-curli (L) and curli-LBT4 (R). The meshes were filter-immobilized onto 5 µm polycarbonate membranes.

Tb^{3+} adsorption using curli-LBT filters

Batch sorption studies with the curli-LBT filters were first performed using Tb^{3+}, a critical rare earth metal and the canonical ligand for LBT. 8 mm filter discs were exposed to various concentrations of Tb^{3+}, and the quantity of metal adsorbed was determined by ICP-MS. The polycarbonate membranes bound a negligible amount of metal. Curli-LBT filters bound ~2.5× more Tb^{3+} than wt-curli filters (Fig. 4.3), with LBT4 binding more Tb^{3+} than LBT2 (~43% vs. ~36% of 200 µM Tb^{3+}). LBT4 did not give double the binding capacity of LBT2, likely because some of the LBTs were occluded and not available for binding. Maximum binding was attained within 30 min (Fig. 4.4). CsgA contains several acidic residues which could interact with metal ions, giving some baseline Tb^{3+} sorption. The addition of the LBTs increased overall binding but also added binding specificity for REEs via chelating residues. This is shown in Fig. 4.3, where modified LBT filters lacking those residues (LBT*) showed much diminished binding capacities

for Tb^{3+}. Binding specificity is further evidenced by examining the luminescent properties of the filters. The LBT contains a tryptophan antenna residue that sensitizes the luminescence of bound lanthanide ions. UV irradiation of Tb^{3+}-exposed filters showed distinctly higher luminescence for curli-LBT compared to wt-curli and curli-LBT* filters (Fig. 4.5), in correspondence with quantitative trends from ICP-MS.

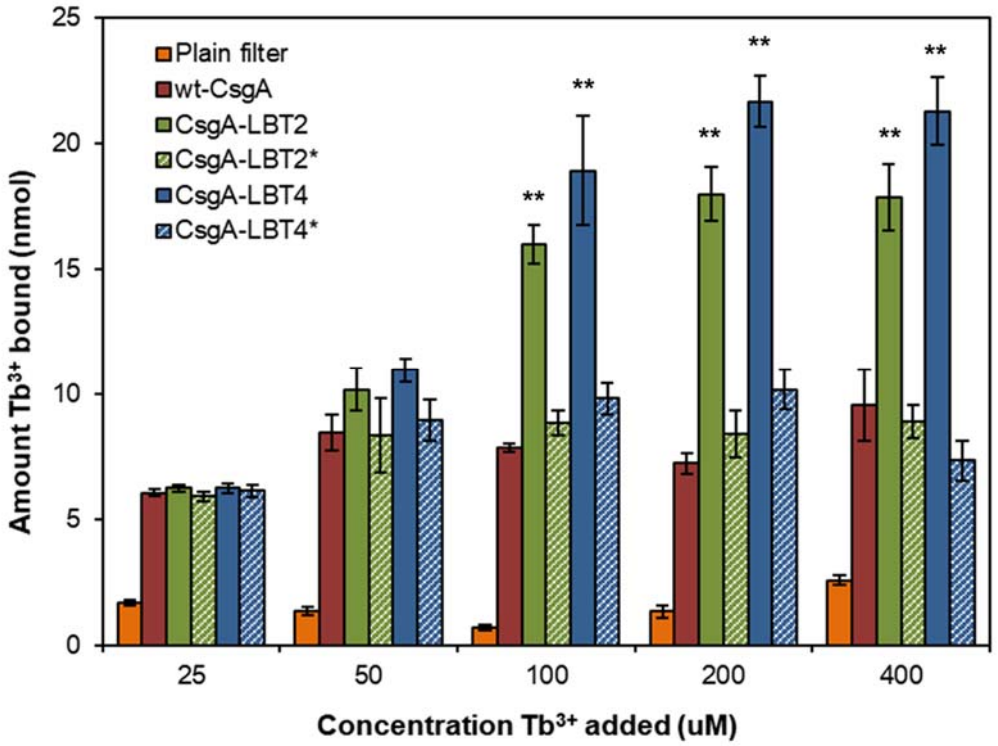

Figure 4.3. Tb^{3+} sorption to curli-LBT filters, as determined by ICP-MS. Curli-LBT filters bound ~2.5× more Tb^{3+} than wt-curli filters at high Tb^{3+} concentrations. ** represents $p < 0.01$ (relative to wt-CsgA binding).

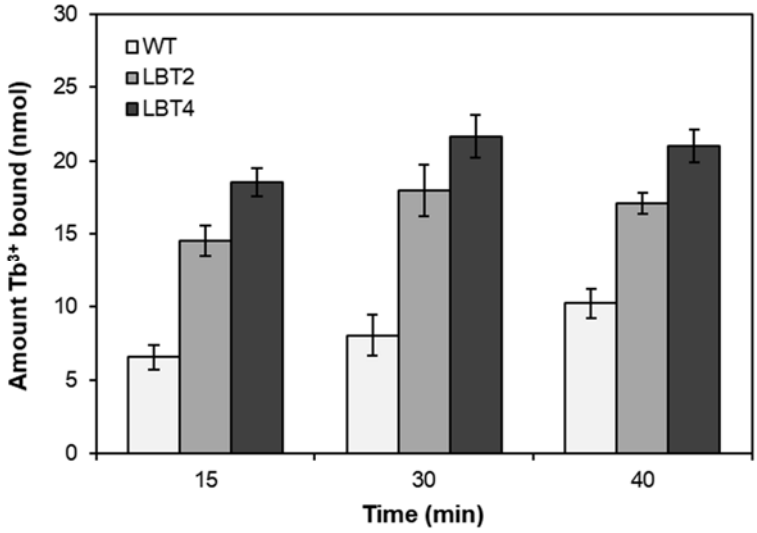

Figure 4.4. Sorption of 200 μM Tb^{3+} to curli filters over time. Sorption was complete within 30 min, and this length of exposure was used for all subsequent binding experiments.

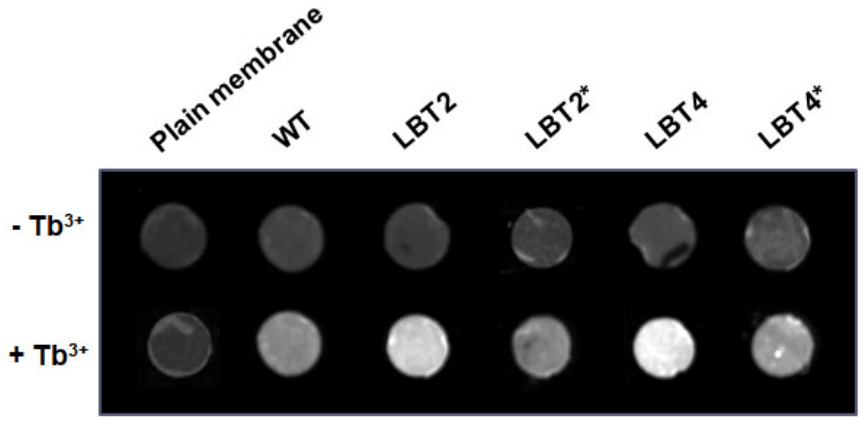

Figure 4.5. Luminesence of filters exposed to 100 μM Tb^{3+}. Consistent with quantitative binding studies, LBT2 and LBT4 filters gave the highest luminescence signals due to strong Tb^{3+}-LBT interactions. LBT2* and LBT4*, which did not contain chelating residues, gave only a low background signal comparable to wt-CsgA.

Sorption capacity peaked at 0.342 ± 0.022 mmol Tb^{3+}/g immobilized biomass for curli-LBT4 filters, which compared favorably to values of 0.01−1 mmol/g reported for cell-based biosorbents.[23, 54, 59] The calculated binding affinity for curli-LBT2 and curli-LBT4 were ~9.9 μM and 14.7 μM respectively. These values are much higher than the reported K_D for Tb^{3+} binding to purified LBT (~57 nM),[52] likely because not all the LBTs were exposed for binding following aggregation of curli fibers and immobilization of the fiber mats. Comparison of the maximum sorption of WT and Curli-LBT2 and Curli-LBT4 filters showed that 1.5 and 2.4 Tb^{3+} ions were bound per molecule of CsgA-LBT2 and CsgA-LBT4 respectively, thus not all the displayed binding tags were available for binding. Because of its higher binding capacity, curli-LBT4 filters were used for all subsequent sorption experiments.

REE extraction typically involves acid leaching, thus Tb^{3+} sorption was measured in a range of acidic conditions (pH 3−6). Higher pH was not investigated as lanthanides formed insoluble hydroxides under basic conditions. Tb^{3+} adsorption by LBT4 filters decreased rapidly at pH values below 5, and was comparable to wt-curli filters at pH 3 (Fig. 4.6). This was likely due to protonation of the chelating glutamate and aspartate residues, which have a pK_a around 3. The filters are thus most effective at pH 5−7.

Since REEs frequently coexist with other metals in ores and waste streams, we examined Tb^{3+} sorption by curli-LBT4 filters in the presence of other metal ions. Al^{3+}, Fe^{3+}, Ni^{2+} and Ca^{2+} did not significantly impact sorption of 100 μM Tb^{3+} at concentrations 10× higher, but Cu^{2+} reduced sorption by 50% (Fig. 4.7). This inhibitory effect of copper was also reported for the original LBT.[48] At concentrations 100× higher, Cu^{2+}, Al^{3+} and Fe^{3+} all led to much reduced Tb^{3+} binding. Overall, Tb^{3+} sorption to LBT4 filters was relatively unaffected by other metal ions except at much higher concentrations. This was unlike wt-curli filters, where equimolar quantities of other

metals effectively outcompeted Tb^{3+} binding (Fig. 4.8). This was further evidence of lanthanide specificity provided by the displayed LBTs.

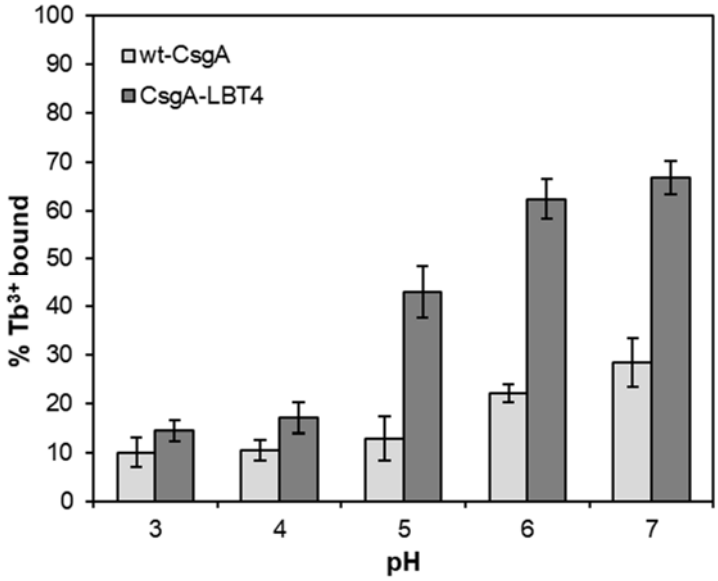

Figure 4.6. Adsorption of 100 μM Tb^{3+} by curli-LBT4 filters at different pH. Progressive protonation of the LBTs at low pH led to loss of Tb^{3+} binding. Optimal binding occurred at pH 6-7; below pH 4, the pK_a of the chelating carboxylate groups in LBTs, little binding was observed.

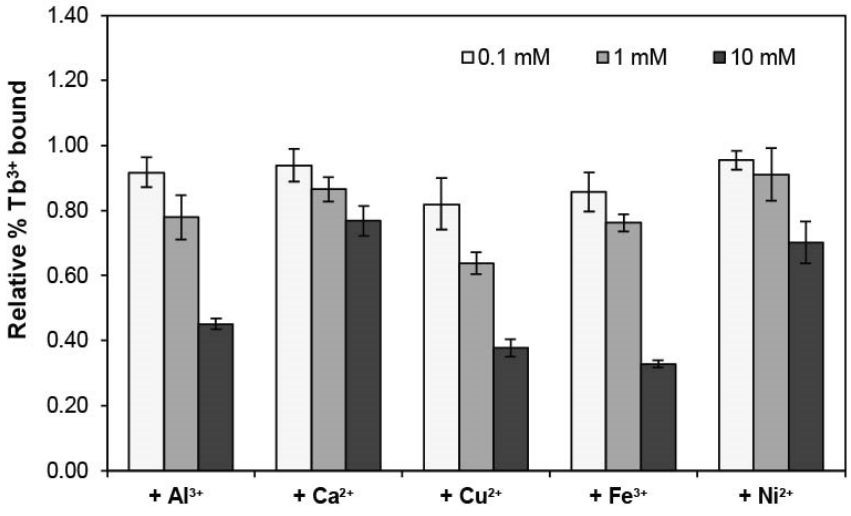

Figure 4.7. Adsorption of 100 µM Tb^{3+} by curli-LBT4 filters in the presence of other metals. Equimolar concentrations of metals (0.1 mM) did not significantly affect Tb^{3+} sorption to LBT4 filters, but sorption capacity decreased over 50% with 100× higher concentrations of Al^{3+}, Cu^{2+} and Fe^{3+}.

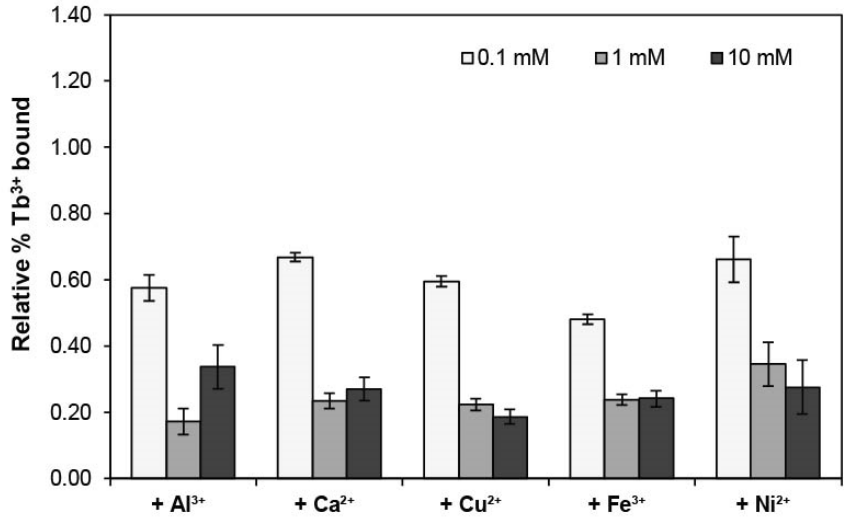

Figure 4.8. Adsorption of 100 µM Tb^{3+} by wt-Curli filters in the presence of other metals. Unlike the LBT4 filters, non-specific sorption of Tb^{3+} to WT filters was much reduced even at equimolar concentrations of competing metals.

Tb^{3+} recovery from curli-LBT filters

Desorption of sequestered Tb^{3+} from the filters was investigated using nitric acid, since low pH disrupts binding to LBT (Fig. 4.6). An initial screen of different pH (using different nitric acid concentrations) showed that complete recovery of bound Tb^{3+} was achieved at pH 2 (Fig. 4.9), and desorption was complete within 20 min (Fig. 4.10). Although organic ligands like citrate are also effective desorbents,[48, 54] they are not specific for REEs, and much higher concentrations might be necessary if other metals are also bound to the filters, potentially increasing the cost of the process. We chose to simplify desorption using an acid wash, which could also facilitate downstream REE sorting processes by not introducing additional ligands. The filters were subjected to multiple cycles of Tb^{3+} sorption/desorption, with a buffered wash following desorption to regenerate the chelating groups. There was no significant reduction in Tb^{3+} binding after three cycles (Fig. 4.11). Unlike with cell-based sorbents, where cell viability could be compromised by acid washes,[23] amyloids are more resilient to a variety of harsh environmental conditions. Curli fibers are able to fibrillate at low pH[60] and only disassemble on exposure to high concentrations of denaturants (e.g. formic acid, hexafluoroisopropanol). The dilute acid used for desorption here is unlikely to cause fiber disassembly, and indeed there was no detectable loss of mass from the filters, and the fiber mats were largely intact after three rounds of acid treatment (Fig. 4.12).

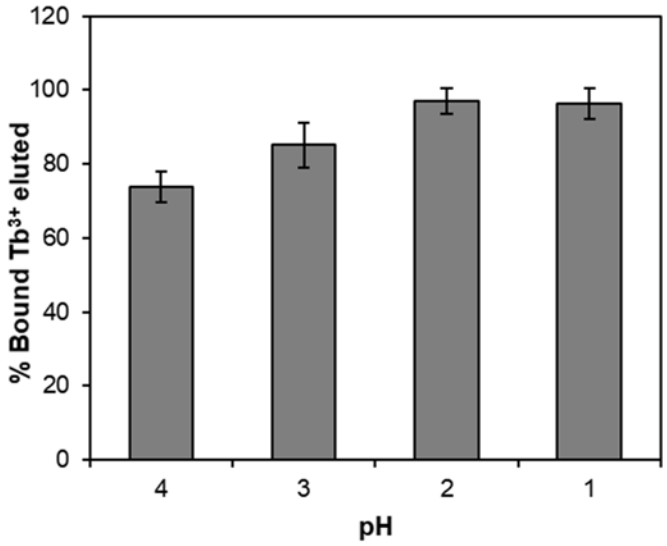

Figure 4.9. Desorption of Tb^{3+} from LBT4 filters using different pH washes. Nitric acid at pH 2 (0.01 M) was sufficient to remove nearly all the bound Tb^{3+}. All subsequent desorption experiments were performed at this pH.

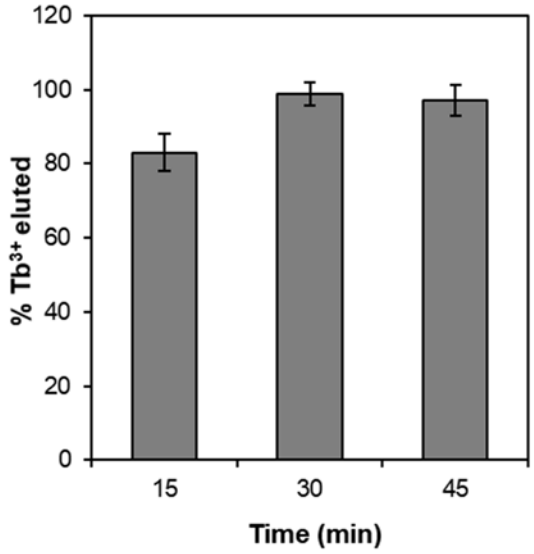

Figure 4.10. Desorption of Tb^{3+} from LBT4 filters over time with pH 2 nitric acid at room remperature. All bound Tb^{3+} was recovered within 30 min.

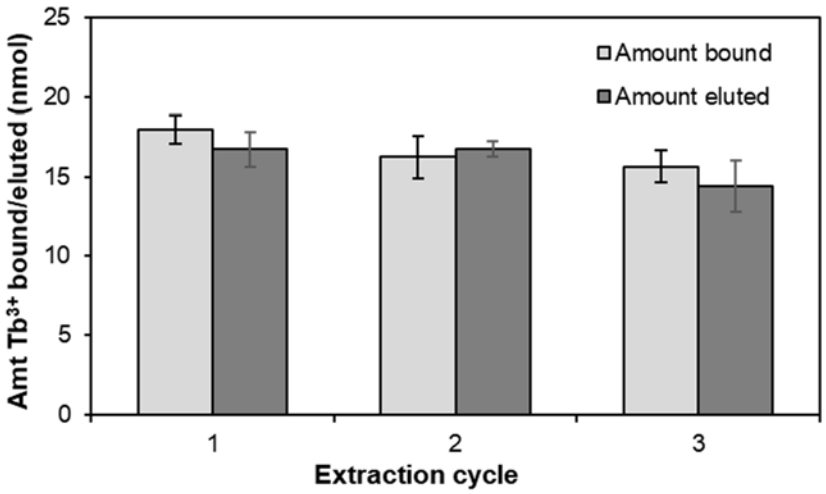

Figure 4.11. Curli-LBT4 filters can be used for multiple cycles of Tb^{3+} sorption/desorption with minimal loss of sorption capacity. 100 μM Tb^{3+} was used for sorption, and desorption was carried out with pH 2 HNO_3.

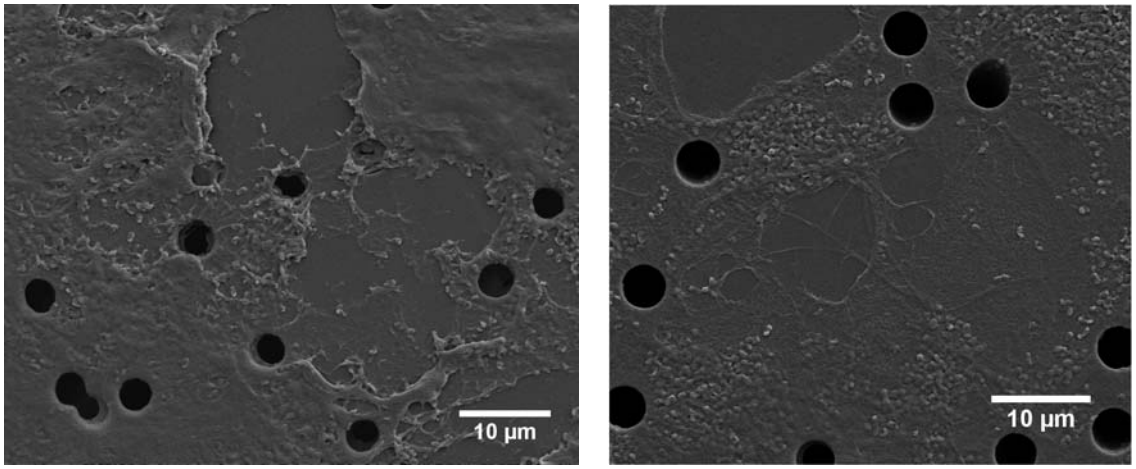

Figure 4.12. Scanning electron micrograph of LBT4 filters before (R) and after (L) three cycles of sorption-desorption, showing that the immobilized fiber mats remained largely intact even after repeated acid washes.

REE adsorption and recovery using curli-LBT filters

We next investigated if curli-LBT4 filters could be used to adsorb other REEs, using a mixed equimolar solution of 15 REEs (abbreviated Ln^{3+}). Although the lanthanides exhibit very similar physicochemical properties, there is a 20% contraction in ionic radii across the series, with a concomitant increase in Lewis acidity that favors binding of the heavier lanthanides to LBTs.[52] As shown in Fig. 4.13, curli-LBT4 filters bound the mid- to heavy lanthanides preferentially, as well as Y^{3+}, whose ionic radius is similar to that of the heavy REEs (HREEs). In contrast, no selectivity was observed for wt-curli filters. Calculated binding affinities for several of the REEs support the binding preference shown in Fig. 4.13, with Tb^{3+}, Eu^{3+} and Dy^{3+} being the strongest binding, followed by Nb^{3+} and Y^{3+}, and Ce^{3+} the weakest binding (Table 4.1). This suggests that curli-LBT filters could be used to selectively sequester most of the critical REEs, including Nb, Tb, Eu, Dy and Y. The bound Ln^{3+} could be recovered by washing with HNO_3 (Fig. 4.14).

We also examined REE adsorption from a metal mixture containing excess Al^{3+}, Ca^{2+}, Cu^{2+}, $Fe^{3+}$and Ni^{2+}, chosen to simulate waste streams from mine tailings and recycled end-of-life sources (Table 4.2).[61-66] Overall REE sorption by curli-LBT4 filters fell by ~50% in the presence of other metals, but selection for REEs improved over wt-Curli filters, for which there was negligible REE adsorption (Fig. 4.15). The LBT filters also retained their selectivity for the HREEs (Fig. 4.15).

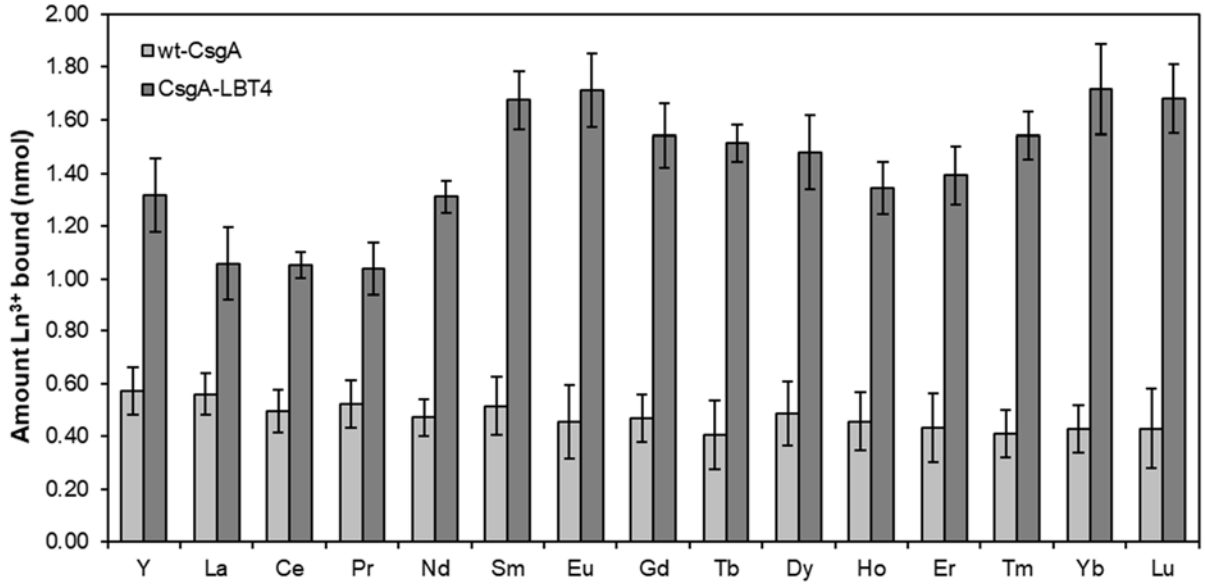

Figure 4.13. Adsorption of 100 μM mixed REEs to wt-Curli and curli-LBT4 filters. The LBT filters showed a preference for binding heavier Ln^{3+}.

Table 4.2. Binding constants of curli-LBT4 filters for individual REEs, determined by exposing various concentrations of the Ln^{3+} to the filters.

REE	K_D (μM)
Tb^{3+}	14.7 ± 6.3
Eu^{3+}	10.9 ± 5.4
Dy^{3+}	15.1 ± 6.9
Nb^{3+}	51.5 ± 14.2
Y^{3+}	54.3 ± 20.7
Ce^{3+}	284 ± 36.5

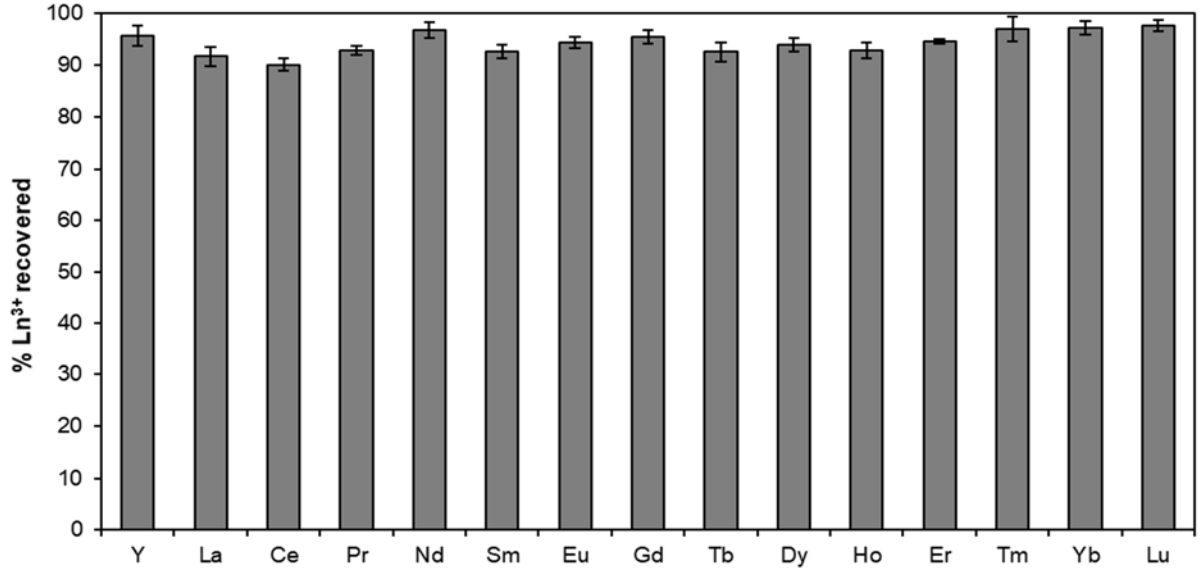

Figure 4.14. Bound Ln^{3+} could be desorbed from LBT4 filters using pH 2 nitric acid.

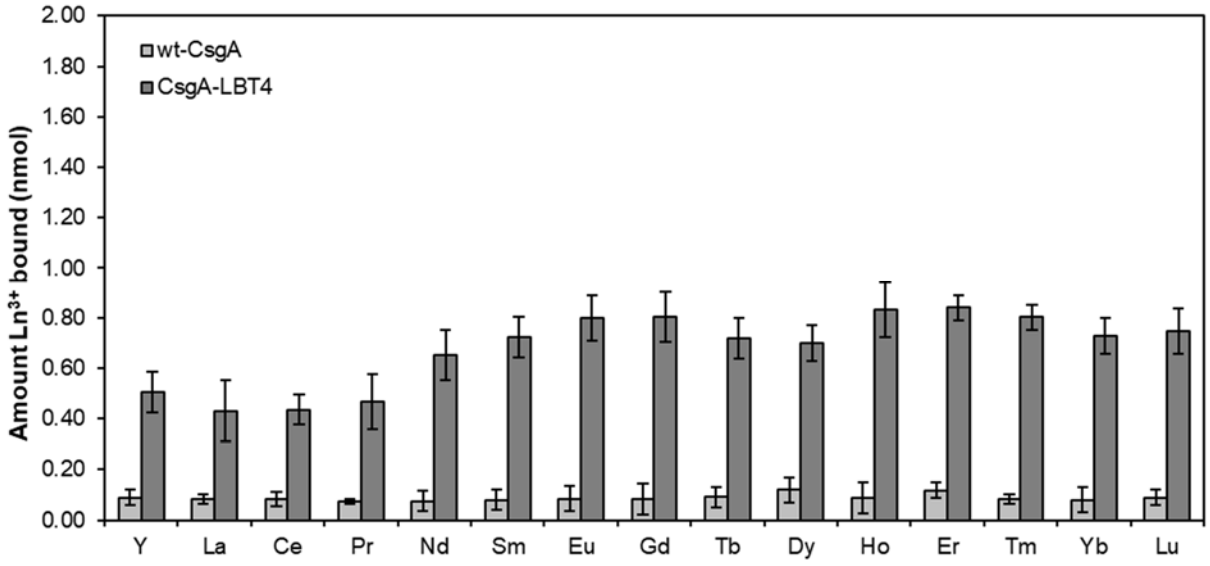

Figure 4.15. Adsorption of 100 μM mixed REEs by wt-Curli and curli-LBT4 filters in the presence of mixed metals. Although overall sorption by the LBT filters decreased by ~50%, selectivity was retained relative to wt-Curli filters.

Table 4.3. Metal composition of simulated waste stream.

Metal	Concentration (μM)
Ln^{3+}	100
Al^{3+}	1000
Ca^{2+}	10,000
Cu^{2+}	1000
Fe^{3+}	1000
Ni^{2+}	10,000

REE adsorption under flow conditions

Curli-LBT4 filters could be adapted for sorption under continuous flow, which is advantageous for REE recovery from more dilute streams. To investigate flow-based sorption, 20 μM of a binary Tb^{3+}-Ce^{3+} mixture was pumped through an encased filter without feed recycling. Breakthrough (measured at C/C_0 = 0.05) occurred earlier for Ce^{3+} (~47 min) compared to Tb^{3+} (~54 min), consistent with higher affinity of the LBTs for Tb^{3+} seen in batch sorption experiments (Fig. 4.16). There was competitive interaction between the two lanthanides, with stronger-binding Tb^{3+} ions displacing bound Ce^{3+} after the latter was saturated, leading to the observed overshoot ($C/C_0 > 1$) between 65−100 min. This was also confirmed by the different quantities of lanthanides adsorbed: 0.22 μmol Tb^{3+} compared to 0.14 μmol Ce^{3+}. Similar selectivity was not evident with wt-curli filters, where breakthrough for both lanthanides occurred at similar times, and the slopes of the breakthrough curves were more similar (Fig. 4.16).

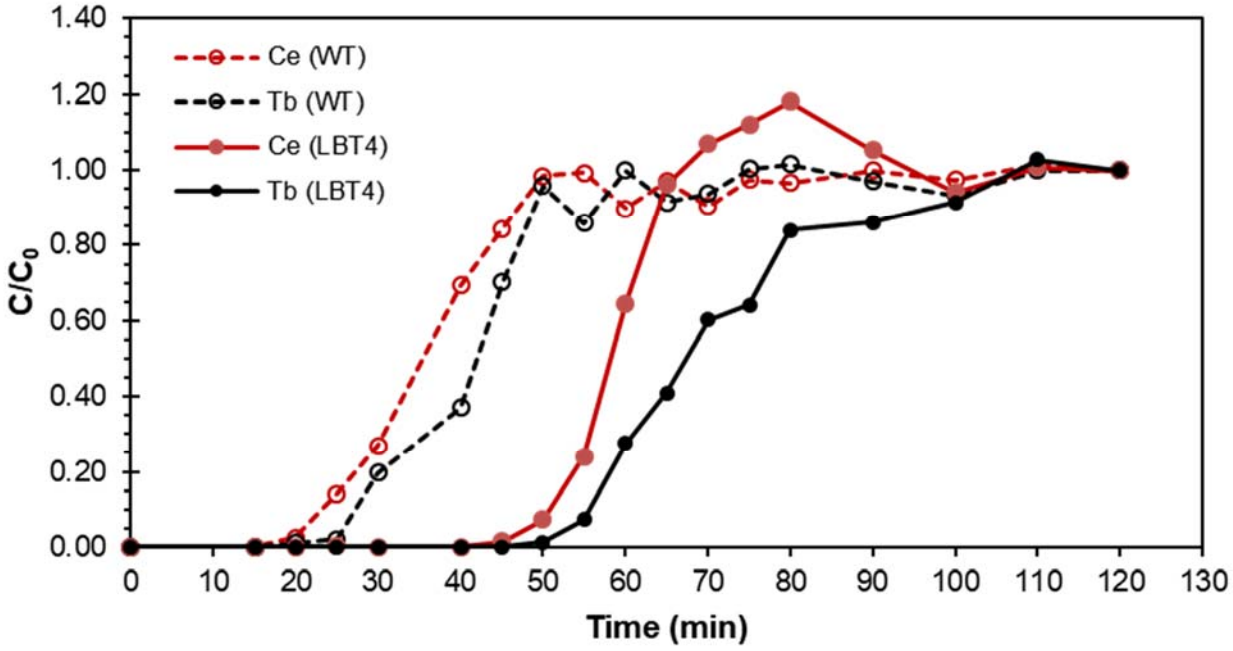

Figure 4.16. Breakthrough curves for Tb^{3+}-Ce^{3+} binary sorption to a curli-LBT4 filter under low-speed single-pass flow. C_0: 20 µM for each species; flow rate: 0.2 ml/min; biomass immobilized: 1.1 mg. Consistent with data from batch sorption, LBT4 filters displayed a higher affinity for Tb^{3+} than Ce^{3+}, as shown by the longer time to breakthrough for Tb^{3+}, the gentler slope of the Tb^{3+} curve, and the overshoot seen with Ce^{3+}, an indication of Ce^{3+} displacement by Tb^{3+}. Data shown is representative of three separate runs using three different sets of filters.

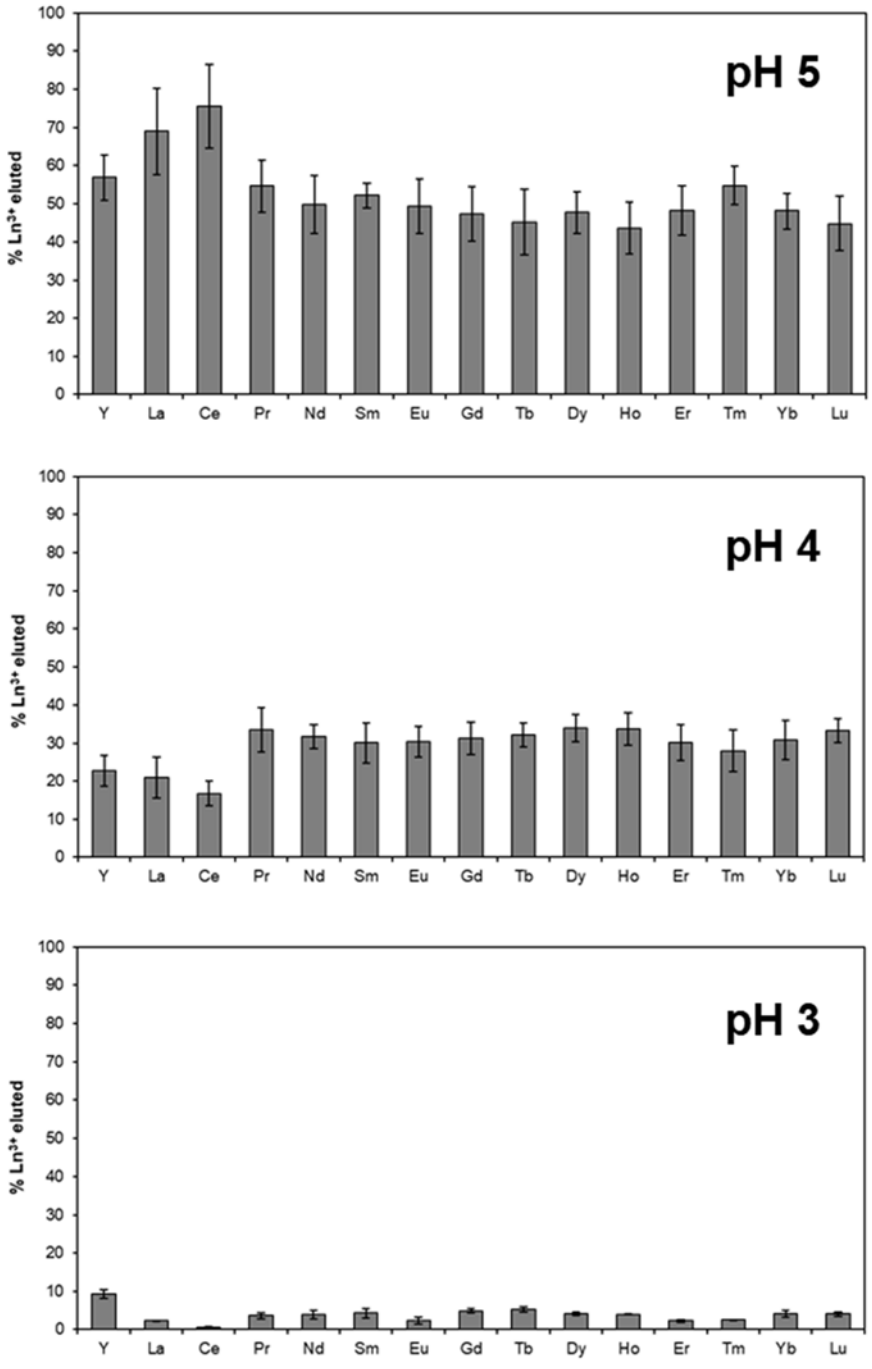

Figure 4.17. Ln^{3+} desorption from curli-LBT filters using a sequential series of acid washes. A proportionally larger amount of the lighter lanthanides (La, Ce) was eluted at higher pH due to their lower affinity to the LBTs.

4.4 Discussion

The rare earth metals are indispensable to much of modern industry and future sustainable technologies, hence the recent push towards green methods of enriching and separating them to reduce the environmental cost of metal processing. A promising approach is the use of microorganisms and microbe-derived materials for biosorption, which has shown good efficacy in bench-scale operations using pure lanthanides.[17, 18, 28, 54, 59] However, industrial application could be hampered by several shortcomings, including the non-selective nature of many biosorbents, leading to unpredictable performance in the presence of contaminating metals; costs associated with maintaining and operating large microbial cultures; and the ability to retrieve the metals while minimizing destruction of the sorbent. Lanthanide-binding peptides offer a way to greatly improve binding selectivity, but it could be a challenge displaying them at high density in a cost-effective and scalable manner.

Our targeted biosorption strategy using genetically engineered bacterial amyloids resolves several of these issues simultaneously. Presentation of LBTs on curli fibers allows high-density extracellular display of REE-specific binding moieties without the need for peptide purification or chemical conjugation. The fibers aggregate into extended networks that could be purified away from the cells via a simple filtration set-up, allowing the bacteria to be reused for further material production without being tied up in metal binding. The curli-based filters are also more robust to treatment conditions that might compromise the viability of cell-based sorbents or the structural integrity of other biopolymeric materials. The curli-LBT filters showed selective REE binding in the presence of competing metals, with a preference for the heavier lanthanides, including Tb, Nd, Eu and Dy—some of the most critical REEs. Metal recovery was complete after a short wash with dilute acid, allowing the filters to be reused multiple times with little loss of efficiency. This simple

desorption step, which exploits the chemical resilience of amyloids compared to cells or other biopolymers, avoids the need for more expensive chelators. The filters can be dried for storage and are easier to handle than whole-cell sorbents.

The sorption capacity of the curli-LBT4 filters was ~0.3 mmol Ln^{3+}/g immobilized biomass when used for batch sorption of pure lanthnides. This value is similar to that reported for *P. aeruginosa* and a range of other bacteria and algae (0.01−1 mmol/g),[23, 59, 67, 68] and better than *Caulobacter crescentus* with surface-displayed LBTs reported by Park *et al* (~0.06 mmol/g).[54] It is also comparable to cellulose phosphate and carboxymethylcellulose-based materials,[21] and DNA-based sorbents derived from salmon milt,[69] although ion exchange resins could potentially offer capacities in excess of ten-fold higher.[70, 71] Further improvement in binding capacity is currently limited by the curli biogenesis pathway, as the attachment of longer LBT repeats led to reduced cell viability during protein expression (Fig. 4.1). However, improvements in curli production—through the use of a more optimal operon and optimized growth conditions in a fermenter—as well as the use of materials that offer greater immobilization capacities (e.g. microporous foam or woven fiber meshes) could further increase the adsorption capacity of curli-LBT-based filters. The specific interaction between rare earth ions and LBTs also offers binding specificity not present in most other biosorbents, especially for adsorption from complex metal mixtures.

From our batch experiments, the curli-LBT filters are best suited for sorption at REE concentrations above 50 μM (>1 ppm), where REE-selective binding is more significant than non-specific background sorption (Fig. 4.3). Such concentrations are often found in bauxite residue (red mud), phosphogypsum, and metallurgical slag derived from recycling waste electric and electronic equipment.[72] In waste streams where REE concentrations are more dilute (e.g. acid

mine drainage, industrial wastewater), preliminary treatment processes often result in precipitates or slurries with enriched REE concentrations.[65, 73-78] Alternatively, the use of a flow-based adsorption system could offer higher binding efficiencies for low-concentration feed streams (Fig. 4.16). An important concern is the composition of other metals in the REE feed, which could reduce REE sorption capacity if they are present in significant quantities (Fig. 4.15). In such instances, it might be necessary to include a pre-treatment step (e.g. oxalate precipitation) to first enrich the REEs.[79]

The curli-LBT filters favored binding of HREEs (Fig. 4.13). Selective recovery of the various REEs could potentially be achieved by rinsing with a gradient of low pH, as has recently been reported by Bonificio *et al.* with lanthanides bound to the surface of *Roseobacter* sp. AzwK-3b.[28] Preliminary studies using a sequence of acidic washes (pH 5, 4, 3) suggested that the lightest lanthanides (La, Ce) eluted at a higher pH and could thus be enriched relative to the heavier lanthanides in a pH gradient wash (Fig. 4.17), although the resolution was not sufficient for proper separation. Greater REE selectivity could also be attained by developing other lanthanide-binding peptides with different affinities for the various REEs,[80, 81]and incorporating a mixture of these peptides on the same filter. For the latter, cells expressing different curli-LBT variants could be co-cultured, or different cultures could be mixed post-expression prior to filtration.[39, 42]

Biofilms have long been utilized as passive sorption vessels to remove toxic species from wastewater, but as the focus of waste management turns towards resource recovery in addition to conventional remediation,[85] there are potentially more lucrative niches which biofilm-based technologies can fill, provided they could be more selective in their binding targets. Here we have demonstrated one general approach to introducing greater selectivity, via the genetic modification of protein nanofibers in the extracellular matrix of biofilms to display binding tags. Our approach

complements existing approaches based on cell surface modification,[54, 86] but is advantageous because it treats the cells as foundries for the continued production of biosorbent, rather than as end-point sorbent products. Filters derived from the engineered fibers showed utility in the selective separation of rare earth metals from complex mixtures in both batch and continuous operations; further optimization of our bench-scale experiments could potentially increase separation efficiency and provide greater resolution for the recovery of the different lanthanides. Overall, our results establish the potential of engineered biofilm-derived materials as biotechnological tools for selective separations processes.

4.6 References

[1] Alonso, E., Sherman, A. M., Wallington, T. J., Everson, M. P., Field, F. R., Roth, R., and Kirchain, R. E. (2012) Evaluating Rare Earth Element Availability: A Case with Revolutionary Demand from Clean Technologies, *Environmental Science & Technology 46*, 3406-3414.

[2] Commission, E. (2014) Critical Raw Materials for the EU: Report of the Ad Hoc Working Group on Defining Critical Raw Materials.

[3] Energy, U. S. D. o. (2011) Critical Materials Strategy Report.

[4] McLellan, C. B., Corder, D. G., and Ali, H. S. (2013) Sustainability of Rare Earths—An Overview of the State of Knowledge, *Minerals 3*.

[5] Xie, F., Zhang, T. A., Dreisinger, D., and Doyle, F. (2014) A critical review on solvent extraction of rare earths from aqueous solutions, *Minerals Engineering 56*, 10-28.

[6] Jha, M. K., Kumari, A., Panda, R., Rajesh Kumar, J., Yoo, K., and Lee, J. Y. (2016) Review on hydrometallurgical recovery of rare earth metals, *Hydrometallurgy 165*, 2-26.

[7] Binnemans, K., Jones, P. T., Blanpain, B., Van Gerven, T., Yang, Y., Walton, A., and Buchert, M. (2013) Recycling of rare earths: a critical review, *Journal of Cleaner Production 51*, 1-22.

[8] Kim, D., Powell, L. E., Delmau, L. H., Peterson, E. S., Herchenroeder, J., and Bhave, R. R. (2015) Selective Extraction of Rare Earth Elements from Permanent Magnet Scraps with Membrane Solvent Extraction, *Environmental Science & Technology 49*, 9452-9459.

[9] Tsamis, A., and Coyne, M. (2015) Recovery of Rare Earths from Electronic wastes: An opportunity for High-Tech SMEs, European Parliament Committee on Industry, Research and Energy.

[10] Gadd, G. M. (2010) Metals, minerals and microbes: geomicrobiology and bioremediation, *Microbiology (Reading, England) 156*, 609-643.

[11] Tay, P. K. R., Nguyen, P. Q., and Joshi, N. S. (2017) A Synthetic Circuit for Mercury Bioremediation Using Self-Assembling Functional Amyloids, *ACS Synthetic Biology*.

[12] Gupta, S., and Singh, D. (2017) Role of Genetically Modified Microorganisms in Heavy Metal Bioremediation, In *Advances in Environmental Biotechnology* (Kumar, R., Sharma, A. K., and Ahluwalia, S. S., Eds.), pp 197-214, Springer Singapore, Singapore.

[13] Perpetuo, E. A., Souza, C. B., and Nascimento, C. A. O. (2011) Engineering Bacteria for Bioremediation, Progress in Molecular and Environmental Bioengineering - From Analysis and Modeling to Technology Applications, (Carpi, P. A., Ed.), InTech.

[14] Pol, A., Barends, T. R. M., Dietl, A., Khadem, A. F., Eygensteyn, J., Jetten, M. S. M., and Op den Camp, H. J. M. (2014) Rare earth metals are essential for methanotrophic life in volcanic mudpots, *Environmental Microbiology 16*, 255-264.

[15] Skovran, E., and Martinez-Gomez, N. C. (2015) Just add lanthanides, *Science 348*, 862.

[16] Wehrmann, M., Billard, P., Martin-Meriadec, A., Zegeye, A., and Klebensberger, J. (2017) Functional Role of Lanthanides in Enzymatic Activity and Transcriptional Regulation of Pyrroloquinoline Quinone-Dependent Alcohol Dehydrogenases in Pseudomonas putida KT2440, *mBio 8*.

[17] Andres, Y., Texier, A. C., and Le Cloirec, P. (2003) Rare earth elements removal by microbial biosorption: A review, *Environ. Technol. 24*, 1367-1375.

[18] Moriwaki, H., and Yamamoto, H. (2013) Interactions of microorganisms with rare earth ions and their utilization for separation and environmental technology, *Applied Microbiology and Biotechnology 97*, 1-8.

[19] Takahashi, Y., Châtellier, X., Hattori, K. H., Kato, K., and Fortin, D. (2005) Adsorption of rare earth elements onto bacterial cell walls and its implication for REE sorption onto natural microbial mats, *Chemical Geology 219*, 53-67.

[20] Ngwenya, B. T., Mosselmans, J. F. W., Magennis, M., Atkinson, K. D., Tourney, J., Olive, V., and Ellam, R. M. (2009) Macroscopic and spectroscopic analysis of lanthanide adsorption to bacterial cells, *Geochimica Et Cosmochimica Acta 73*, 3134-3147.

[21] Takahashi, Y., Yamamoto, M., Yamamoto, Y., and Tanaka, K. (2010) EXAFS study on the cause of enrichment of heavy REEs on bacterial cell surfaces, *Geochimica et Cosmochimica Acta 74*, 5443-5462.

[22] Moriwaki, H., Masuda, R., Yamazaki, Y., Horiuchi, K., Miyashita, M., Kasahara, J., Tanaka, T., and Yamamoto, H. (2016) Application of Freeze-Dried Powders of Genetically Engineered Microbial Strains as Adsorbents for Rare Earth Metal Ions, *ACS Applied Materials & Interfaces 8*, 26524-26531.

[23] Philip, L., Iyengar, L., and Venkobachar, C. (2000) Biosorption of U, La, Pr, Nd, Eu and Dy by Pseudomonas aeruginosa, *Journal of Industrial Microbiology and Biotechnology 25*, 1-7.

[24] Texier, A. C., Andrès, Y., Faur-Brasquet, C., and Le Cloirec, P. (2002) Fixed-bed study for lanthanide (La, Eu, Yb) ions removal from aqueous solutions by immobilized Pseudomonas aeruginosa: experimental data and modelization, *Chemosphere 47*, 333-342.

[25] Ozaki, T., Gillow, J., Francis, A., Kimura, T., Ohnuki, T., and Yoshida, Z. (2002) Association of Eu(III) and Cm(III) with Bacillus subtilis and Halobacterium salinarum, *Journal of Nuclear Science and Technology 39*, 950-953.

[26] Texier, A. C., Andrès, Y., and Cloirec, P. L. (1997) Selective Biosorption of Lanthanide (La, Eu) Ions by Mycobacterium Smegmatis, *Environ. Technol. 18*, 835-841.

[27] Hosomomi, Y., Baba, Y., Kubota, F., Kamiya, N., and Goto, M. (2013) Biosorption of Rare Earth Elements by Escherichia coli, *J. Chem. Eng. Jpn. 46*, 450-454.

[28] Bonificio, W. D., and Clarke, D. R. (2016) Rare-Earth Separation Using Bacteria, *Environmental Science & Technology Letters 3*, 180-184.

[29] Texier, A. C., Andrès, Y., and Le Cloirec, P. (2000) Selective biosorption of lanthanide (La, Eu, Yb) ions by an immobilized bacterial biomass, *Water Science and Technology 42*, 91.

[30] Dash, H. R., and Das, S. (2016) Interaction between mercuric chloride and extracellular polymers of biofilm-forming mercury resistant marine bacterium Bacillus thuringiensis PW-05, *RSC Advances 6*, 109793-109802.

[31] Upadhyay, A., Kochar, M., Rajam, M. V., and Srivastava, S. (2017) Players over the Surface: Unraveling the Role of Exopolysaccharides in Zinc Biosorption by Fluorescent Pseudomonas Strain Psd, *Frontiers in Microbiology 8*.

[32] Zhang, P., Chen, Y. P., Peng, M. W., Guo, J. S., Shen, Y., Yan, P., Zhou, Q. H., Jiang, J., and Fang, F. (2017) Extracellular polymeric substances dependence of surface interactions of Bacillus subtilis with Cd2+ and Pb2+: An investigation combined with surface plasmon resonance and infrared spectra, *Colloids and Surfaces B-Biointerfaces 154*, 357-364.

[33] Ueshima, M., Ginn, B. R., Haack, E. A., Szymailowski, J. E. S., and Fein, F. B. (2008) Cd adsorption onto Pseudomonas putida in the presence and absence of extracellular polymeric substances, *Geochimica Et Cosmochimica Acta 72*, 5885-5895.

[34] Vijayaraghavan, K., Sathishkumar, M., and Balasubramanian, R. (2010) Biosorption of Lanthanum, Cerium, Europium, and Ytterbium by a Brown Marine Alga, Turbinaria Conoides, *Industrial & Engineering Chemistry Research 49*, 4405-4411.

[35] Wang, F., Zhao, J., Pan, F., Zhou, H., Yang, X., Li, W., and Liu, H. (2013) Adsorption Properties toward Trivalent Rare Earths by Alginate Beads Doping with Silica, *Industrial & Engineering Chemistry Research 52*, 3453-3461.

[36] Wang, S., Hamza, M. F., Vincent, T., Faur, C., and Guibal, E. (2017) Praseodymium sorption on Laminaria digitata algal beads and foams, *Journal of Colloid and Interface Science 504*, 780-789.

[37] Wang, F., Zhao, J., Wei, X., Huo, F., Li, W., Hu, Q., and Liu, H. (2014) Adsorption of rare earths (III) by calcium alginate–poly glutamic acid hybrid gels, *Journal of Chemical Technology & Biotechnology 89*, 969-977.

[38] Chen, A. Y., Deng, Z., Billings, A. N., Seker, U. O. S., Lu, M. Y., Citorik, R. J., Zakeri, B., and Lu, T. K. (2014) Synthesis and patterning of tunable multiscale materials with engineered cells, *Nature materials 13*, 515-523.

[39] Nguyen, P. Q., Botyanszki, Z., Tay, P. K. R., and Joshi, N. S. (2014) Programmable biofilm-based materials from engineered curli nanofibres, *5*, 4945.

[40] Zhong, C., Gurry, T., Cheng, A. A., Downey, J., Deng, Z., Stultz, C. M., and Lu, T. K. (2014) Strong underwater adhesives made by self-assembling multi-protein nanofibres, *Nat Nano 9*, 858-866.

[41] Botyanszki, Z., Tay, P. K. R., Nguyen, P. Q., Nussbaumer, M. G., and Joshi, N. S. (2015) Engineered catalytic biofilms: Site-specific enzyme immobilization onto E. coli curli nanofibers, *Biotechnology and Bioengineering 112*, 2016-2024.

[42] Nussbaumer, M. G., Nguyen, P. Q., Tay, P. K. R., Naydich, A., Hysi, E., Botyanszki, Z., and Joshi, N. S. (2017) Bootstrapped biocatalysis: biofilm-derived materials as reversibly functionalizable multi-enzyme surfaces, *ChemCatChem*, n/a-n/a.

[43] Seker, U. O. S., Chen, A. Y., Citorik, R. J., and Lu, T. K. (2017) Synthetic Biogenesis of Bacterial Amyloid Nanomaterials with Tunable Inorganic–Organic Interfaces and Electrical Conductivity, *ACS Synthetic Biology 6*, 266-275.

[44] Dorval Courchesne, N.-M., Duraj-Thatte, A., Tay, P. K. R., Nguyen, P. Q., and Joshi, N. S. (2017) Scalable Production of Genetically Engineered Nanofibrous Macroscopic Materials via Filtration, *ACS Biomaterials Science & Engineering 3*, 733-741.

[45] Barthelmes, D., Granz, M., Barthelmes, K., Allen, K. N., Imperiali, B., Prisner, T., and Schwalbe, H. (2015) Encoded loop-lanthanide-binding tags for long-range distance measurements in proteins by NMR and EPR spectroscopy, *Journal of Biomolecular Nmr 63*, 275-282.

[46] Barthelmes, K., Reynolds, A. M., Peisach, E., Jonker, H. R. A., DeNunzio, N. J., Allen, K. N., Imperiali, B., and Schwalbe, H. (2011) Engineering Encodable Lanthanide-Binding Tags into Loop Regions of Proteins, *Journal of the American Chemical Society 133*, 808-819.

[47] Daughtry, K. D., Martin, L. J., Sarraju, A., Imperiali, B., and Allen, K. N. (2012) Tailoring Encodable Lanthanide-Binding Tags as MRI Contrast Agents, *Chembiochem 13*, 2567-2574.

[48] Franz, K. J., Nitz, M., and Imperiali, B. (2003) Lanthanide-binding tags as versatile protein coexpression probes, *Chembiochem 4*, 265-271.

[49] Martin, L. J., Hahnke, M. J., Nitz, M., Wohnert, J., Silvaggi, N. R., Allen, K. N., Schwalbe, H., and Imperiali, B. (2007) Double-lanthanide-binding tags: Design, photophysical properties, and NMR applications, *Journal of the American Chemical Society 129*, 7106-7113.

[50] Sculimbrene, B. R., and Imperiali, B. (2006) Lanthanide-binding tags as luminescent probes for studying protein interactions, *Journal of the American Chemical Society 128*, 7346-7352.

[51] Silvaggi, N. R., Martin, L. J., Schwalbe, H., Imperiali, B., and Allen, K. N. (2007) Double-lanthanide-binding tags for macromolecular crystallographic structure determination, *Journal of the American Chemical Society 129*, 7114-7120.

[52] Nitz, M., Sherawat, M., Franz, K. J., Peisach, E., Allen, K. N., and Imperiali, B. (2004) Structural Origin of the High Affinity of a Chemically Evolved Lanthanide-Binding Peptide, *Angewandte Chemie International Edition 43*, 3682-3685.

[53] Liang, H., Deng, X., Bosscher, M., Ji, Q., Jensen, M. P., and He, C. (2013) Engineering Bacterial Two-Component System PmrA/PmrB to Sense Lanthanide Ions, *Journal of the American Chemical Society 135*, 2037-2039.

[54] Park, D. M., Reed, D. W., Yung, M. C., Eslamimanesh, A., Lencka, M. M., Anderko, A., Fujita, Y., Riman, R. E., Navrotsky, A., and Jiao, Y. (2016) Bioadsorption of Rare Earth Elements through Cell Surface Display of Lanthanide Binding Tags, *Environmental Science & Technology 50*, 2735-2742.

[55] Bolisetty, S., and Mezzenga, R. (2016) Amyloid–carbon hybrid membranes for universal water purification, *Nat Nano 11*, 365-371.

[56] Van Gerven, N., Goyal, P., Vandenbussche, G., De Kerpel, M., Jonckheere, W., De Greve, H., and Remaut, H. (2014) Secretion and functional display of fusion proteins through the curli biogenesis pathway, *Molecular microbiology 91*, 1022-1035.

[57] Evans, M. L., Chorell, E., Taylor, J. D., Aden, J., Gotheson, A., Li, F., Koch, M., Sefer, L., Matthews, S. J., Wittung-Stafshede, P., Almqvist, F., and Chapman, M. R. (2015) The bacterial curli system possesses a potent and selective inhibitor of amyloid formation, *Molecular cell 57*, 445-455.

[58] Taylor, J. D., Hawthorne, W. J., Lo, J., Dear, A., Jain, N., Meisl, G., Andreasen, M., Fletcher, C., Koch, M., Darvill, N., Scull, N., Escalera-Maurer, A., Sefer, L., Wenman, R., Lambert, S., Jean, J., Xu, Y., Turner, B., Kazarian, S. G., Chapman, M. R., Bubeck, D., de Simone, A., Knowles, T. P., and Matthews, S. J. (2016) Electrostatically-guided inhibition of Curli amyloid nucleation by the CsgC-like family of chaperones, *Scientific reports 6*, 24656.

[59] Tsuruta, T. (2007) Accumulation of Rare Earth Elements in Various Microorganisms, *Journal of Rare Earths 25*, 526-532.

[60] Dueholm, M. S., Nielsen, S. B., Hein, K. L., Nissen, P., Chapman, M., Christiansen, G., Nielsen, P. H., and Otzen, D. E. (2011) Fibrillation of the Major Curli Subunit CsgA under a Wide Range of Conditions Implies a Robust Design of Aggregation, *Biochemistry 50*, 8281-8290.

[61] Gergoric, M., Ekberg, C., Foreman, M. R. S. J., Steenari, B.-M., and Retegan, T. (2017) Characterization and Leaching of Neodymium Magnet Waste and Solvent Extraction of the Rare-Earth Elements Using TODGA, *Journal of Sustainable Metallurgy 3*, 638-645.

[62] Tunsu, C., Petranikova, M., Gergorić, M., Ekberg, C., and Retegan, T. (2015) Reclaiming rare earth elements from end-of-life products: A review of the perspectives for urban mining using hydrometallurgical unit operations, *Hydrometallurgy 156*, 239-258.

[63] Yang, Y., Walton, A., Sheridan, R., Güth, K., Gauß, R., Gutfleisch, O., Buchert, M., Steenari, B.-M., Van Gerven, T., Jones, P. T., and Binnemans, K. (2017) REE Recovery from End-of-Life NdFeB Permanent Magnet Scrap: A Critical Review, *Journal of Sustainable Metallurgy 3*, 122-149.

[64] Ayora, C., Macías, F., Torres, E., Lozano, A., Carrero, S., Nieto, J.-M., Pérez-López, R., Fernández-Martínez, A., and Castillo-Michel, H. (2016) Recovery of Rare Earth Elements and Yttrium from Passive-Remediation Systems of Acid Mine Drainage, *Environmental Science & Technology 50*, 8255-8262.

[65] Stewart, B. W., Capo, R. C., Hedin, B. C., and Hedin, R. S. (2017) Rare earth element resources in coal mine drainage and treatment precipitates in the Appalachian Basin, USA, *International Journal of Coal Geology 169*, 28-39.

[66] Bandara, H. M. D., Field, K. D., and Emmert, M. H. (2016) Rare earth recovery from end-of-life motors employing green chemistry design principles, *Green Chemistry 18*, 753-759.

[67] Ilyas, S., and Lee, J.-c. (2014) Biometallurgical Recovery of Metals from Waste Electrical and Electronic Equipment: a Review, *ChemBioEng Reviews 1*, 148-169.

[68] Dodson, J. R., Parker, H. L., Munoz Garcia, A., Hicken, A., Asemave, K., Farmer, T. J., He, H., Clark, J. H., and Hunt, A. J. (2015) Bio-derived materials as a green route for precious & critical metal recovery and re-use, *Green Chemistry 17*, 1951-1965.

[69] Takahashi, Y., Kondo, K., Miyaji, A., Watanabe, Y., Fan, Q., Honma, T., and Tanaka, K. (2014) Recovery and Separation of Rare Earth Elements Using Salmon Milt, *PLOS ONE 9*, e114858.

[70] Bobkova, L. A., Skvortsova, L. N., Naumova, L. B., and Kashkan, G. V. (2015) Ion-Exchange Separation and Concentration of Ions of Rare-Earth Elements on Fibrous Sorbents, *Key Engineering Materials 670*, 270-275.

[71] Kołodyńska, D., and Hubicki, Z. (2012) Investigation of Sorption and Separation of Lanthanides on the Ion Exchangers of Various Types, In *Ion Exchange Technologies* (Kilislioğlu, A., Ed.), p Ch. 06, InTech, Rijeka.

[72] Binnemans, K., Jones, P. T., Blanpain, B., Van Gerven, T., and Pontikes, Y. (2015) Towards zero-waste valorisation of rare-earth-containing industrial process residues: a critical review, *Journal of Cleaner Production 99*, 17-38.

[73] Grauch, R. I., Verplanck, P. L., Seeger, C. M., Budahn, J. R., and Van Gosen, B. S. (2010) Chemistry of Selected Core Samples, Concentrate, Tailings, and Tailings Pond Waters: Pea Ridge Iron (-Lanthanide-Gold) Deposit, Washington County, Missouri, p 15, U.S. Geological Survey.

[74] Zhao, F., Cong, Z., Sun, H., and Ren, D. (2007) The geochemistry of rare earth elements (REE) in acid mine drainage from the Sitai coal mine, Shanxi Province, North China, *International Journal of Coal Geology 70*, 184-192.

[75] Jannesar Malakooti, S., Shafaei Tonkaboni, S. Z., Noaparast, M., Doulati Ardejani, F., and Naseh, R. (2014) Characterisation of the Sarcheshmeh copper mine tailings, Kerman province, southeast of Iran, *Environmental Earth Sciences 71*, 2267-2291.

[76] Soltani, N., Moore, F., Keshavarzi, B., and Sharifi, R. (2014) Geochemistry of Trace Metals and Rare Earth Elements in Stream Water, Stream Sediments and Acid Mine Drainage from Darrehzar Copper Mine, Kerman, Iran, *Water Quality, Exposure and Health 6*, 97-114.

[77] Sahoo, P., Tripathy, S., Sk, Equeenuddin, S., and Panigrahi, M. (2012) *Geochemical characteristics of coal mine discharge vis-à-vis behavior of rare earth elements at Jaintia Hills coalfield, northeastern India*.

[78] Li, X., and Wu, P. (2017) Geochemical characteristics of dissolved rare earth elements in acid mine drainage from abandoned high-As coal mining area, southwestern China, *Environmental Science and Pollution Research 24*, 20540-20555.

[79] Chi, R., and Xu, Z. (1999) A solution chemistry approach to the study of rare earth element precipitation by oxalic acid, *Metallurgical and Materials Transactions B 30*, 189-195.

[80] Hatanaka, T., Matsugami, A., Nonaka, T., Takagi, H., Hayashi, F., Tani, T., and Ishida, N. (2017) Rationally designed mineralization for selective recovery of the rare earth elements, *8*, 15670.

[81] Lederer, F. L., Curtis, S. B., Bachmann, S., Dunbar, W. S., and MacGillivray, R. T. A. (2017) Identification of lanthanum-specific peptides for future recycling of rare earth elements from compact fluorescent lamps, *Biotechnology and Bioengineering 114*, 1016-1024.

[82] Guyonnet, D., Planchon, M., Rollat, A., Escalon, V., Tuduri, J., Charles, N., Vaxelaire, S., Dubois, D., and Fargier, H. (2015) Material flow analysis applied to rare earth elements in Europe, *Journal of Cleaner Production 107*, 215-228.

[83] Rademaker, J. H., Kleijn, R., and Yang, Y. (2013) Recycling as a Strategy against Rare Earth Element Criticality: A Systemic Evaluation of the Potential Yield of NdFeB Magnet Recycling, *Environmental Science & Technology 47*, 10129-10136.

[84] Meyer, H.-P., Minas, W., and Schmidhalter, D. (2017) Industrial-Scale Fermentation, In *Industrial Biotechnology*, pp 1-53, Wiley-VCH Verlag GmbH & Co. KGaA.

[85] Puyol, D., Batstone, D. J., Hülsen, T., Astals, S., Peces, M., and Krömer, J. O. (2016) Resource Recovery from Wastewater by Biological Technologies: Opportunities, Challenges, and Prospects, *Frontiers in Microbiology 7*, 2106.

[86] Li, P.-S., and Tao, H.-C. (2015) Cell surface engineering of microorganisms towards adsorption of heavy metals, *Critical Reviews in Microbiology 41*, 140-149.

5

Conclusions

5.1 Summary of findings

This thesis presents ways to rationally engineer biofilm properties for the selective removal of pollutants, using metal binding to curli fibers in *E. coli* biofilms as a practical illustration. Specifically, we showed that both the cells and the extracellular matrix of biofilms could be genetically programmed as selective agents, the former through its recognition of and response to specific pollutants, the latter through the display of specific binding moieties. We demonstrated ways of implementing the biofilm-based materials for the remediation of mercury and the recovery of rare earth metals.

Chapter 2 described the environmentally-triggered production of curli fibers for mercury biosorption. We exploited a mercury-responsive bacterial promoter and the natural affinity of curli fibers for mercury to create a synthetic gene circuit that coupled mercury sensing to curli production for mercury removal. The circuit tuned curli expression according to environmental mercury concentrations so there was no need for constant sorbent production. It was responsive to mercury in a range (> 400 ppb) that was above the tolerable limit for soil health in terms of plants and micro-organisms (130 ppb).[1] It was also selective for mercury in mixed metal environments common to contaminated sites. Curli fibers induced flocculation of the cells, further consolidating mercury for retrieval, and bound mercury was not easily washed off the biofilm. Overall, the work presented in Chapter 2 highlights the potential for creating environmentally-responsive biofilms for *in situ* bioremediation.

The work in Chapter 3 was motivated by the need for biosorbents with high sorption capacity and regenerability that were also easy to fabricate in a scalable manner. We showed that by eliminating anchoring proteins in curli biogenesis, we could produce extensive curli networks tens to hundreds of microns in size that were untethered from the bacteria and thus easier to separate. We then developed a rapid and scalable process for the filtration-purification of these curli matrices that also immobilized them onto a substrate, while concurrently recovering the bacteria for further material generation. Genetically modified curli retained the ability to display binding tags after immobilization.

Curli-based filters displaying lanthanide-binding tags (LBTs) were utilized in Chapter 4 for the selective recovery of rare earth elements (REEs). Curli-LBT filters selectively bound REEs from complex metal mixtures, with some preference for valuable heavy REEs like Nd, Tb and Eu. Bound metals were readily desorbed with a mild acid wash without affecting curli integrity, allowing multiple extraction cycles with minimal loss of efficiency. Further, the filters were readily adaptable for sorption under continuous flow. Taken together, the results in Chapters 2 and 3 demonstrate a strategy for creating functionalized, extractable biofilm polymers for use as selective *ex situ* separations matrices. The exclusion of cells from the sorption process allows continuous production of these biopolymers.

5.2 Limitations and future directions

The goal of this thesis was to highlight methods of biofilm engineering for targeted environmental remediation, as such, some of our designs were exploratory and would need further refinement for actual field or commercial implementation. This section discusses some of the limitations of our approach and avenues for further research.

For mercury bioremediation, several aspects of our current circuit could be improved to provide better response. Its sensitivity could be enhanced by introducing a mercury transporter (e.g. MerP, MerF) downstream of *merR* to increase intracellular mercury concentrations, and also by further *in vitro* evolution of MerR to increase its binding affinity to mercury.[2, 3] The addition of a downstream reporter gene (e.g. a chromoprotein or UV- or infrared-responsive fluorescent protein) would enable field detection of the biofilm for removal once it has been formed. Finally, the circuit would need to be genomically integrated into a suitable chassis so that it operates in the absence of an external selection agent.

The synthetic *csgBACEFG* operon we employed in our study could also be further optimized for curli production, since there was significant toxicity associated with high-level expression at high mercury concentrations. The various Csg proteins need to be exported into the periplasm through the Sec translocon prior to secretion,[4] and rapid protein expression could overwhelm this pathway. Improper protein export—especially of the aggregation-prone CsgA and CsgB—could then lead to rampant intracellular self-assembly and induce cell death. One way to evolve the operon would be a combinatorial screen for ribosomal-binding sites (RBS) for the individual *csg* genes that result in the highest curli production under strongly inducing conditions without compromising cell growth. This is the goal of ongoing work in the lab.

Our initial attempts to improve mercury sorption using mercury-binding motifs for BIND display were not successful, likely because the displayed thiol moieties were irreversibly oxidized and so could not function in mercury binding. Better understanding of the mechanism of curli-mediated sorption would likely improve the design of future variants. This interaction could be affected by a variety of environmental conditions, including pH, ionic strength, the presence of other metals, and the redox environment, thus a combinatorial screen of conditions would be

necessary. Structural modeling of potential chelating or stabilizing interactions between mercury and exposed side chains in assembled curli fibers could also inform our understanding of the binding interaction. The effect of mercury speciation is another important consideration, since divalent mercury is readily converted by many bacteria to methylmercury, a much more toxic species. Native *mer* operons typically contain the *merB* gene, which encodes an organomercury lyase that degrades methylmercury. It would be interesting to investigate whether curli could bind methylmercury, and if the inclusion of *merB* would increase binding, since Hg^{2+} released by MerB-mediated degradation could induce higher curli expression levels. Finally, it would be useful to investigate if curli also binds other toxic heavy metals and metalloids like cadmium, lead, copper, arsenite or chromate, since transcriptional regulators exist for many of these species that could be incorporated into future gene circuits for remediation.[5, 6]

We used *E. coli* in our experiments due to the extensive knowledge and genetic tools available for its engineering, and our understanding of the curli biogenesis pathway. However, given its potential for pathogenicity, *E. coli* biofilms would not be practical as field-deployable systems for *in situ* bioremediation. Instead, bacteria like *Bacillus spp*. or *Shewanella spp.* that are adapted for the colonization of soil—the most likely environment for deployment—would be more suitable chassis for further genetic engineering. TasA in *Bacillus subtilis*, which self-assembles to form amyloid fibers analogous to CsgA/curli in *E. coli*, was recently engineered for domain display à la curli BIND,[7] while *Shewanella oneidensis* expresses CsgA homologs that might be amenable to similar genetic modification,[8] making these two species attractive candidates for future studies in field deployment. *Bacillus subtilis* is also a good starting point for additional engineering because it thrives in the rhizosphere—the microenvironment surrounding plant roots—and is a microbe generally recognized as safe by the FDA. We tested our circuit in suspension culture,

which was helpful in our initial characterizations of circuit performance, but not truly representative of the ultimate environment for mercury binding. Future studies would look into circuit activation and mercury binding by curli in simulated soil environments, and also explore bacteria encapsulation in a viable state for field dispersion.[9-11]

For lanthanide recovery using curli-based filters, there were limitations to our determination of certain sorption parameters. Knowledge of the mean number of metal ions bound per CsgA-LBT4 molecule would give an indication of the availability of the displayed LBTs for binding, but we were unable to determine that parameter because of residual cell debris adding to the measured weight of immobilized material (Fig. 4.2 and Fig. 4.12). The cell bodies also contributed an unknown but non-negligible amount of background sorption that affected our calculations of the binding constants (K_D), giving rise to large variations in K_D figures (Table 4.2). More stringent decellularization involving extended treatments with lysozyme, nuclease and base to remove all cellular remnants would enable accurate calculations of those binding parameters. The dependence of LBTs on circumneutral pH for effective metal binding is a fundamental limitation of our sorption system; it necessitates an additional neutralization step, since most waste streams are acidic, and acids are typically used to leach metals from recylable materials. Future work could look into developing other lanthanide-binding peptides that operate in a wider pH range and show better REE selectivity in complex metal mixtures. Another area for further improvement is REE resolution during acid desorption, which would be better achieved using an acidic pH gradient under flow.

The flow experiments in this work were operated as single passes through one filter at a low flowrate to prevent early saturation of the filter. To increase the adsorption efficiency, future work could look into multi-pass filtration systems using a stack of filters, which would enable

good metal capture at higher flowrates, and also potentially improve REE separation. It would also be interesting to explore other form factors besides filtration membranes. For instance, monolithic polyurethane foams and hollow-fiber cartridges lend themselves well to the curli filtration-immobilization process, and could be more easily developed for commercial filtration. The use of immobilization matrices with more open microstructures (e.g. glass fiber materials) could potentially increase the amount of immobilized curli and thus the adsorption capacity.

Finally, the engineered curli-based filters described here could be adapted to remove other entities beyond rare earth metals, including precious metals like gold and platinum (for which various binding peptides have been developed),[12-15] and small molecules like pesticides and waste pharmaceuticals.[16] The large surface area provided by the curli fiber mats could also be used to immobilize catalysts for the degradation of pollutants in wastewater treatment, e.g. titanium dioxide or zinc oxide nanoparticles for photocatalytic degradation of dyes, organophosphates and other emerging pollutants.[17-22]

In sum, this thesis explored ways of rationally engineering biofilms to create targeted biosorbents for pollutant removal and resource recovery. We hope that the design principles established in this work will be useful for the development of other novel biofilm-based material platforms for environmental remediation.

5.3 References

[1] Tipping, E., Lofts, S., Hooper, H., Frey, B., Spurgeon, D., and Svendsen, C. (2010) Critical Limits for Hg(II) in soils, derived from chronic toxicity data, *Environmental pollution (Barking, Essex : 1987) 158*, 2465-2471.

[2] Hakkila, K. M., Nikander, P. A., Junttila, S. M., Lamminmaki, U. J., and Virta, M. P. (2011) Cd-specific mutants of mercury-sensing regulatory protein MerR, generated by directed evolution, *Appl Environ Microbiol 77*, 6215-6224.

[3] Li, L., Liang, J., Hong, W., Zhao, Y., Sun, S., Yang, X., Xu, A., Hang, H., Wu, L., and Chen, S. (2015) Evolved bacterial biosensor for arsenite detection in environmental water, *Environ Sci Technol 49*, 6149-6155.

[4] Evans, M. L., and Chapman, M. R. (2014) Curli biogenesis: order out of disorder, *Biochimica et biophysica acta 1843*, 1551-1558.

[5] Branco, R., Chung, A. P., Johnston, T., Gurel, V., Morais, P., and Zhitkovich, A. (2008) The Chromate-Inducible chrBACF Operon from the Transposable Element TnOtChr Confers Resistance to Chromium(VI) and Superoxide, *Journal of Bacteriology 190*, 6996-7003.

[6] Fernandez-Lopez, R., Ruiz, R., de la Cruz, F., and Moncalian, G. (2015) Transcription factor-based biosensors enlightened by the analyte, *Front Microbiol 6*, 648.

[7] Huang, J., Zhang, C., Zhao, T., Li, K., Wang, X., and Zhong, C. Engineering Bacillus subtilis Biofilms as Living Functional Materials, *Frontiers in Bioengineering and Biotechnology*.

[8] Zhou, Y., Smith, D., Leong, B. J., Brännström, K., Almqvist, F., and Chapman, M. R. (2012) Promiscuous Cross-seeding between Bacterial Amyloids Promotes Interspecies Biofilms, *The Journal of Biological Chemistry 287*, 35092-35103.

[9] Kane, A. L., Al-Shayeb, B., Holec, P. V., Rajan, S., Le Mieux, N. E., Heinsch, S. C., Psarska, S., Aukema, K. G., Sarkar, C. A., Nater, E. A., and Gralnick, J. A. (2016) Toward Bioremediation of Methylmercury Using Silica Encapsulated Escherichia coli Harboring the mer Operon, *PLOS ONE 11*, e0147036.

[10] McCarthy, D., Edwards, G. C., Gustin, M. S., Care, A., Miller, M. B., and Sunna, A. (2017) An innovative approach to bioremediation of mercury contaminated soils from industrial mining operations, *Chemosphere 184*, 694-699.

[11] Yin, K., Lv, M., Wang, Q., Wu, Y., Liao, C., Zhang, W., and Chen, L. (2016) Simultaneous bioremediation and biodetection of mercury ion through surface display of carboxylesterase E2 from Pseudomonas aeruginosa PA1, *Water research 103*, 383-390.

[12] Cetinel, S., Dincer, S., Cebeci, A., Oren, E. E., Whitaker, J. D., Schwartz, D. T., Karaguler, N. G., Sarikaya, M., and Tamerler, C. (2012) Peptides to bridge biological-platinum materials interface, *Bioinspired, Biomimetic and Nanobiomaterials 1*, 143-153.

[13] Chiu, C.-Y., Li, Y., Ruan, L., Ye, X., Murray, C. B., and Huang, Y. (2011) Platinum nanocrystals selectively shaped using facet-specific peptide sequences, *Nat Chem 3*, 393-399.

[14] Kim, J., Kim, D. H., Lee, S. J., Rheem, Y., Myung, N. V., and Hur, H. G. (2016) Synthesis of gold structures by gold-binding peptide governed by concentration of gold ion and peptide, *Bioscience, biotechnology, and biochemistry 80*, 1478-1483.

[15] Slocik, J. M., Govorov, A. O., and Naik, R. R. (2008) Photoactivated biotemplated nanoparticles as an enzyme mimic, *Angewandte Chemie (International ed. in English) 47*, 5335-5339.

[16] Lanzone, V., Sergi, M., Mascini, M., Scarpone, R., Della Pelle, F., Del Carlo, M., Scortichini, G., and Compagnone, D. (2015) Solid-Phase Extraction of Pesticides by Using Bioinspired Peptide Receptors, *Journal of Chemistry 2015*, 7.

[17] Chen, S. F., and Cao, G. Y. (2005) Photocatalytic degradation of organophosphorus pesticides using floating photocatalyst TiO2 center dot SiO2/beads by sunlight, *Solar Energy 79*, 1-9.

[18] Echavia, G. R. M., Matzusawa, F., and Negishi, N. (2009) Photocatalytic degradation of organophosphate and phosphonoglycine pesticides using TiO2 immobilized on silica gel, *Chemosphere 76*, 595-600.

[19] Ameta, R., Benjamin, S., Ameta, A., and Ameta, S. (2012) *Photocatalytic Degradation of Organic Pollutants: A Review*, Vol. 734.

[20] Mirzaei, A., Chen, Z., Haghighat, F., and Yerushalmi, L. (2016) Removal of pharmaceuticals and endocrine disrupting compounds from water by zinc oxide-based photocatalytic degradation: A review, *Sustainable Cities and Society 27*, 407-418.

[21] Molinari, R., Lavorato, C., and Argurio, P. (2017) Recent progress of photocatalytic membrane reactors in water treatment and in synthesis of organic compounds. A review, *Catalysis Today 281*, 144-164.

[22] Rimoldi, L., Meroni, D., Falletta, E., Pifferi, V., Falciola, L., Cappelletti, G., and Ardizzone, S. (2017) Emerging pollutant mixture mineralization by TiO2 photocatalysts. The role of the water medium, *Photochemical & Photobiological Sciences 16*, 60-66.

6

Appendix

Table 6.1. Plasmid inserts used in the mercury bioremediation study in Chapter 2. All plasmids used the pET30a backbone. Inserts were cloned by Gibson Assembly into pET30a, replacing the T7 promoter in the plasmid. Flanking regions corresponding to the pET30a vector are highlighted in gray.

Plasmid Name	Nucleotide Sequence of Insert	Comments
pET30a-P_{merR}:YFP	CGTCCGGCGTAGAGGATCGAGATCGATCTCGCGGAAAATAAAGCACG**CTA**AGGCA TAGCTGACCTTGCCAGGCCTGCTTCGCCCTGTAGTGACGCGATCAACGGGCAGGA AACATTCCCCTTTCGTGCATGGCAGGCGCACACGAGTTCAGACAGCACGGTTTCC ATGCGCGCCAAGTCGGCCATCTTCTCGCGCACGTCCTTGAGCTTGTGTTCGGCCA GGCTGCTGGCCTCCTCGCAGTGGGTGCCATCGTCGAGCCGCAACAGCTCGGCAAT CTCGTCCAGACTGAACCCCAGCCGCTGTGCCGATTTCACGAATTTCACCCGAACC ACGTCCGCCTCCCCATAGCGGCGGATGCTGCCGTAAGGCTTGTCCGGTTCCCGCA ACAGGCCCTTGCGCTGATAGAAGCGGATTGTCTCCACGTTGACCCCGGCCGCCTT GGCAAAAACGCCAATGGTCAGGTTTTCCAAATTATTTTC**CAT**ATCGCTTGACTCC GTACATGAGTACGGAAGTAAGGTTACGCTATCCAATCCAAATTCAAAAGAGGAGA AATTAACT**ATG**AGGGGATCCTTAGGTGGCGTGAGCAAGGGCGAGGAGCTGTTCAC CGGGGTGGTGCCCATCCTGGTCGAGCTGGACGGCGACGTAAACGGCCACAAGTTC AGCGTGTCCGGCGAGGGCGAGGGCGATGCCACCTACGGCAAGCTGACCCTGAAGC TGATCTGCACCACCGGCAAGCTGCCCGTGCCCTGGCCCACCCTCGTGACCACCCT GGGCTACGGCCTGCAGTGCTTCGCCCGCTACCCCGACCACATGAAGCAGCACGAC TTCTTCAAGTCCGCCATGCCCGAAGGCTACGTCCAGGAGCGCACCATCTTCTTCA AGGACGACGGCAACTACAAGACCCGCGCCGAGGTGAAGTTCGAGGGCGACACCCT GGTGAACCGCATCGAGCTGAAGGGCATCGACTTCAAGGAGGACGGCAACATCCTG GGGCACAAGCTGGAGTACAACTACAACAGCCACAACGTCTATATCACCGCCGACA AGCAGAAGAACGGCATCAAGGCCAACTTCAAGATCCGCCACAACATCGAGGACGG CGGCGTGCAGCTCGCCGACCACTACCAGCAGAACACCCCCATCGGCGACGGCCCC GTGCTGCTGCCCGACAACCACTACCTGAGCTACCAGTCCGCCCTGAGCAAAGACC CCAACGAGAAGCGCGATCACATGGTCCTGCTGGAGTTCGTGACCGCCGCCGGGAT CACTCTCGGCATGGACGAGCTGTACAAG**TGA**GATCCGGCTGCTAACAAAGCCCGA AAGGAAGC	Gray = Flanking pET30a plasmid region; Cyan = *merR* gene, showns as complement (transcribed divergently to the reporter gene); Yellow = Promoter controlling expression of *merR* and the *merR*-controlled reporter gene; Green = *yfp* reporter gene;
pET30a-P_{merR}:curli	CGTCCGGCGTAGAGGATCGAGATCGATCTCGCGGAAAATAAAGCACG**CTA**AGGCA TAGCTGACCTTGCCAGGCCTGCTTCGCCCTGTAGTGACGCGATCAACGGGCAGGA AACATTCCCCTTTCGTGCATGGCAGGCGCACACGAGTTCAGACAGCACGGTTTCC ATGCGCGCCAAGTCGGCCATCTTCTCGCGCACGTCCTTGAGCTTGTGTTCGGCCA GGCTGCTGGCCTCCTCGCAGTGGGTGCCATCGTCGAGCCGCAACAGCTCGGCAAT CTCGTCCAGACTGAACCCCAGCCGCTGTGCCGATTTCACGAATTTCACCCGAACC ACGTCCGCCTCCCCATAGCGGCGGATGCTGCCGTAAGGCTTGTCCGGTTCCCGCA ACAGGCCCTTGCGCTGATAGAAGCGGATTGTCTCCACGTTGACCCCGGCCGCCTT GGCAAAAACGCCAATGGTCAGGTTTTCCAAATTATTTTC**CAT**ATCGCTTGACTCC GTACATGAGTACGGAAGTAAGGTTACGCTATCGACCAGGTCCAGGGTGACAAC**ATG** AAAAACAAATTGTTATTTATGATGTTAACAATACTGGGTGCGCCTGGGATTGCA GCCGCAGCAGGTTATGATTTAGCTAATTCAGAATATAACTTCGCGGTAAATGAAT TGAGTAAGTCTTCATTTAATCAGGCAGCCATAATTGGTCAAGCTGGGACTAATAA TAGTGCTCAGTTACGGCAGGGAGGCTCAAAACTTTTGGCGGTTGTTGCGCAAGAA GGTAGTAGCAACCGGGCAAAGATTGACCAGACAGGAGATTATAACCTTGCATATA TTGATCAGGCGGGCAGTGCCAACGATGCCAGTATTTCGCAAGGTGCTTATGGTAA TACTGCGATGATTATCCAGAAAGGTTCTGGTAATAAAGCAAATATTACACAGTAT GGTACTCAAAAAACGGCAATTGTAGTGCAGAGACAGTCGCAAATGGCTATTCGCG TGACACAACGT**TAA**TTTCCATTCGACTTTTAAATCAATCCGATGGGGGTTTTACA	Gray = Flanking pET30a plasmid region; Cyan = *merR* gene (transcribed divergently to the reporter gene); Yellow = Promoter controlling expression of *merR* and the *merR*-controlled reporter gene; Orange = *csgB* from

	TGAAACTTTTAAAAGTAGCAGCAATTGCAGCAATCGTATTCTCCGGTAGCGCTCT GGCAGGTGTTGTTCCTCAGTACGGCGGCGGCGGTAACCACGGTGGTGGCGGTAAT AATAGCGGCCCAAATTCTGAGCTGAACATTTACCAGTACGGTGGCGGTAACTCTG CACTTGCTCTGCAAACTGATGCCCGTAACTCTGACTTGACTATTACCCAGCATGG CGGCGGTAATGGTGCAGATGTTGGTCAGGGCTCAGATGACAGCTCAATCGATCTG ACCCAACGTGGCTTCGGTAACAGCGCTACTCTTGATCAGTGGAACGGCAAAAATT CTGAAATGACGGTTAAACAGTTCGGTGGTGGCAACGGTGCTGCAGTTGACCAGAC TGCATCTAACTCCTCCGTCAACGTGACTCAGGTTGGCTTTGGTAACAACGCGACC GCTCATCAGTACTAATACATCATTTGTATTACAGAAACAGGGCGCAAGCCCTGTT TTTTTTCGGGAGAAGAATATGAATACGTTATTACTCCTTGCGGCACTTTCCAGTC AGATAACCTTTAATACGACCCAGCAAGGGGATGTGTATACCATTATTCCTGAAGT CACTCTTACTCAATCTTGTCTGTGCAGAGTACAAATATTGTCCCTGCGCGAAGGC AGTTCAGGGCAAAGTCAGACGAAGCAAGAAAAGACCCTTTCATTGCCTGCTAATC AACCCATTGCTTTGACGAAGTTGAGTTTAAATATTTCCCCGGACGATCGGGTGAA AATAGTTGTTACTGTTTCTGATGGACAGTCACTTCATTTATCACAACAATGGCCG CCCTCTTCAGAAAAGTCTTAAGGTTTCCTGGGCAAACGATAACCTCAGGCGATAA AGCCATGAAACGTTATTTACGCTGGATTGTGGCGGCAGAATTTCTGTTCGCCGCA GGGAATCTTCACGCCGTTGAGGTAGAAGTCCCGGGATTGCTAACTGACCATACTG TTTCATCTATTGGCCATGATTTTTACCGAGCCTTTAGTGATAAATGGGAAAGTGA CTATACGGGTAACTTAACGATTAATGAAAGGCCCAGTGCACGATGGGGAAGCTGG ATCACTATAACGGTCAATCAGGACGTTATTTTCCAGACTTTTTTATTTCCGTTGA AAAGAGACTTCGAGAAAACTGTCGTCTTTGCACTGATTCAAACTGAAGAAGCACT AAATCGTCGCCAGATAAATCAGGCGTTATTAAGTACGGGCGATTTGGCGCATGAT GAATTCTAAATAAAAAATTGTTCGGAGGCTGCAATGCGTGTCAAACATGCAGTAG TTCTACTCATGCTTATTTCGCCATTAAGTTGGGCTGGAACCATGACTTTCCAGTT CCGTAATCCAAACTTTGGTGGTAACCCAAATAATGGCGCTTTTTTATTAAATAGC GCTCAGGCCCAAAACTCTTATAAAGATCCGAGCTATAACGATGACTTTGGTATTG AAACACCCTCAGCGTTAGATAACTTTACTCAGGCCATCCAGTCACAAATTTTAGG TGGGCTACTGTCGAATATTAATACCGGTAAACCGGGCCGCATGGTGACCAACGAT TATATTGTCGATATTGCCAACCGCGATGGTCAATTGCAGTTGAACGTGACAGATC GTAAAACCGGACAAACCTCGACCATCCAGGTTTCGGGTTTACAAAATAACTCAAC CGATTTTTAAGCCCCAGCTTCATAAGGAAAATAATCATGCAGCGCTTATTTCTTT TGGTTGCCGTCATGTTACTGAGCGGATGCTTAACCGCCCCGCCTAAAGAAGCCGC CAGACCGACATTAATGCCTCGTGCTCAGAGCTACAAAGATTTGACCCATCTGCCA GCGCCGACGGGTAAAATCTTTGTTTCGGTATACAACATTCAGGACGAAACCGGGC AATTTAAACCCTACCCGGCAAGTAACTTCTCCACTGCTGTTCCGCAAAGCGCCAC GGCAATGCTGGTCACGGCACTGAAAGATTCTCGCTGGTTTATACCGCTGGAGCGC CAGGGCTTACAAAACCTGCTTAACGAGCGCAAGATTATTCGTGCGGCACAAGAAA ACGGCACGGTTGCCATTAATAACCGAATCCCGCTGCAATCTTTAACGGCGGCAAA TATCATGGTTGAAGGTTCGATTATCGGTTATGAAAGCAACGTCAAATCTGGCGGG GTTGGGGCAAGATATTTTGGCATCGGTGCCGACACGCAATACCAGCTCGATCAGA TTGCCGTGAACCTGCGCGTCGTCAATGTGAGTACCGGCGAGATCCTTTCTTCGGT GAACACCAGTAAGACGATACTTTCCTATGAAGTTCAGGCCGGGGTTTTCCGCTTT ATTGACTACCAGCGCTTGCTTGAAGGGGAAGTGGGTTACACCTCGAACGAACCTG TTATGCTGTGCCTGATGTCGGCTATCGAAACAGGGGTCATTTTCCTGATTAATGA TGGTATCGACCGTGGTCTGTGGGATTTGCAAAATAAAGCAGAACGGCAGAATGAC ATTCTGGTGAAATACCGCCATATGTCGGTTCCACCGGAATCCTGAGATCCGGCTG CTAACAAAGCCCGAAAGG	MG1655, contains 22 bp upstream region. Red = *csgA* from MG1655. Purple = *csgC* from MG1655. Magenta = *csgE* from MG1655. Turquiose = *csgF* from MG1655 Blue = *csgG* from MG1655
pET30a-Ctrl	CGATGCGTCCGGCGTAGAGGATCGAGATCGAT***CTCGAG***CACCACCACCACCACCA CTGAGATCCGGCTGC	Gray = Flanking pET30a plasmid region; *Italicized* = restriction site introduced by PCR for removal of T7 promoter.

Table 6.2. Plasmid inserts used to produce the CsgA and CsgB variants in Chapter 3. All plasmids used the pET21d backbone. All inserts were cloned by Gibson Assembly.

Plasmid Name	Nucleotide Sequence of Insert	Comments
pET21d-P_{T7}:WT	GTTTAACTTTAAGAAGGAGATATACAT**ATG**AAAAACAAATTGTTATTTATGATGT TAACAATACTGGGTGCGCCTGGGATTGCAGCCGCAGCAGGTTATGATTTAGCTAA TTCAGAATATAACTTCGCGGTAAATGAATTGAGTAAGTCTTCATTTAATCAGGCA GCCATAATTGGTCAAGCTGGGACTAATAATAGTGCTCAGTTACGGCAGGGAGGCT CAAAACTTTTGGCGGTTGTTGCGCAAGAAGGTAGTAGCAACCGGGCAAAGATTGA CCAGACAGGAGATTATAACCTTGCATATATTGATCAGGCGGGCAGTGCCAACGAT GCCAGTATTTCGCAAGGTGCTTATGGTAATACTGCGATGATTATCCAGAAAGGTT CTGGTAATAAAGCAAATATTACACAGTATGGTACTCAAAAAACGGCAATTGTAGT GCAGAGACAGTCGCAAATGGCTATTCGCGTGACACAACGT**TAA**TTTCCATTCGAC TTTTAAATCAATCCGATGGGGGTTTTAC**ATG**AAACTTTTAAAAGTAGCAGCAATT GCAGCAATCGTATTCTCCGGTAGCGCTCTGGCAGGTGTTGTTCCTCAGTACGGCG GCGGCGGTAACCACGGTGGTGGCGGTAATAATAGCGGCCCAAATTCTGAGCTGAA CATTTACCAGTACGGTGGCGGTAACTCTGCACTTGCTCTGCAAACTGATGCCCGT AACTCTGACTTGACTATTACCCAGCATGGCGGCGGTAATGGTGCAGATGTTGGTC AGGGCTCAGATGACAGCTCAATCGATCTGACCCAACGTGGCTTCGGTAACAGCGC TACTCTTGATCAGTGGAACGGCAAAAATTCTGAAATGACGGTTAAACAGTTCGGT GGTGGCAACGGTGCTGCAGTTGACCAGACTGCATCTAACTCCTCCGTCAACGTGA CTCAGGTTGGCTTTGGTAACAACGCGACCGCTCATCAGTAC**TAA**TACATCATTTG TATTACAGAAACAGGGCGCAAGCCCTGTTTTTTTTCGGGAGAAGAAT**ATG**AATAC GTTATTACTCCTTGCGGCACTTTCCAGTCAGATAACCTTTAATACGACCCAGCAA GGGGATGTGTATACCATTATTCCTGAAGTCACTCTTACTCAATCTTGTCTGTGCA GAGTACAAATATTGTCCCTGCGCGAAGGCAGTTCAGGGCAAAGTCAGACGAAGCA AGAAAAGACCCTTTCATTGCCTGCTAATCAACCCATTGCTTTGACGAAGTTGAGT TTAAATATTTCCCCGGACGATCGGGTGAAAATAGTTGTTACTGTTTCTGATGGAC AGTCACTTCATTTATCACAACAATGGCCGCCCTCTTCAGAAAAGTCTT**TAA**GGTTT CCTGGGCAAACGATAACCTCAGGCGATAAAGCC**ATG**AAACGTTATTTACGCTGGA TTGTGGCGGCAGAATTTCTGTTCGCCGCAGGGAATCTTCACGCCGTTGAGGTAGA AGTCCCGGGATTGCTAACTGACCATACTGTTTCATCTATTGGCCATGATTTTTAC CGAGCCTTTAGTGATAAATGGGAAAGTGACTATACGGGTAACTTAACGATTAATG AAAGGCCCAGTGCACGATGGGGAAGCTGGATCACTATAACGGTCAATCAGGACGT TATTTTCCAGACTTTTTTATTTCCGTTGAAAAGAGACTTCGAGAAAACTGTCGTC TTTGCACTGATTCAAACTGAAGAAGCACTAAATCGTCGCCAGATAAATCAGGCGT TATTAAGTACGGGCGATTTGGCGCATGATGAATTC**TAA**ATAAAAAATTGTTCGGA GGCTGCA**ATG**CGTGTCAAACATGCAGTAGTTCTACTCATGCTTATTTCGCCATTA AGTTGGGCTGGAACCATGACTTTCCAGTTCCGTAATCCAAACTTTGGTGGTAACC CAAATAATGGCGCTTTTTTATTAAATAGCGCTCAGGCCCAAAACTCTTATAAAGA TCCGAGCTATAACGATGACTTTGGTATTGAAACACCCTCAGCGTTAGATAACTTT ACTCAGGCCATCCAGTCACAAATTTTAGGTGGGCTACTGTCGAATATTAATACCG GTAAACCGGGCCGCATGGTGACCAACGATTATATTGTCGATATTGCCAACCGCGA TGGTCAATTGCAGTTGAACGTGACAGATCGTAAAACCGGACAAACCTCGACCATC CAGGTTTCGGGTTTACAAAATAACTCAACCGATTTT**TAA**GCCCCAGCTTCATAAG GAAAATAATC**ATG**CAGCGCTTATTTCTTTTGGTTGCCGTCATGTTACTGAGCGGA TGCTTAACCGCCCCGCCTAAAGAAGCCGCCAGACCGACATTAATGCCTCGTGCTC AGAGCTACAAAGATTTGACCCATCTGCCAGCGCCGACGGGTAAAATCTTTGTTTC GGTATACAACATTCAGGACGAAACCGGGCAATTTAAACCCTACCCGGCAAGTAAC TTCTCCACTGCTGTTCCGCAAAGCGCCACGGCAATGCTGGTCACGGCACTGAAAG ATTCTCGCTGGTTTATACCGCTGGAGCGCCAGGGCTTACAAAACCTGCTTAACGA GCGCAAGATTATTCGTGCGGCACAAGAAAACGGCACGGTTGCCATTAATAACCGA ATCCCGCTGCAATCTTTAACGGCGGCAAATATCATGGTTGAAGGTTCGATTATCG GTTATGAAAGCAACGTCAAATCTGGCGGGGTTGGGGCAAGATATTTTGGCATCGG TGCCGACACGCAATACCAGCTCGATCAGATTGCCGTGAACCTGCGCGTCGTCAAT GTGAGTACCGGCGAGATCCTTTCTTCGGTGAACACCAGTAAGACGATACTTTCCT ATGAAGTTCAGGCCGGGGTTTTCCGCTTTATTGACTACCAGCGCTTGCTTGAAGG GGAAGTGGGTTACACCTCGAACGAACCTGTTATGCTGTGCCTGATGTCGGCTATC GAAACAGGGGTCATTTTCCTGATTAATGATGGTATCGACCGTGGTCTGTGGGATT TGCAAAATAAAGCAGAACGGCAGAATGACATTCTGGTGAAATACCGCCATATGTC GGTTCCACCGGAATCC**TGA**GATCCGGCTGCTAACAAAGCCCGAAAGG	Gray = Flanking pET21d plasmid region Cyan = *csgB* from MG1655 Red = *csgA* from MG1655 Blue = *csgC* from MG1655 Magenta = *csgE* from MG1655 Purple = *csgF* from MG1655 Green = *csgG* from MG1655
pET21d-P_{T7}:ΔB	GTTTAACTTTAAGAAGGAGATATACAT**ATG**AAACTTTTAAAAGTAGCAGCAATTG CAGCAATCGTATTCTCCGGTAGCGCTCTGGCAGGTGTTGTTCCTCAGTACGGCGG CGGCGGTAACCACGGTGGTGGCGGTAATAATAGCGGCCCAAATTCTGAGCTGAAC	Gray = Flanking pET21d plasmid region

	ATTTACCAGTACGGTGGCGGTAACTCTGCACTTGCTCTGCAAACTGATGCCCGTA ACTCTGACTTGACTATTACCCAGCATGGCGGCGGTAATGGTGCAGATGTTGGTCA GGGCTCAGATGACAGCTCAATCGATCTGACCCAACGTGGCTTCGGTAACAGCGCT ACTCTTGATCAGTGGAACGGCAAAAATTCTGAAATGACGGTTAAACAGTTCGGTG GTGGCAACGGTGCTGCAGTTGACCAGACTGCATCTAACTCCTCCGTCAACGTGAC TCAGGTTGGCTTTGGTAACAACGCGACCGCTCATCAGTACTAATACATCATTTGT ATTACAGAAACAGGGCGCAAGCCCTGTTTTTTTTCGGGAGAAGAATATGAATACG TTATTACTCCTTGCGGCACTTTCCAGTCAGATAACCTTTAATACGACCCAGCAAG GGGATGTGTATACCATTATTCCTGAAGTCACTCTTACTCAATCTTGTCTGTGCAG AGTACAAATATTGTCCCTGCGCGAAGGCAGTTCAGGGCAAAGTCAGACGAAGCAA GAAAAGACCCTTTCATTGCCTGCTAATCAACCCATTGCTTTGACGAAGTTGAGTT TAAATATTTCCCCGGACGATCGGGTGAAAATAGTTGTTACTGTTTCTGATGGACA GTCACTTCATTTATCACAACAATGGCCGCCCTCTTCAGAAAAGTCTTAAGGTTTC CTGGGCAAACGATAACCTCAGGCGATAAAGCCATGAAACGTTATTTACGCTGGAT TGTGGCGGCAGAATTTCTGTTCGCCGCAGGGAATCTTCACGCCGTTGAGGTAGAA GTCCCGGGATTGCTAACTGACCATACTGTTTCATCTATTGGCCATGATTTTTACC GAGCCTTTAGTGATAAATGGGAAAGTGACTATACGGGTAACTTAACGATTAATGA AAGGCCCAGTGCACGATGGGGAAGCTGGATCACTATAACGGTCAATCAGGACGTT ATTTTCCAGACTTTTTTATTTCCGTTGAAAAGAGACTTCGAGAAAACTGTCGTCT TTGCACTGATTCAAACTGAAGAAGCACTAAATCGTCGCCAGATAAATCAGGCGTT ATTAAGTACGGGCGATTTGGCGCATGATGAATTCTAAATAAAAAATTGTTCGGAG GCTGCAATGCGTGTCAAACATGCAGTAGTTCTACTCATGCTTATTTCGCCATTAA GTTGGGCTGGAACCATGACTTTCCAGTTCCGTAATCCAAACTTTGGTGGTAACCC AAATAATGGCGCTTTTTTATTAAATAGCGCTCAGGCCCAAAACTCTTATAAAGAT CCGAGCTATAACGATGACTTTGGTATTGAAACACCCTCAGCGTTAGATAACTTTA CTCAGGCCATCCAGTCACAAATTTTAGGTGGGCTACTGTCGAATATTAATACCGG TAAACCGGGCCGCATGGTGACCAACGATTATATTGTCGATATTGCCAACCGCGAT GGTCAATTGCAGTTGAACGTGACAGATCGTAAAACCGGACAAACCTCGACCATCC AGGTTTCGGGTTTACAAAATAACTCAACCGATTTTTAAGCCCCAGCTTCATAAGG AAAATAATCATGCAGCGCTTATTTCTTTTGGTTGCCGTCATGTTACTGAGCGGAT GCTTAACCGCCCCGCCTAAAGAAGCCGCCAGACCGACATTAATGCCTCGTGCTCA GAGCTACAAAGATTTGACCCATCTGCCAGCGCCGACGGGTAAAATCTTTGTTTCG GTATACAACATTCAGGACGAAACCGGGCAATTTAAACCCTACCCGGCAAGTAACT TCTCCACTGCTGTTCCGCAAAGCGCCACGGCAATGCTGGTCACGGCACTGAAAGA TTCTCGCTGGTTTATACCGCTGGAGCGCCAGGGCTTACAAAACCTGCTTAACGAG CGCAAGATTATTCGTGCGGCACAAGAAAACGGCACGGTTGCCATTAATAACCGAA TCCCGCTGCAATCTTTAACGGCGGCAAATATCATGGTTGAAGGTTCGATTATCGG TTATGAAAGCAACGTCAAATCTGGCGGGGTTGGGGCAAGATATTTTGGCATCGGT GCCGACACGCAATACCAGCTCGATCAGATTGCCGTGAACCTGCGCGTCGTCAATG TGAGTACCGGCGAGATCCTTTCTTCGGTGAACACCAGTAAGACGATACTTTCCTA TGAAGTTCAGGCCGGGGTTTTCCGCTTTATTGACTACCAGCGCTTGCTTGAAGGG GAAGTGGGTTACACCTCGAACGAACCTGTTATGCTGTGCCTGATGTCGGCTATCG AAACAGGGGTCATTTTCCTGATTAATGATGGTATCGACCGTGGTCTGTGGGATTT GCAAAATAAAGCAGAACGGCAGAATGACATTCTGGTGAAATACCGCCATATGTCG GTTCCACCGGAATCCTGAGATCCGGCTGCTAACAAAGCCCGAAAGG	Red = *csgA* from MG1655 Blue = *csgC* from MG1655 Magenta = *csgE* from MG1655 Purple = *csgF* from MG1655 Green = *csgG* from MG1655
pET21d-P_{T7}:ΔBF	GTTTAACTTTAAGAAGGAGATATACATATGAAACTTTTAAAAGTAGCAGCAATTG CAGCAATCGTATTCTCCGGTAGCGCTCTGGCAGGTGTTGTTCCTCAGTACGGCGG CGGCGGTAACCACGGTGGTGGCGGTAATAATAGCGGCCCAAATTCTGAGCTGAAC ATTTACCAGTACGGTGGCGGTAACTCTGCACTTGCTCTGCAAACTGATGCCCGTA ACTCTGACTTGACTATTACCCAGCATGGCGGCGGTAATGGTGCAGATGTTGGTCA GGGCTCAGATGACAGCTCAATCGATCTGACCCAACGTGGCTTCGGTAACAGCGCT ACTCTTGATCAGTGGAACGGCAAAAATTCTGAAATGACGGTTAAACAGTTCGGTG GTGGCAACGGTGCTGCAGTTGACCAGACTGCATCTAACTCCTCCGTCAACGTGAC TCAGGTTGGCTTTGGTAACAACGCGACCGCTCATCAGTACTAATACATCATTTGT ATTACAGAAACAGGGCGCAAGCCCTGTTTTTTTTCGGGAGAAGAATATGAATACG TTATTACTCCTTGCGGCACTTTCCAGTCAGATAACCTTTAATACGACCCAGCAAG GGGATGTGTATACCATTATTCCTGAAGTCACTCTTACTCAATCTTGTCTGTGCAG AGTACAAATATTGTCCCTGCGCGAAGGCAGTTCAGGGCAAAGTCAGACGAAGCAA GAAAAGACCCTTTCATTGCCTGCTAATCAACCCATTGCTTTGACGAAGTTGAGTT TAAATATTTCCCCGGACGATCGGGTGAAAATAGTTGTTACTGTTTCTGATGGACA GTCACTTCATTTATCACAACAATGGCCGCCCTCTTCAGAAAAGTCTTAAGGTTTC CTGGGCAAACGATAACCTCAGGCGATAAAGCCATGAAACGTTATTTACGCTGGAT TGTGGCGGCAGAATTTCTGTTCGCCGCAGGGAATCTTCACGCCGTTGAGGTAGAA GTCCCGGGATTGCTAACTGACCATACTGTTTCATCTATTGGCCATGATTTTTACC GAGCCTTTAGTGATAAATGGGAAAGTGACTATACGGGTAACTTAACGATTAATGA AAGGCCCAGTGCACGATGGGGAAGCTGGATCACTATAACGGTCAATCAGGACGTT ATTTTCCAGACTTTTTTATTTCCGTTGAAAAGAGACTTCGAGAAAACTGTCGTCT TTGCACTGATTCAAACTGAAGAAGCACTAAATCGTCGCCAGATAAATCAGGCGTT ATTAAGTACGGGCGATTTGGCGCATGATGAATTCTAAGCCCCAGCTTCATAAGGA	Gray = Flanking pET21d plasmid region Red = *csgA* from MG1655 Blue = *csgC* from MG1655 Magenta = *csgE* from MG1655 Green = *csgG* from MG1655

	AAATAATC**ATG**CAGCGCTTATTTCTTTTGGTTGCCGTCATGTTACTGAGCGGATG CTTAACCGCCCCGCCTAAAGAAGCCGCCAGACCGACATTAATGCCTCGTGCTCAG AGCTACAAAGATTTGACCCATCTGCCAGCGCCGACGGGTAAAATCTTTGTTTCGG TATACAACATTCAGGACGAAACCGGGCAATTTAAACCCTACCCGGCAAGTAACTT CTCCACTGCTGTTCCGCAAAGCGCCACGGCAATGCTGGTCACGGCACTGAAAGAT TCTCGCTGGTTTATACCGCTGGAGCGCCAGGGCTTACAAAACCTGCTTAACGAGC GCAAGATTATTCGTGCGGCACAAGAAAACGGCACGGTTGCCATTAATAACCGAAT CCCGCTGCAATCTTTAACGGCGGCAAATATCATGGTTGAAGGTTCGATTATCGGT TATGAAAGCAACGTCAAATCTGGCGGGGTTGGGGCAAGATATTTTGGCATCGGTG CCGACACGCAATACCAGCTCGATCAGATTGCCGTGAACCTGCGCGTCGTCAATGT GAGTACCGGCGAGATCCTTTCTTCGGTGAACACCAGTAAGACGATACTTTCCTAT GAAGTTCAGGCCGGGGTTTTCCGCTTTATTGACTACCAGCGCTTGCTTGAAGGGG AAGTGGGTTACACCTCGAACGAACCTGTTATGCTGTGCCTGATGTCGGCTATCGA AACAGGGGTCATTTTCCTGATTAATGATGGTATCGACCGTGGTCTGTGGGATTTG CAAAATAAAGCAGAACGGCAGAATGACATTCTGGTGAAATACCGCCATATGTCGG TTCCACCGGAATCC**TGA**GATCCGGCTGCTAACAAAGCCCGAAAGG	
pET21d-P_{T7}:BΔR5	GTTTAACTTTAAGAAGGAGATATACAT**ATG**AAAAACAAATTGTTATTTATGATGT TAACAATACTGGGTGCGCCTGGGATTGCAGCCGCAGCAGGTTATGATTTAGCTAA TTCAGAATATAACTTCGCGGTAAATGAATTGAGTAAGTCTTCATTTAATCAGGCA GCCATAATTGGTCAAGCTGGGACTAATAATAGTGCTCAGTTACGGCAGGGAGGCT CAAAACTTTTGGCGGTTGTTGCGCAAGAAGGTAGTAGCAACCGGGCAAAGATTGA CCAGACAGGAGATTATAACCTTGCATATATTGATCAGGCGGGCAGTGCCAACGAT GCCAGTATTTCGCAAGGTGCTTATGGTAATACTGCGATGATTATCCAGAAAGGTT CTGGTAATAAAGCAAATATTACACAGTATGGTACTCAA**TAA**TTTCCATTCGACTT TTAAATCAATCCGA	Gray = Flanking plasmid region in pET21d-P_{T7}:WT Cyan = gene for $CsgB^{\Delta R5}$ (truncated CsgB)
pET21d-P_{T7}:CsgA*	GTTTAACTTTAAGAAGGAGATATACAT**ATG**AAACTGCTGAAAGTTGCGGCGATCG CGGCGATCGTTTTCTCTGGTTCTGCGCTGGCGGGTGTTGTTCCGCAGTACGGTGG TGGTGGTAACCACGGTGGTGGTGGTAACAACTCTGGTCCGAACTCTGAACTGAAC ATCTACCAGTACGGTGGTGGTAACTCTGCGCTGGCGCTGCAGACCGACGCGCGTA ACTCTGACCTGACCATCACCCAGCACGGTGGTGGTAACTCTGCGCTGGTTCTGCA GGGTTCTGACGACTCTTCTATCAACCTGACCCAGCGTGGTTTCGGTAACTCTGCG ACCCTGCTGCAGTGGAACGGTAAAAACTCTGAAATGACCGTTAAACAGTTCGGTG GTGGTAACAACGCGGCGGTTCACCAACCGCGTCTAACTCTTCTGTTAACGTTACC CAGGTTGGTTTCGGTAACAACGCGACCGCGCACCAGTACTACATCATTTGTATTA CAGAAACAGGGCG	Gray = Flanking plasmid region in pET21d-P_{T7}:ΔB Red = gene for CsgA*
pET21d-P_{T7}:WT^{his}	CGACTTTTAAATCAATCCGATGGGGGTTTTAC**ATG**AAACTTTTAAAAGTAGCAGC AATTGCAGCAATCGTATTCTCCGGTAGCGCTCTGGCAGGTGTTGTTCCTCAGTAC GGCGGCGGCGGTAACCACGGTGGTGGCGGTAATAATAGCGGCCCAAATTCTGAGC TGAACATTTACCAGTACGGTGGCGGTAACTCTGCACTTGCTCTGCAAACTGATGC CCGTAACTCTGACTTGACTATTACCCAGCATGGCGGCGGTAATGGTGCAGATGTT GGTCAGGGCTCAGATGACAGCTCAATCGATCTGACCCAACGTGGCTTCGGTAACA GCGCTACTCTTGATCAGTGGAACGGCAAAAATTCTGAAATGACGGTTAAACAGTT CGGTGGTGGCAACGGTGCTGCAGTTGACCAGACTGCATCTAACTCCTCCGTCAAC GTGACTCAGGTTGGCTTTGGTAACAACGCGACCGCTCATCAGTACGGTGGATCTG GTAGCAGCGGCTCTGGTGGTTCTGGGGGCGGAAGTGGCTCCTCTGGGAGCGGGGG GTCGGGTGGTGGCTCGGGTTCATCTGGTAGTGGCGGTTCGGGTCATCACCACCAC CATCATTAA**TAA**TACATCATTTGTATTACAGAAACAGGGCG	Gray = Flanking plasmid region in pET21d-P_{T7}:WT Red = gene for CsgA-6xHis (tag underlined along with 36-amino acid linker)
pET21d-P_{T7}:ΔBF^{his}	GTTTAACTTTAAGAAGGAGATATACAT**ATG**AAACTTTTAAAAGTAGCAGCAATTG CAGCAATCGTATTCTCCGGTAGCGCTCTGGCAGGTGTTGTTCCTCAGTACGGCGG CGGCGGTAACCACGGTGGTGGCGGTAATAATAGCGGCCCAAATTCTGAGCTGAAC ATTTACCAGTACGGTGGCGGTAACTCTGCACTTGCTCTGCAAACTGATGCCCGTA ACTCTGACTTGACTATTACCCAGCATGGCGGCGGTAATGGTGCAGATGTTGGTCA GGGCTCAGATGACAGCTCAATCGATCTGACCCAACGTGGCTTCGGTAACAGCGCT ACTCTTGATCAGTGGAACGGCAAAAATTCTGAAATGACGGTTAAACAGTTCGGTG GTGGCAACGGTGCTGCAGTTGACCAGACTGCATCTAACTCCTCCGTCAACGTGAC TCAGGTTGGCTTTGGTAACAACGCGACCGCTCATCAGTACGGTGGATCTGGTAGC AGCGGCTCTGGTGGTTCTGGGGGCGGAAGTGGCTCCTCTGGGAGCGGGGGGTCGG GTGGTGGCTCGGGTTCATCTGGTAGTGGCGGTTCGGGTCATCACCACCACCATCA TTAA**TAA**TACATCATTTGTATTACAGAAACAGGGCG	Gray = Flanking plasmid region in pET21d-P_{T7}:ΔBF Red = gene for CsgA-6xHis (tag underlined along with 36-amino acid linker)
pET21d-P_{T7}:MBP	gtttaactttaagaaggagatatacat**ATG**aaaatcgaagaaggtaaactggtaa tctggattaacggcgataaaggctataacggtctcgctgaagtcggtaagaaatt	Gray = Flanking pET21d plasmid

	cgagaaagataccggaattaaagtcaccgttgagcatccggataaactggaagag aaattcccacaggttgcggcaactggcgatggccctgacattatcttctgggcac acgaccgctttggtggctacgctcaatctggcctgttggctgaaatcaccccgga caaagcgttccaggacaagctgtatccgtttacctgggatgccgtacgttacaac ggcaagctgattgcttacccgatcgctgttgaagcgttatcgctgatttataaca aagatctgctgccgaacccgccaaaaacctgggaagagatcccggcgctggataa agaactgaaagcgaaaggtaagagcgcgctgatgttcaacctgcaagaaccgtac ttcacctggccgctgattgctgctgacgggggttatgcgttcaagtatgaaaacg gcaagtacgacattaaagacgtgggcgtggataacgctggcgcgaaagcgggtct gaccttcctggttgacctgattaaaaacaaacacatgaatgcagacaccgattac tccatcgcagaagctgcctttaataaaggcgaaacagcgatgaccatcaacggcc cgtgggcatggtccaacatcgacaccagcaaagtgaattatggtgtaacggtact gccgaccttcaagggtcaaccatccaaaccgttcgttggcgtgctgagcgcaggt attaacgccgccagtccgaacaaagagctggcaaaagagttcctcgaaaactatc tgctgactgatgaaggtctggaagcggttaataaagacaaaccgctgggtgccgt agcgctgaagtcttacgaggaagagttggcgaaagatccacgtattgccgccact atggaaaacgcccagaaaggtgaaatcatgccgaacatcccgcagatgtccgctt tctggtatgccgtgcgtactgcggtgatcaacgccgccagcggtcgtcagactgt cgatgaagccctgaaagacgcgcagactaattcgagctcg**TGA**gatccggctgct aacaaagcccg	region; Yellow = gene for maltose binding protein (excluding the signal sequence)

Table 6.3. Plasmid inserts used in the lanthanide recovery study in Chapter 4. All plasmids used the pET21d backbone. Inserts were cloned by Gibson Assembly into the pET21d-P_{T7}:ΔBF^{his} construct (Table 6.2), replacing the sequence for 6×His.

Plasmid Name	Nucleotide Sequence of Insert	Comments
pET21d-P_{T7}:LBT2	GGTTCATCTGGTAGTGGCGGTTCGGGTTACATTGACACTAATAACGATGGATGGA TTGAGGGAGATGAGCTTTACATTGACACGAACAATGATGGATGGATCGAAGGCGA CGAATTACTTGCG**TAA**TACATCATTTGTATTACAGAAACAGGG	Gray = Flanking plasmid region in pET21d-P_{T7}:ΔBF Red = gene for CsgA-LBT2
pET21d-P_{T7}:LBT4	GGTTCATCTGGTAGTGGCGGTTCGGGTTACATCGATACCAATAACGACGGCTGGA TCGAGGGGGATGAATTATACATCGACACAAACAATGATGGTTGGATCGAGGGAGA TGAGCTGTACATCGACACGAATAACGATGGGTGGATCGAAGGTGATGAGTTGTAT ATCGACACTAATAATGATGGTTGGATCGAAGGCGACGAATTG**TAA**TACATCATTT GTATTACAGAAACAGGG	Gray = Flanking plasmid region in pET21d-P_{T7}:ΔBF Red = gene for CsgA-LBT4
pET21d-P_{T7}:LBT6	GGTTCATCTGGTAGTGGCGGTTCGGGTTACATTGACACAAACAATGACGGGTGGA TCGAAGGGGACGAGTTATATATCGACACAAACAACGACGGCTGGATTGAAGGCGA TGAGCTTTACATCGACACCAACAACGATGGATGGATCGAGGGGGATGAACTTTAC ATCGATACTAACAATGATGGATGGATTGAGGGTGACGAGCTTTACATTGATACTA ACAATGATGGGTGGATTGAAGGTGATGAATTATATATCGACACCAATAATGACGG ATGGATTGAGGGCGATGAGTTGCTTGCC**TAA**TACATCATTTGTATTACAGAAACA GGG	Gray = Flanking plasmid region in pET21d-P_{T7}:ΔBF Red = gene for CsgA-LBT6
pET21d-P_{T7}:LBT2*	GGTTCATCTGGTAGTGGCGGTTCGGGTTACATCGGGACTAATAATGGTGGTTGGA TCGGGGGCGGTGGTCTTTATATCGGCACGAACAATGGTGGGTGGATCGGCGGGGG AGGGTTGCTTGCC**TAA**TACATCATTTGTATTACAGAAACAGG	Gray = Flanking plasmid region in pET21d-P_{T7}:ΔBF Red = gene for CsgA-LBT2*
pET21d-P_{T7}:LBT4*	GGTTCATCTGGTAGTGGCGGTTCGGGTTACATTGGGACGAATAACGGAGGGTGGA TTGGCGGTGGTGGCCTTTACATTGGCACGAACAATGGTGGGTGGATTGGAGGTGG AGGATTATATATCGGTACTAACAACGGAGGGTGGATTGGTGGGGGCGGTCTTTAT ATCGGGACAAACAACGGAGGATGGATTGGCGGTGGTGGCCTGCTTGCG**TAA**TACA TCATTTGTATTACAGAAACAGGG	Gray = Flanking plasmid region in pET21d-P_{T7}:ΔBF Red = gene for CsgA-LBT4*
pET21d-P_{T7}:LBT6*	GGTTCATCTGGTAGTGGCGGTTCGGGTTACATCGGAACCAATAATGGCGGATGGA TCGGGGGAGGGGGCCTTTACATTGGGACTAATAACGGGGGATGGATCGGGGGAGG AGGGTTGTATATCGGGACCAACAATGGGGGTTGGATTGGGGGCGGCGGGTTATAT ATTGGGACAAACAACGGGGGCTGGATCGGAGGCGGTGGTCTTTATATCGGAACAA ACAACGGGGGATGGATTGGAGGGGGTGGACTGTATATCGGAACAAATAATGGAGG GTGGATTGGTGGAGGGGGTTTGTTGGCA**TAA**TACATCATTTGTATTACAGAAACA GGG	Gray = Flanking plasmid region in pET21d-P_{T7}:ΔBF Red = gene for CsgA-LBT6*